Università degli studi di Genova - Istituto Italiano di Tecnologia

Ph.D. Program in Bioengineering and Robotics

Curriculum in Bionanotechnology

XXXII cycle

Functional Materials for Active and Intelligent Food Packaging Applications

Jasim Zia

S4174347

Thesis submitted for the degree of Doctor of Philosophy

Tutors:

Dr. Despina Fragouli

Dr. Athanassia Athanassiou

Group of Smart Materials

Department of Informatics, Bioengineering, Robotics and Systems Engineering (DIBRIS)

Genova, July 2020

Declaration

I hereby declare that except where specific reference is made to the work of others, the contents of this dissertation are original and have not been submitted in whole or in part for consideration for any other degree or qualification in this, or any other university. This dissertation is my own work and contains nothing which is the outcome of work done in collaboration with others, except as specified in the text and Acknowledgements. This dissertation contains fewer than 40,000 words including appendices, bibliography, footnotes, tables and equations and has fewer than 80 figures.

Jasim Zia

July 2020

Functional Materials for Active and Intelligent Food Packaging Applications

Abstract

Food products undergo numerous spoilage processes due to their highly perishable nature. Decreased food quality causes food borne diseases that affect the public health and well-being of the society. Therefore, manufacturers, retailers, consumers and regulatory agencies demand higher quality standards, and the adoption of strategies that enable the real time monitoring/traceability of the food quality throughout the supply chain. Recently the advances in the food packaging led to the development of active, intelligent and smart packaging materials able to improve the food quality, to increase the shelf life and to provide real time information about the condition of the food products. Although in the field numerous studies are continuously reported, there is still the need for the development of biocompatible, cost effective and highly performant systems easily scalable and applicable in everyday life.

This thesis is focused on the development of active, and intelligent packaging biocomposite materials by utilizing functional fillers of natural origin, following cost effective, and easily scalable methods. Specifically, the first part of this study is focused on the modification of an already widely used polymer in food packaging, the low-density polyethylene, in order to improve its water vapor barrier properties and to transform it to a functional material with antioxidant properties, expanding thus its use in active packaging. This is succeeded by introducing into the polymer curcumin powder as filler, following the most common method for polyethylene processing used in industry, the melt processing. The developed composite shows excellent water vapor barrier and antioxidant properties making thus possible its use in active packaging for the shelf life increase of food products. In the second part of this study, an intelligent packaging porous indicator is developed by the combination of polyvinyl alcohol, microcrystalline cellulose and anthocyanins extracted from red cabbage. The specific material is able to indicate the food spoilage through a distinct color change that can be perceived by the naked eye and by non-expert users. In the third part of the present study, an smart packaging material is developed based on red cabbage powder and chitosan that combines the properties of both the active and intelligent packaging materials in a single system. The developed bioplastic presents excellent antioxidant activity, biodegradability and rapid color changes to the food's pH fluctuations during the spoilage process indicating thus its quality deterioration.

Acknowledgments

I would like to acknowledge my advisor, Dr. Despina Fragouli, whom I am exceptionally fortunate to have had the opportunity to work under. She provided an extremely supportive and collaborative environment to work in while taking care of my freedom to pursue my own research interests. I would also like to acknowledge Dr. Athanassia Athanassiou, who motivated and encouraged me throughout my PhD journey along with helpful feedback at many points.

In addition, I would like to pay my gratitude to many of my laboratory colleagues have been incredibly helpful over the years. In particular, I would like to acknowledge Lara Marini, Giorgio Mancini and Riccardo Carzino, who have contributed to my research endeavors. I also had fortune to have colleague friends Muhammad Zahid, Muhammad Tamoor Masood, Zeeshan Hamid Shah and Sara Naderizadeh for supporting me and accompanying.

I am immensely grateful for my friends and family who have been continuously provided me support, encouraged me to pursue my goals and motivated me in bad times. Most of all, they have kept me modest and grounded.

Finally, I would like to gratitude my mother Nasreen Akhtar (Late) and father Abdul Ghaffar, my brother Adarsh Junaid Bastami, my uncle Abid Iqbal, my aunt Azra Yasmeen and my cousins Sabrina Abid and Shanza Abid; who prayed for me and supported me at every stage of life.

Table of Contents

List of Figure

List of Tables

Chapter 1: Introduction to conventional, active and intelligent food packaging

1. Introduction

Food packaging preserves the quality of perishable food products for easy transportation, storage and end use. It slows down the quality decay of the food and makes marketing and distribution more efficient. In fact, packaging materials for food have four basic functions: protection, convenience, communication and containment (Figure 1) [1]. Packages protect the food products from the external environment and offer convenient features like microwaveability, easy opening and resealability. They allow to the consumers to enjoy the food in the way they want; packages communicate with the consumers and retailers with the help of graphics, brand logos, written text about the nutritional facts and preparation guidelines, and finally, food containers are aimed for easy handling and transportation [1].

Figure 1. Basic functions of food packaging.

The deterioration in the food quality occurs during storage and distribution due to various degradation processes, and the consumers and manufacturers request specific strategies and systems that enable the real time monitoring of the food products and also increase their shelf lives [2]. For this reason, in the last 15 years, have been developed diverse active packaging materials with the aim to increase the shelf life of the packaged food [2]. In fact, active packaging refers to a type of packaging, which allows the absorption or release of some substances into or from packaged food or the surrounding environment in order to enhance the shelf life [3].

Unfortunately, active packaging does not give us information about the quality of food before or at the point of consumption. For this reason, intelligent packaging systems have been proposed and used in the last 10 years to carry out such tasks. Intelligent packaging is a type of packaging that can sense, detect and record any changes of the food, and at the same time improves the food quality by releasing specific substances, enhances the safety and warns about the possible problems during food storage

and transportation [2]. Intelligent packaging offers direct information about the quality of packaged food, and can indicate its freshness, or whether its shelf life has, or will, expire soon. It can also control the microwave dosage for ready to eat meals. Intelligent packaging can also be employed as an important tool for monitoring the effectiveness of active packaging [1].

1.1 Sensory manifestations of food spoilage

Many food products are highly perishable due to the inherent susceptibility of their components to microbial and physicochemical degradation. Despite the availability of both conventional and recently developed methods for food preservation such as salting, curing, refrigeration, freezing, freeze-drying, heat treatments, ultrafiltration, use of preservatives, and exposure to irradiation and high hydrostatic pressure, food spoilage remains inevitable, constituting a serious financial burden and raising safety concerns. Food spoilage refers to an ensemble of complex and often interconnected intrinsic and extrinsic factors associated with microbial, chemical and physical processes that render a food product undesirable or unacceptable for human consumption (Figure 2). The manifestations of food spoilage can vary and may become evident through a sensory assessment of the food appearance (discoloration, slime production, colony formation, breakdown of structure, blowing of the container), smell (off-odors) and taste (off-flavors) [4].

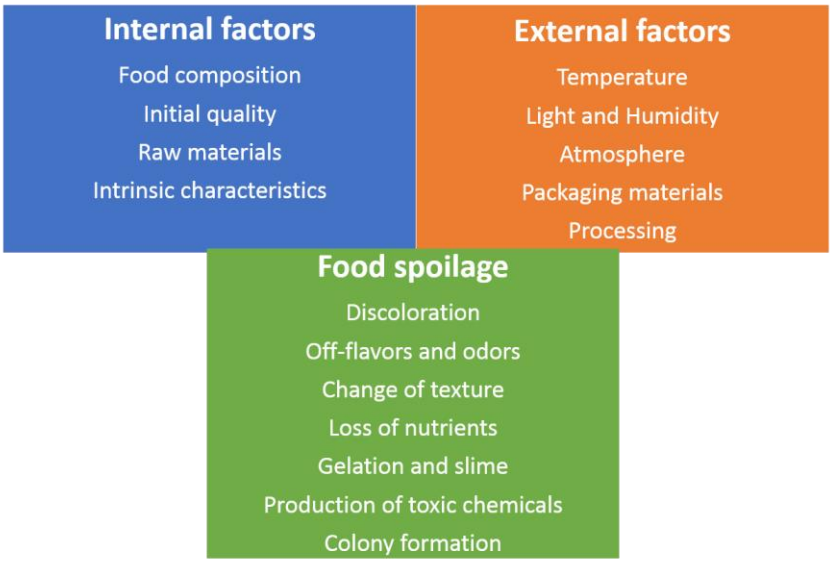

Figure 2. Internal and external factors and sensory manifestations of food spoilage.

1.1.1 Microbial spoilage

Microbial activity is the most impactful cause of food spoilage in terms of financial losses and health concerns. It has been estimated that microbial spoilage alone accounts for the loss of a quarter of the global food supply, reaching 50% of losses for non-grain staples, fruits and vegetables [4]. Based on findings by Pereira et al., more than 6 million cases of foodborne diseases occur every year in the US,

and 60 cases for every 100.000 inhabitants in Spain [5].

The factors affecting microbial spoilage can be classified into extrinsic, intrinsic, implicit and modes of production processing and preservation. Intrinsic factors are related to the inherent chemical, structural and physical properties of the food itself such as pH, chemical composition, redox potential, natural antimicrobial substances, nutrients and water content. Extrinsic factors refer to external conditions in which food is stored and includes temperature, humidity and atmospheric composition. Implicit parameters are defined as the synergistic or antagonistic influences among microorganisms [6], [7]. Finally, the methods followed in the production, processing, preservation and the associated physical and chemical treatments induce changes in the characteristics of a food product determining a microflora, which can widely differ because of the specific effects of such practices.

The range of spoilage microorganisms is wide and comprises bacteria, yeasts and fungi. Bacteria can be both Gram-negative such as Pseudomonas, Escherichia coli and Salmonella and Gram-positive such as Clostridium, Micrococcus, Bacillus and lactic acid bacteria [4]. Bacteria induce a rapid and evident spoilage of protein rich foods such as meat, fish, shellfish, milk and some dairy products [7]. Yeasts and molds grow more slowly compared to bacteria but they can proliferate on a variety of substrates such as pectin and other carbohydrates, organic acids, proteins and lipids and they tolerate more extreme conditions of pH, water activity, temperature and the presence of preservatives. It is also notable that yeasts can utilize food ingredients, such as organic acids (e.g. lactic, citric and acetic acids) that are generally considered to have an inhibitory effect on the growth of many other microorganisms [7]. For instance, Zygosaccharomyces spoil high sugar and salt products, and Dekkera and Brettanomyces are primary spoilers of alcoholic beverages. Concerning to the fungi, Zygomycetes, Penicillia, Aspergilli and Fusaria are the most common species and can grow on all kinds of food including cereals, meat, milk, fruits, vegetables and nuts. Until recently, fungi were generally considered to cause only the unaesthetic spoilage of food. After 1960, when the famous "TurkeyX" disease killed 100.000 turkey poults in Great Britain, it became evident that common spoilage molds could produce dangerous toxins [8]. Today more than 400 mycotoxins exhibiting diverse toxicity levels and effects have been identified, with aflatoxins being the best known [9].

1.1.2 Physical and chemical spoilage

Food spoilage is not only caused by the action of microorganisms but also by a wide range of physical and chemical processes, which may be triggered by light, metal ions or excessive heat during processing or storage, such as oxidation and lipolysis, leading to changes in color, flavor, viscosity or gelation and sedimentation phenomena. Oxidation reactions are among the most common causes of food deterioration and typically occur in food containing pigments and polyphenols, like fruits, and unsaturated fats, like oils, and can be initiated by photosensitizers as well as by naturally

occurring enzymes (e.g. lipoxygenase and peroxidases). Fats can also undergo enzymatic hydrolysis by lipases responsible for the common off-flavor, referred to as rancidity [7], [10].

1.2 Active food packaging

The current focus of the food packaging sector is to provide appropriate food packaging materials and methods in order to ensure the food safety and to minimize the food loss [11], and it is associated with the intensified consumer demands for fresh, convenient and better quality food [11]. In fact, consumers, manufactures and retailers concerns over food quality and safety issues result in the development of active packaging systems [12]. Active packaging is a kind of innovative packaging technology that performs specific functions for the preservation of the food, that cannot be achieved with the use of conventional packaging materials [12], [13].

Specifically, active packaging aims to enhance the shelf life of the food products while maintaining their nutritional quality by preventing the oxidation of the food, inhibiting the growth of microorganisms and preventing the migration of the contaminants, ensuring thus the food quality and safety [13], [14]. Active packaging includes antioxidants and antimicrobial releasing agents, CO_2 absorbers/emitters, moisture absorbers etc. [1], [13], and some of them will be described in detail in the next subchapters.

1.2.1 Antioxidants

Oxygen present in the packaged environment facilitates the microbial growth and lipid oxidation which leads to the color change, the development of off-odors and off-flavors, and nutritional losses, thereby reduces the shelf life of the foods significantly [11]. Consequently, the level of oxygen needs to be controlled carefully in the food environment to restrict such kinds of spoilage reactions. To this aim, oxygen absorbing systems are used to enhance the product quality and shelf life as an alternative to vacuum and gas flushing packaging. In most of these systems, oxygen scavengers are used, which react chemically (oxidation) with the oxygen present in the headspace of the packaged food and prevent the food from oxidative spoilage [11].

The most used scavenging agents for this scope, are iron based substances, englobed in highly permeable sachets that allow the oxygen molecules to pass through them facilitating, thus, the oxidation of iron to iron oxide. This type of oxygen scavenging system was first introduced in the market by the Mitsubishi Gas Chemical Company. The amount of iron required in the sachet depends on the type of package and the type of food, as it is based on the initial oxygen level in the package, dissolved oxygen present in the food, the water activity of the food, and the permeability of the packaging material [11].

Another type of oxygen scavengers is the enzymatic oxygen scavengers, where enzymes that react with the substrate to scavenge oxygen are utilized. Enzymatic oxygen scavengers are very sensitive

to pH, water activity, temperature and solvent/substrate present in the sachet that is essential for the activation of the enzyme, but they are pretty expensive compared to the iron based scavenging systems and therefore their use is significantly restricted.

Most importantly, oxygen scavenging sachets are not considered safe due to the possible spillage of the sachet content, which leads to the contamination of the foodstuff. In addition, sachets may cause accidental consumption with the food or may be consumed by children [11].

When the antioxidants are incorporated in the packaging materials, the sachet-related problems are prevented, and also the performance is significantly enhanced. Specifically, scavengers englobed in films allow the absorption of oxygen from all the food surface in contact with the film [11]. Therefore, recently the research is focused on the development of antioxidant food packaging films. A great part of the research is focused on the development of polymer composite films containing antioxidants that can sufficiently extend the shelf life of the packaged food even for 30 days depending on the type of food [15]. For such scope synthetic antioxidants such as butylated hydroxyanisole (BHA), butylated hydroxytoluene (BHT), propyl gallate (PG), and tert-butyl hydroquinone (TBHQ) Irganox 1076 etc.[16] [17] [18]. were mainly used in the past. However, due to the adverse effects that may cause the synthetic antioxidants to the human health and environment, there is an increasing trend in the use of phenolic antioxidants based on natural resources like essential oils, extracts from herbs, plants and spices etc. with very good performances [13], [14], [19], [20], [21], [22]. For example, it has been proved that active packaging films of low-density polyethylene (LDPE) and antioxidants from barley husks improved the lipid stability of frozen fish compared to control films for an observed time period of 12 months [23]. In another study, the use of nisin (antioxidant) packaging with a modified atmosphere extended the shelf life of the seabream slices to 48 days at 0 °C from the original shelf life of 10 days [24]. Similarly, the combination of modified atmosphere and active LDPE packaging films embedded with a-tocopherol (vitamin E, natural antioxidant) extends the shelf life of the bluefin tuna fillet to 18 days from 2 days [25].

1.2.2 Carbon dioxide scavengers and emitters

The presence of high levels of CO_2 generally plays a useful role in delaying the respiration rate of vegetables and fruits and slows down the microbial growth on meat surfaces. Most of the food packaging films are highly permeable to CO_2, but in such cases, most of the CO_2 inside the package usually infuses through the film. Therefore, where the package has a high permeability to CO_2, a CO_2 releasing system is used to decrease the respiration rate and prevent the microbial growth [11]. In the food packaging industry to increase the shelf life of the highly perishable foods, are usually used antioxidants in combination with a CO_2 releasing system.

1.2.3 Moisture scavengers

The excess of moisture inside the package decreases the product quality and shelf life by facilitating the growth of molds and microbes [11]. Therefore, the prevention of excess moisture buildup in food packages is important to restrict microbial growth. Usually, moisture accumulation takes place inside the packages due to their low permeability to water vapors and the respiration of fresh products triggered by the temperature fluctuations in food packages. The best way to counter this problem in a food package, which usually presents high water vapor barrier properties, is to use a moisture scavenger e.g. silica gel, natural clays, calcium chloride, calcium oxide and modified starch. Silica gel is the most widely used desiccant because it is non-toxic and non-corrosive, and poultry, meat and fish products are usually wrapped to such desiccant pad which absorbs the water. On the other hand, moisture absorbing systems in sachet forms are usually used to maintain low levels of moisture in dried food packages, such as nuts, chips, biscuits, spices, crackers, instant coffee and milk powder [11].

1.2.4 Ethylene absorbers

The shelf life of the climacteric and leafy vegetables and fruits decreases in the presence of ethylene (growth hormone) because it accelerates the ripening due to the increase in the respiration rate and chlorophyll degradation. Hence, the removal of ethylene gas from the package headspace is necessary to slow down the senescence and increase of shelf life. Mostly potassium permanganate embedded in silica is used as ethylene absorber in a highly permeable sachet pack. The function of silica is to absorb the ethylene, while potassium permanganate oxidizes it to ethylene glycol [11]. The performance of such a system depends on the amount of potassium permanganate and substrate surface area. Another system used to scavenge ethylene is zeolite impregnated with potassium permanganate, coated with a quaternary ammonium cation. This system is not only capable of absorbing ethylene from the medium, but also other organic compounds, such as toluene, benzene and xylene. Ethylene scavengers are effective for the storage of packaged vegetables and fruits [11].

1.2.5 Flavor absorbing and releasing systems

Flavor scalping occurs when packaging materials interact with food flavors, resulting in their loss from the food products. Furthermore, high temperature processing of foods results in the loss or degradation of the flavors. Therefore, there is a need to replace these lost flavor constituents when scalping or degradation occurs. Although the high barrier food packaging materials can keep the food flavors in the package, supplementary flavor releasing systems can be effective in diverse cases, such as when heat seal layers of a package have a high affinity to flavors. In addition, consumers always like to smell pleasant flavors when they first open a food package. In contrast to flavor releasing

systems, flavor absorbers scavenge unwanted odors, flavors and aromas present in the package headspace. The formation of off-flavors and off-odors in food products results by the oxidation of oils and fats, or degradation of proteins that lead to the formation of aldehydes and amines respectively that can be removed effectively with the help of active flavor scavengers [11].

1.2.6 Antimicrobial films

Different methods like pasteurization, canning, freezing, refrigeration, dehydration, evaporation, and fermentation are used for food preservation. However, when these methods are combined with chemical preservatives, stronger inhibitory effects against microorganisms occur. Sachets and films containing antimicrobials can be of great value in suppressing surface microbial growth and increasing shelf life. Chemical preservatives that are used in active antimicrobial releasing systems include organic acids and their salts (primarily sorbates, benzoates, and propionates), sulfites, nitrites, chlorides, phosphates, epoxides, alcohols, ozone, diethyl pyrocarbonate, antibiotics, and bacteriocins [11].

Antimicrobial compounds have also been incorporated into films for use in active packaging. For more sustainable and safe packaging materials, are also utilized natural antimicrobial ingredients like coffee, curcumin, clove, pepper and cinnamon [11], or chitosan, due to their natural antimicrobial activities and nontoxicity. For example, Oussalah et al. [26] developed antimicrobial packaging films based on alginate, winter savory, oregano and cinnamon essential oils and found that the cinnamon packaging films are more efficient, compared to winter savory and oregano active packaging.

1.3 Intelligent food packaging

In 2017, as reported by the World Health Organization (WHO) about 600 million cases of illness were caused due to the contaminated food, while around 420.000 people lose their lives every year due to foodborne diseases [27]. Food quality is an important indicator for human health and depends on several factors like food stability, nutritional value and consumer standards. The lack of real time information about the food quality and the inability of reporting the real time condition of the food put the consumers at risk for foodborne diseases. Therefore, since the beginning of the current millennium, researchers have been trying to develop systems able to give information about the food quality in real time. Currently, these efforts have led to the development of a new class of food packaging known as intelligent food packaging [27].

Intelligent packaging contains a component that enables the monitoring of the condition of packaged food or the environment surrounding the food during transport and storage. Intelligent packaging is thus a system that provides to the user with reliable and correct information on the conditions of the food, the environment and/or the packaging integrity [27]. Intelligent packaging is an extension of the communication function of traditional food packaging and communicates information to the

consumer based on its ability to sense, detect, or record changes in the product or its environment. Intelligent packaging offers thus to the consumers and retailers a tool to estimate the quality attributes that are difficult to estimate, and thereby can assist in assuring good product quality to consumers.

1.3.1 Sensors

Sensors provide information about the packaged food product and its environment throughout the supply chain and are used as an alternative to destructive, time consuming and expensive techniques that are currently used in the industry. Sensors are used to measure humidity, temperature, pH-level and light exposure. In addition to this, chemical sensors have gained widespread attention in the last couple of years for the monitoring of food quality and package integrity. Most sensors consist of two components [28]: The sensing part (receptor), which is a coating capable of detecting the presence, activity, concentration or composition of specific chemicals or gases via surface adsorption. The detection occurs through a change of a certain property of the coating, then converted into an output signal by the second component, the transducer that is the actual measuring part of the sensor. This can be an electrical, chemical, optical or thermal signal. Chemical sensors are used to monitor gas molecules (O_2, H_2, CO, CO_2, H_2S, NO_2, NH_3, CH_4, etc) and organic volatile compounds related to food spoilage and package leaking and can be used to evaluate the product quality and the package integrity, important in cases where the modified atmosphere packaging (MAP) is used [28].

1.3.2 Indicators

Indicators in contrast to sensors cannot provide quantitative information (e.g. concentration, temperature) and cannot store the data of measurement over time. However, they provide immediate qualitative information about the packaged food through a mechanical deformation, a color change, an increase in color intensity or diffusion of a dye along a straight path. In most of the cases, the basic requirement of an indicator is that the changes should be irreversible, in order to avoid false information [29]. Intelligent indicators can be based on measuring the condition of the package on the outside, or on measuring directly the quality of the food product, i.e. inside the packaging. In the latter case, there is direct contact with the food or with the headspace. Indicators offer some advantages over sensors such as their low cost, and being user friendly, e.g. can be used by non-expert users. In particular, in the case of indicators, the information regarding the product quality can be perceived directly just by the naked eye while in case of sensors, they have to be connected to a separate device to transduce the sensor signal to an observable response [30]–[38]. For example, a pH electrode is considered a sensor and pH paper is considered an indicator.

1.3.2.1 Time-temperature indicators (TTI)

Temperature plays an important role in determining the shelf life of a food product [28]. Fluctuations in the temperature profile can result in the growth of microorganisms that result in spoilage of the food. TTIs are used to monitor the temperature during storage and distribution, which is particularly useful for warning of temperature abuse for chilled or frozen food products and thus for ensuring food safety [28]. TTIs are placed outside of the package and their working principle is based on a chemical, mechanical, electrochemical, enzymatic or microbiological time and temperature dependent change, mostly expressed as a visible color change [27], [28].

1.3.2.2 Integrity Indicators

Package integrity is essential for maintaining the quality and safety of food products in MAP. An alternative approach to package-destructive, quality assurance techniques is the use of non-invasive indicator systems as part of the MAP. Such systems usually provide information through visual colorimetric changes or comparison with standard references. For example, oxygen indicators composed of redox dyes change their color upon the oxidation of the dye molecules, which is caused by changes in the oxygen concentration in the package due to leakages [39], [40]. One of the main disadvantages of such a system is that it requires the use of highly sensitive redox dyes and the oxygen already present in the package may also interact with the dye to give false indications.

1.3.2.3 Freshness Indicators

Food freshness indicators provide direct information about the quality of the product resulting from chemical changes or microbial growth within a food product [2]. Most of the concepts that the freshness indicators exploit rely on the interaction between the functional component of the indicators and specific by-products of the food originating from deterioration reactions give rise to a change in color of the indicator [2], [41]–[43]. They, thus, indicate the real spoilage or lack of freshness of the product instead of just temperature abuse or package leaks and have to be placed inside the package [2]. Food freshness indicators can also be used for the estimation of the remaining shelf life of perishable products.

In general, colorimetric indicators functionalized with synthetic dyes e.g. methylene blue and red, bromocresol green and purple, bromothymol blue, chlorophenol and xylenol have been utilized extensively as freshness indicators for intelligent packaging applications [41]. Colorimetric indicators enable the real time monitoring in a user friendly manner through an optical color change observable by the naked eye [41]. However, they do not meet strict consumers and regulatory agencies food safety demands due to their potential toxicity [41]. Therefore, as an alternative approach, natural dyes extracted from different plants e.g. curcumin, alizarin and anthocyanin are used due to their negligible toxicity, easy preparation, cost effectiveness and renewability [41]–[43]. In the next sub-chapters, the most important types of freshness indicators are presented.

1.3.2.3.1 Indicators for CO_2

CO_2 gas is produced during bacterial and mold growth on foods. Therefore, CO_2 detection can be used to indicate the deterioration of foods as it changes the pH of the packaged environment. CO_2 indicators typically function following the principle of Severinghaus CO_2 electrode [44], which involves the diffusion of CO_2 from the test medium (gaseous or aqueous) through a thin gas permeable membrane, and a quick establishment of equilibrium with the entrapped aqueous layer, which contains a pH-sensitive dye [2]. Therefore, the detection occurs upon the interaction of the gas to be tested with a chemical reagent/dye of the indicator which results in a color change/shift of the system [2], [27]. However, these technologies still present some drawbacks, as indicators containing pH-sensitive dyes generally suffer from physical (e.g. humidity and temperature) and chemical interferences (e.g. other volatile acid or basic gases produced during spoilage).

1.3.2.3.2 Indicators for amines

Biogenic amines are low molecular weight organic bases that possess biological activity. They include tyramine, trimethylamine, 2-phenylethylamine, histamine, putrescine, cadaverine, spermine, spermidine, tryptamine, and agmatine. They are generated from the decarboxylation of amino acids in meat, fish, and milk by bacteria [45], [46], and their presence in foods causes the alteration of the pH of the packaged environment. Biogenic amines in foods are of concern in relation to both food spoilage and food safety. They are generated either as the result of endogenous amino acid decarboxylase activity in raw food materials or by the growth of decarboxylase-positive microorganisms under favorable enzymatic activity. As the microbial spoilage of food may be accompanied by the increased production of decarboxylases, the presence of biogenic amines might serve as a useful indicator of food spoilage [47], [48]. The presence of amines changes the pH of the packaged environment. Mostly pH-sensitive dyes are used for the detection of amines that indicates the spoilage just by producing the optical color change [30], [31], [49]–[73].

1.3.3 Radio frequency identification (RFID)

RFID is particularly suitable for large production networks such as food supply chains. Compared to sensors and indicators, these technologies do not provide qualitative or quantitative information about the product quality status. They are typically applied for purposes such as identification, atomization, antitheft prevention or counterfeit protection [27].

1.4 Smart food packaging

Smart packaging is a food packaging system that has the functions of both the active and intelligent packaging. Smart packaging provides the complete packaging solution by enhancing the protection

and the communication functions of food packaging materials. With the smart packaging, the food spoilage due to not appropriate storage can be sufficiently controlled while information about the quality of food throughout its distribution chain is provided. In fact, to achieve the smart packaging functions, active and intelligent packaging technologies have been integrated into the packaging system. Currently, there is considerable research activity for the development of individual active and intelligent packaging systems, but research on the integration of these technologies or the development of a single food packaging system with both functions still needs to be explored.

1.5 Thesis motivation and outlook

This thesis focuses on the development of materials for active and intelligent food packaging, and specifically on the development of novel active films and colorimetric indicators based on natural and biodegradable materials.

Concerning the active food packaging, synthetic antioxidants that are used in the polymer industry to prevent the thermal degradation (thermal oxidation) of the polymers during industrial processing, are also proposed for the development of packaging films with antioxidant properties able to effectively prevent the lipid oxidation of the foods [16]–[18], [74]–[77]. However, their potential toxicity due to the migration to the food products restricts their wide use in active food packaging materials. As an alternative approach, natural antioxidants, mainly from essential oils, plant extracts, herbs and spices are widely utilized in combination with natural or synthetic polymers (see Appendix-I, Table S1). In most of the studies, novel combinations with natural polymers are explored following fabrication methods that are not industrially scalable for bulk production, e.g. solution casting, as are required large amounts of solvents, and time consuming processes. When commercial food packaging polymers such as polyethylene and polypropylene are considered, their combination with the natural antioxidants is performed only for the prevention of the polymers' thermal oxidation during their thermal processing without any further discussion on whether or not such system can be used for antioxidant food packaging applications [18], [74]–[77]. In the second chapter of this thesis, we will focus on the development of active food packaging materials following an industrially applicable fabrication method, easily scalable, and based on the combination of the commercial low-density polyethylene, widely used as food packaging material, and the natural antioxidant curcumin via extrusion and compression molding.

In the third chapter, this thesis will focus on the development of a porous colorimetric food indicator based on natural and biodegradable materials, and on the engineering of its pores structure in order to obtain rapid color changes upon a large range of pH. Nowadays, colorimetric natural indicators mostly in the form of films are widely investigated to monitor the real time freshness of the meat and

seafood [30], [31], [49]–[73]. However, due to the highly compact structure of the films, their responsiveness and sensitivity against rapid pH fluctuations (e.g. acidic or basic vapors), and reversibility is highly questionable and not addressed adequately. In fact, to best of our knowledge, not even a single study addresses the response kinetics of the color change of the developed indicators. Moreover, the developed natural indicator films are application specific e.g. not used for acidic or basic vapors sensing (see Appendix-I, Table S2). Therefore, the focus of the second chapter will be the development of highly porous natural pH indicators, which demonstrate good reversibility, reusability and responsivity to a wide pH range, but also to acidic and basic vapors. Most importantly, it will be proved that by specifically tunning the characteristics of the pores of the indicators, the response kinetics to defined pH changes can be efficiently controlled.

Finally, in the fourth chapter will be presented the development of bioplastic films by the combination of red cabbage powder and chitosan. The presented films provide the complete food packaging solution by combining the advantages of active and intelligent food packaging in a single system that give rise to a smart food packaging material. The smart food packaging films demonstrated excellent mechanical and water vapor barrier properties, biodegradability in the sea water and on top of that excellent antioxidant activity and faster response to acidic or basic vapors. The focus on whole natural composite system is motivated by the current need to focus on the development of innovative plastic materials from renewable resources with minimal environmental impact. In fact, petroleum based plastics have a negative impact on the environment as most of them are not biodegradable and they remain in the environment as persistent wastes (Figure 3a). A great source of such plastic pollution is the packaging sector, and therefore packaging plastic materials significantly contribute to the specific problem (Figure 3b). Additionally, the depletion of the nonrenewable resources of petroleum is on the cards, as millions of oil barrels are used for the production of plastics.

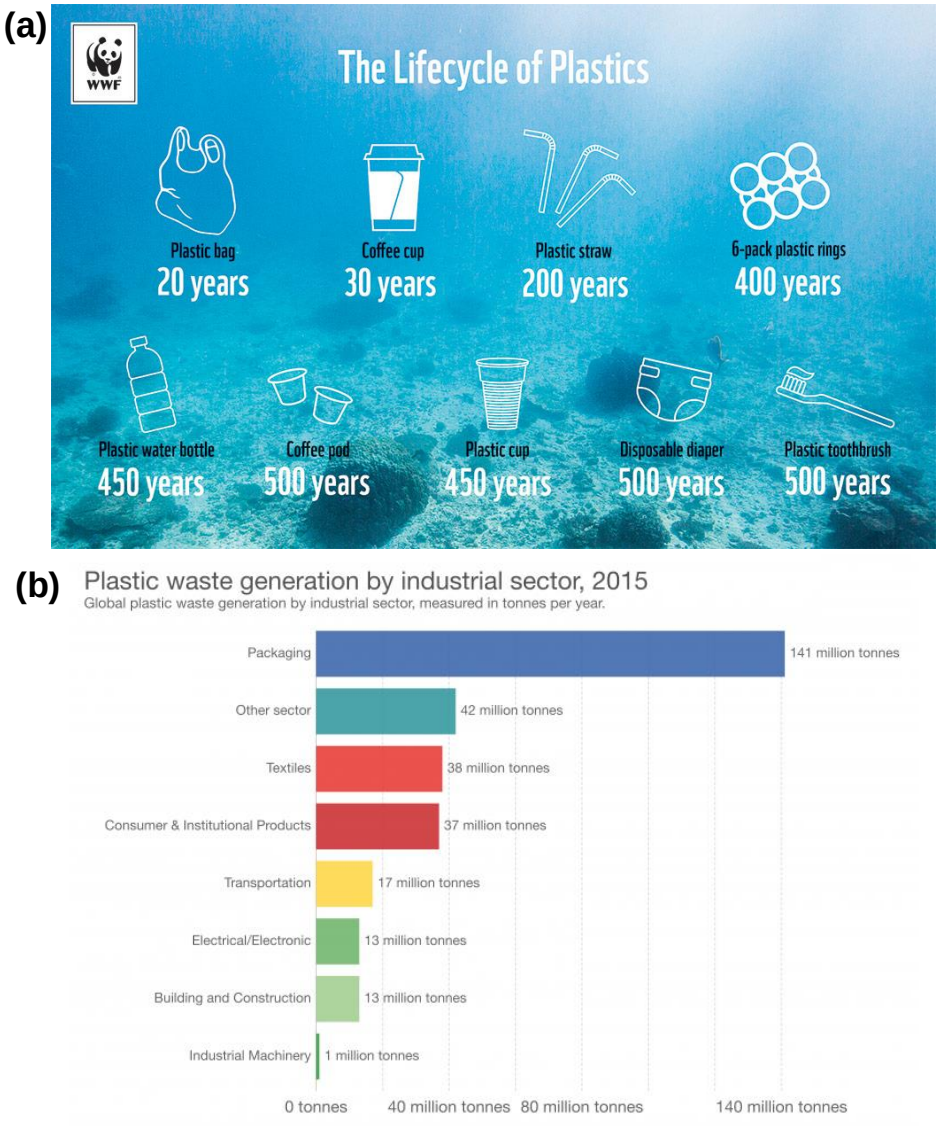

Figure 3. (a) Life cycle of the plastics in the ocean and (b) classification of the plastic waste with respect to industrial sector [78].

Chapter 2: Active food packaging films based on low-density polyethylene (LDPE) and curcumin

Abstract

In this study, active film composites of low-density polyethylene and curcumin powder are developed by extrusion and compression molding, thus, via the conventional industrial methods that such polymer is usually processed. The aim is to develop active food packaging materials based on a natural and biocompatible active filler and a conventional polymer widely used in the packaging industry in the form of pure polymer films, but rarely studied in combination with active molecules in order to be transformed into an advanced packaging material. The effect of the curcumin concentration on the morphology of the active packaging films was studied with scanning electron microscopy (SEM), the possible chemical interactions between the LDPE and the curcumin were studied with fourier transform infrared spectroscopy (FTIR), the thermal properties of the developed films and the effect of the curcumin filler present in different concentrations were studied with differential scanning calorimetry (DSC), and thermo-gravimetric analysis (TGA), and the wetting properties of the films and how they were affected by the curcumin filler in different concentrations was studied with water contact angle (WCA). Furthermore, the performance of the composite films as novel active packaging systems was explored through the characterization of the water vapor permeability (WVP), oxygen permeability (OP), mechanical properties and free radical scavenging potential (antioxidant activity). The results of this study reveal that the morphology of the films is not significantly affected by the presence of curcumin. Furthermore, the presence of curcumin increases the thermal stability of the biocomposite films without altering their thermal processability. In addition to this, curcumin enhances the elastic modulus, and water vapor barrier performance of the polymer and offers an excellent antioxidant activity to the polymer. The results of this study suggest that the active films based on the combination of low-density polyethylene and curcumin can be used for active food packaging applications.

2.1 Introduction

The oxidation together with microbial growth is the main cause of the quality loss of packaged food [13], [19], [79]. The oxidation reactions degrade the proteins, lipids and pigments resulting in the decrease of the shelf life of the packaged food products [13], [24], [79] [80]. Most strategies that are commonly used to control the lipid oxidation of packaged foods deal with the direct addition of antioxidants to the food, or the packaging under modified atmospheres in which the oxygen presence is limited [81]. Active packaging that carries antioxidants in the packaging system has been proved to be more effective compared to the packaging systems in which antioxidants are directly applied to

the food surface [80], [81]. This is attributed to the continuous/sustained release of the active components from the packaging system towards the food. Therefore, the antioxidant activity is guaranteed during the time, and so also the stability of the food products, in contrary to the direct addition of the antioxidant in the food where once the active compound is consumed, the protection level decreases and the food starts to deteriorate rapidly [81].

Currently synthetic antioxidants, for example butylated hydroxyanisole (BHA), propyl gallate (PG), butylated hydroxytoluene (BHT) and tert-butyl hydroquinone (TBHQ) are widely used in the food industry [12], [16], [17], [19], [79]. However, their use is restricted by the Codex Alimentarius (FAO/WHO Food Standards, 2005) as well as by European Regulation (Directive 2006/52/EC, 2006) and FDA Food Additive Status List (US Food and Drug Administration, 2006) [19]. Similarly, to improve the barrier performance of the polymeric packaging materials, synthetic additives, such as silicate, clays and other nanomaterials, have been employed [82]–[84]. However, their migration towards food and the effects on the health is still under consideration and therefore the, still not defined, acceptable limits for migration of these substances into food may restrict their large scale application in the food packaging field [84]–[86]. Due to the adverse effects of synthetic antioxidants on the human health and environment, there is an increasing trend in the use of phenolic antioxidants based on natural resources like essential oils, extracts from herbs, plants and spices etc. [13], [14], [19], [20] and fillers of natural origin [87]–[89]. Some of them can significantly increase the antioxidant activity of the films [90], [91] but at the same time, they do not contribute sufficiently to the enhancement of the water vapor barrier properties, essential for food packaging films. However, the utilization of phenolic compounds, like tea extracts [13], [80] and curcumin [92] may offer the possibility to improve simultaneously both properties if combined with the right polymers, making possible the development of packaging materials with improved properties.

Curcumin is a naturally occurring polyphenolic compound derived from the roots of curcuma longa (turmeric plant) [93], [94]. The Food and Drug Administration Department of USA (USFDA) has declared curcumin as a nontoxic compound [95]. Currently, curcumin is used in the food industries and pharmaceuticals due to its excellent biological activities such as antiviral, anticancer, antimicrobial, anti-inflammatory and antioxidant properties [94]–[100]. Recently due to its powerful antioxidant potential and its ability to change color upon pH modifications [42], [53] has led to the research of curcumin for use in smart packaging systems.

In food packaging, curcumin is mainly blended with natural polymers e.g. cellulose, chitosan, gelatin, corn zein, k-carrageenan and tara gum [12], [13], [42], [53], [80], [92], [95], [100]–[104] in order to achieve antioxidant properties. In most of the studies, solution casting methods are utilized for the fabrication of active packaging films that are not directly correlated with the conventional industrial

techniques for large scale production fact that restricts the wide use of curcumin for the food packaging.

Polyethylene (PE) is widely used in the packaging due to its versatility, easy processability, recyclability, low cost and more recently the availability of the feedstock from renewable resources [105]–[107]. However, there is still a limited number of studies on the use of curcumin as an antioxidant incorporated in the PE, following melt flow processes [108], [109]. In particular, the PE has never been functionalized before with curcumin for active food packaging applications. Moreover, to the best of our knowledge, the antioxidant potential of curcumin in active food packaging systems after going through a substantial heating process is yet to be reported. Hence, it is necessary to investigate the antioxidant activity of curcumin incorporated within the packaging system.

In this study, active food packaging films based on low-density polyethylene (LDPE) were developed by incorporating natural antioxidant curcumin through industrially applied methods: extrusion molding and compression molding. The active films were characterized in terms of thermal, chemical, mechanical, and physical properties including wetting properties, oxygen permeability and water vapor permeability. The 2,2-diphenyl-1-picrylhydrazyl free radical scavenging assay was used in order to evaluate the antioxidant potential of the active films. The results of this study showed that the addition of curcumin does not alter the melting behavior of the active films, and therefore the thermal processability of the LDPE based films is not altered. 5%wt curcumin in the LDPE matrix improves the polymer's tensile modulus (21.24%) and water vapor barrier property by 51.48%. The active packaging films showed excellent antioxidant activity of 44.5%. The results of this study indicate that following the already widely used industrially applicable processing methods for the processing of LDPE it is possible to develop active LDPE/curcumin films which are ideal candidates for active food packaging systems.

2.2 Material and methods

2.2.1 Materials

Low-density polyethylene (LDPE), curcumin from Curcuma longa (Turmeric powder), ethanol with 96% purity and 2,2-diphenyl-1-picrylhydrazyl (DPPH) were purchased from Sigma Aldrich and were used without further purification.

2.2.2 Fabrication of the films

The extrusion of the pure LDPE and LDPE containing 1, 2, 3, 5% and 7%wt. of curcumin (Cur/LDPE) was carried out through a single-screw Rheoscam extruder (Scamex-France) having three heating zones (Figure 4a,b) with a screw of 20 mm diameter, and length to diameter ratio (L/D) of 20. The screw was attached to a die of 2 mm diameter at the extrusion point, and its rotation speed was maintained at 50 rpm throughout the extrusion process. During the process, the temperature of the three heating zones was set at 145 °C, while the entire length of the heating zones is 11.5 cm. The extruded filaments were further pelletized and were used for the fabrication of the active films. Following this process, pure LDPE and Cur/LDPE composite films (Figure 4c,d) were produced by compression molding (Carver Inc., Model 3850, USA) at 145 °C for 40 minutes with a 10 MPa applied pressure. The dimensions of the final films were 9.8 cm × 9.8 cm and their thickness 450 μm.

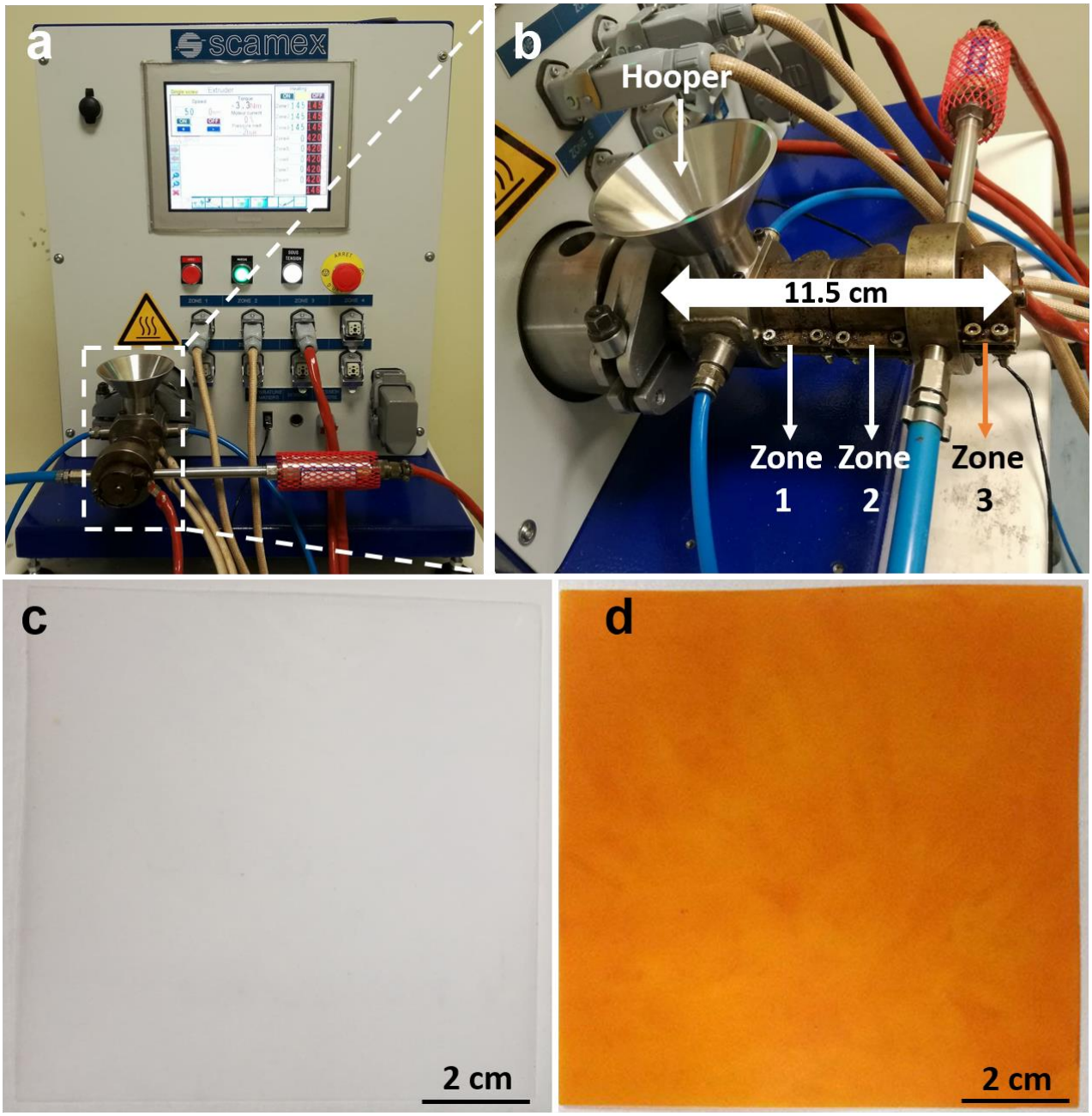

Figure 4. Photograph of (a) Rheoscam single-screw extruder used for the fabrication of pure LDPE and Cur/LDPE films, (b) detailed configuration of three heating zones, (c) pure LDPE film and (d) 5% Cur/LDPE film.

2.2.3 Scanning electron microscopy (SEM)

To study the surface and cryo-fractured cross-sectional morphologies of the pure LDPE and Cur/LDPE filaments and films, scanning electron microscopy imaging was performed (SEM, JEOL JSM-6490AL) after coating the specimens with 10 nm thin gold layer using a Cressington 208HR high-resolution sputter coater (Cressington Scientific Instrument Ltd., UK).

2.2.4 Fourier transform infrared spectroscopy (FTIR)

Infrared spectroscopy was used to investigate the possible intermolecular interactions between curcumin and LDPE. Infrared spectra were obtained with a Fourier Transform Infrared (FTIR) spectrometer (Equinox 70 FT-IR, Bruker) in transmittance mode. All spectra were recorded in the range from 3800 to 600 cm^{-1} with a resolution of 4 cm^{-1}, accumulating 128 scans.

2.2.5 Differential scanning calorimetry (DSC)

The thermal behavior of the fabricated films was studied through differential scanning calorimetry (Diamond-DSC, Perkin Elmer, USA). The 20±1 mg of pure LDPE and Cur/LDPE films were weighed accurately in sealed aluminum pans and heated from 30 °C to 220 °C with a rate of 20 °C /min under a dry nitrogen purge (flow rate 20 ml/min). After keeping the samples at 220 °C for 1 min, they were then cooled down from 220 °C to 30 °C with a rate of 20 °C/min. After 1 min at 30 °C, they were subsequently subjected to a second heating cycle with the same parameters. An empty pan was used as the reference cell. The instrument was calibrated using indium before testing the samples. The first heating cycle was performed in order to erase any aging event occurring during sample storage, and the second one was conducted to determine the melting temperature (T_m) while the first cooling cycle was carried out to determine the crystallization temperatures (T_c).

2.2.6 Thermo-gravimetric analysis (TGA)

The thermal stability of the pure curcumin powder, pure LDPE and Cur/LDPE films was investigated by means of thermo-gravimetric analysis (TGA) using a TGA Q500 system (TA Instruments USA). The measurements were carried out on 14 mg samples weighed in aluminum pans and heated from 30 °C to 800 °C with a heating rate of 10 °C/min under the air of a constant flow rate of 50 ml/min.

2.2.7 Interaction of the films with water

The static water contact angle of pure LDPE and curcumin LDPE films were obtained by an optical contact angle measurement instrument (Data Physics OCAH 200, Germany). A droplet volume of 5µl (distilled water) and a droplet age of 30 seconds was used for all water contact angle experiments. Three different films of each type were used for experiments and for each film ten measurements were taken at different places and average values are reported.

The water vapor permeability (WVP) of the pure LDPE and Cur/LDPE films was determined gravimetrically according to the ASTM E96/E96M standard method [110], [111]. The tests were carried out at ambient temperature under 100% relative humidity gradient (ΔRH%). 400 µl of distilled water (which provides 100% RH inside the permeation cell) was placed in each of the permeation cells with a 10 mm inner depth and an inner diameter of 7 mm. The test films were cut in circular form using a dye cutting press and then were mounted on the top of the permeation cells. The permeation cells were placed in a desiccator, which contained anhydrous silica gel as a desiccant in

order to maintain 0% RH [112]. The water transferred through the test films and absorbed by the desiccant was determined from the weight loss of the permeation cell after every hour for an 8 hour period using an electronic weighing balance (0.0001 g accuracy). The weight loss of the permeation cells was plotted as a function of time. Then, the water vapor transmission rate (WVTR) was determined from the slope of each line obtained from the linear regression, as shown by the following expression.

$$\text{WVTR} = \frac{\text{Slope}}{\text{Area of the film}} \qquad \text{Equation 1}$$

The WVP of the films was calculated as follows [111], [112].

$$\text{WVP} = \frac{\text{WVTR} \times \text{L} \times 100}{\text{P}_S \times \Delta\text{RH}} \qquad \text{Equation 2}$$

Where, L (m) is the film thickness, ΔRH (%) is the relative humidity gradient and P_s (Pa) is the saturation water vapor pressure at 25 °C. The results are reported as a mean of 10 repetitions from different films with their standard deviation.

2.2.8 Oxygen permeability

The oxygen permeability (OP) of the pure LDPE and Cur/LDPE films was evaluated using an Oxysense device (Oxysense 5250i, USA) equipped with a film permeation chamber, according to the ASTM F3136-15 standard method. The films were cut in a rectangular shape with dimensions of 6 cm × 6 cm and placed in the permeation chamber. The oxygen transmission rate (OTR) of the films was measured automatically by the Oxysense software by monitoring the oxygen uptake after 30 minute time intervals. The OP was calculated by the following formula [113], [114].

$$\text{OP} = \frac{\text{OTR} \times \text{L}}{\Delta\text{P}} \qquad \text{Equation 3}$$

Where L (μm) is the film thickness and ΔP is the difference in the oxygen pressure between both sides of the films that is 1 atm.

2.2.9 Mechanical properties

The mechanical properties of the pure LDPE and Cur/LDPE composite films were determined using an Instron (3365 Instron, USA) dual column tabletop universal testing system, with a load cell of 5 kN at a crosshead speed of 5 mm/min, following the ASTM D882-12 standard method. The specimens were cut into a dog-bone shape with a dimension of 35 mm × 4 mm using a mechanical cutter. The tensile modulus in MPa and elongation at break in % were automatically calculated by the Instron software. In each case, 5 different samples were tested from different films and the average values are reported.

2.2.10 Release kinetics

The release kinetics of the curcumin from the Cur/LDPE films and the antioxidant tests were performed by UV-visible (UV-Vis) spectroscopy in the range of 200-800 nm, using a Varian UV–Vis spectrophotometer (CARY 6000i, USA). For the release kinetics, samples of 60 mg weight were cut with a dye cutting press and placed in ethanol solution such that the sample concentration in the solution to be 1% (w/v). The evolution of the absorbance of the extracted curcumin in the solution was recorded after defined time intervals up to 24 hour using pure ethanol for the baseline correction. Following this process, 10 different samples were tested, and the average absorbance value of the characteristic peak of the curcumin (428 nm), was calculated for each time interval. In order to evaluate the concentration of the curcumin in solution in each case, the absorption spectra of five different curcumin solutions with known concentrations ranging between 1-5 µg/ml were recorded. The intensity of the absorption peak at 428 nm was then plotted and the equation which gives the dependence of the absorption intensity to the curcumin concentration was defined by a linear fit (Figure 5). According to the linear fitting, the concentration of the curcumin in unknown solutions was calculated by the equation

$$I_{abs} = 181.25 \times C \qquad \text{Equation 4}$$

Where I_{abs} is the intensity of the absorbance peak at 428 nm and C is the curcumin concentration.

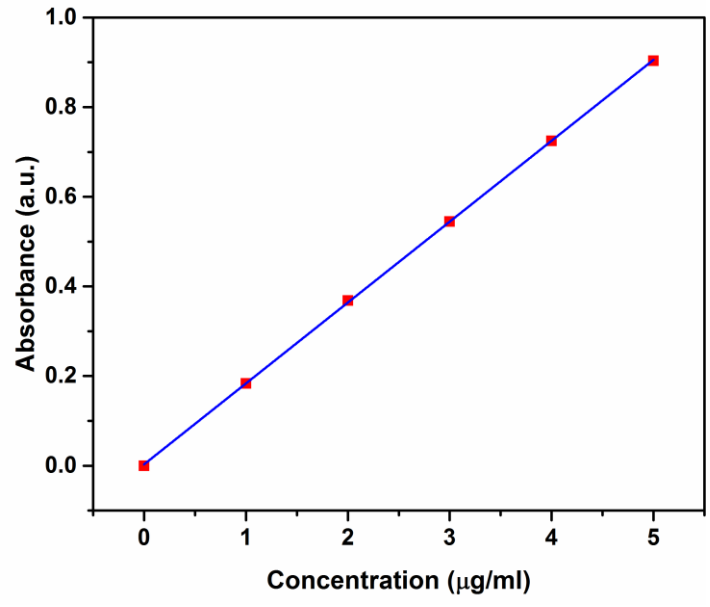

Figure 5**.** Linear fitting of the absorption intensity at 428nm vs curcumin concentration.

2.2.11 Antioxidant properties

To investigate the antioxidant activity of Cur/LDPE films, the curcumin extract from different vials containing 1% (w/v) Cur/LDPE films were collected after time intervals of 1 hour for a period of 24

hour. For comparison reasons, the antioxidant activity of pure curcumin powder was also evaluated by preparing the same concentrations of curcumin powder in ethanol (measured through the process described above (Equation 4)). The antioxidant activity of the Cur/LDPE films was determined by using a slightly modified standard DPPH• free radical scavenging method [115], [116]. In particular, 2 ml of the curcumin extract solution was mixed with 2 ml of 50 μM solution of DPPH• in ethanol and kept in the dark. After 30 minutes, the absorbance of this solution was measured. The absorbance of a second solution was measured by mixing 2 ml of curcumin extract solution with 2 ml of ethanol. Finally, the spectrum of the absorbance was obtained by mixing 2 ml of 50 μM solution of DPPH• in ethanol with 2 ml of ethanol. The percentage of DPPH• scavenging activity was calculated according to the following equation.

$$\text{Radical scavenging activity (\%)} = \left[1 - \frac{A_1 - A_2}{A_3}\right] \times 100 \qquad \text{Equation 5}$$

Where A_1 is the absorbance value at 517 nm of the solution containing the curcumin extract and the DPPH• radical, A_2 is the absorbance at 517 nm of the curcumin extract with ethanol and A_3 refers to the absorbance of DPPH• control solution at the same wavelength. All the results are reported as an average of three repetitions of different samples.

2.3 Results and discussion

2.3.1 Bio-composites morphology and SEM

In Figure 6, SEM images for the fabricated filaments and hot pressed films are presented. It is evident that following the fabrication process described in the experimental part, the LDPE filaments and films have a compact, nonporous and smooth surface morphology. By adding the curcumin filler (5% wt.), films' top and cross-section surface become slightly less smooth, but no cracks, air bubbles and big particle agglomerates are evident showing a uniform dispersion of the curcumin filler in the polymer matrix. Moreover, the compression molding step did not have a significant effect on the surface and cross-sectional morphologies of the LDPE and 5% Cur/LDPE films.

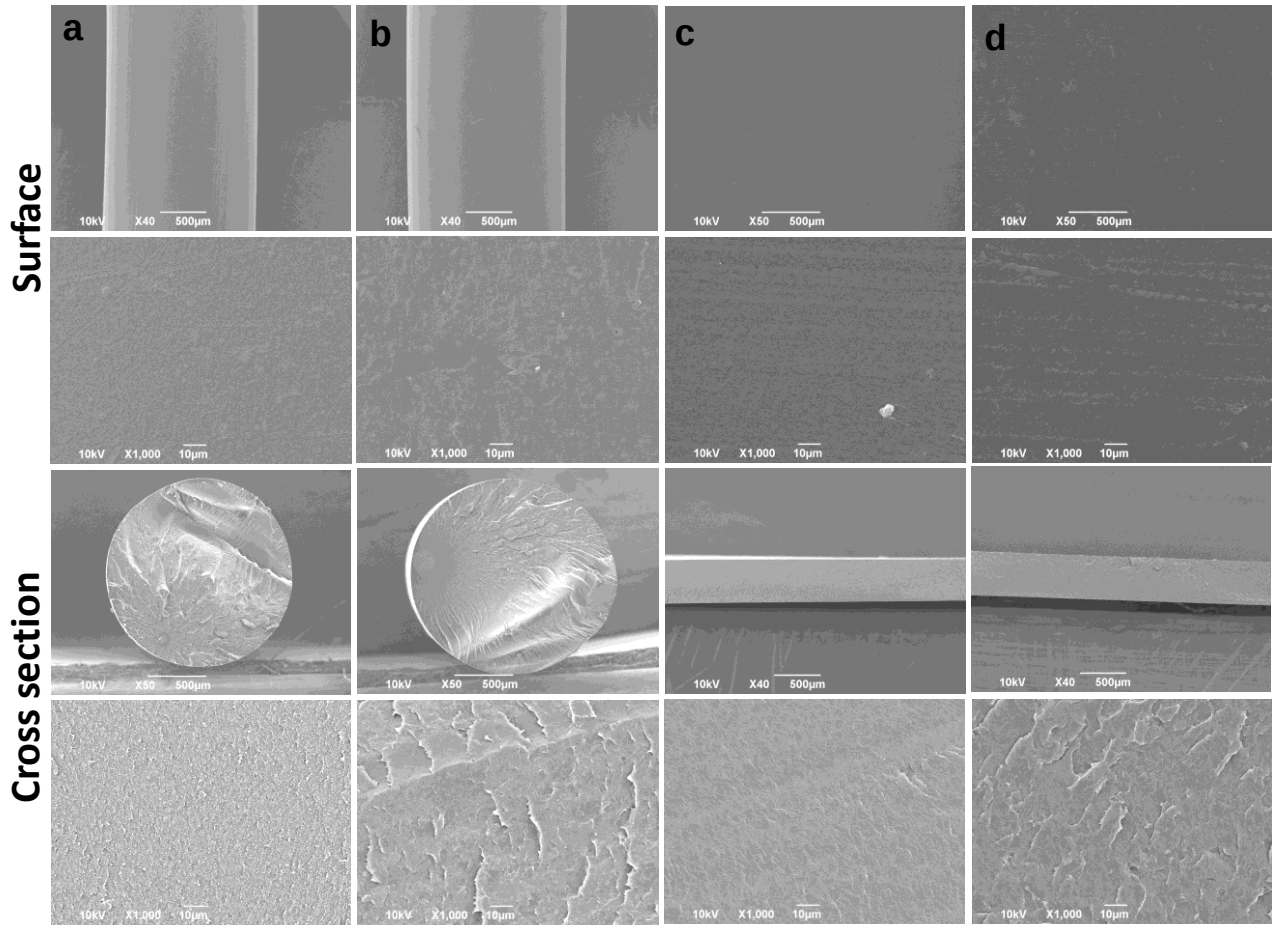

Figure 6. Surface and cryo-fractured cross-sectional morphologies of (a) pure LDPE filament, (b) 5% Cur/LDPE filament, (c) pure LDPE film and (d) 5% Cur/LDPE film

2.3.2 Fourier transform infrared spectroscopy (FTIR)

To see the possible chemical interactions between the components the ATR-FTIR spectra of the pure curcumin, the LDPE and Cur/LDPE films is analyzed. The main assignments of the pure curcumin (Figure 7 and Figure 8) are the OH stretching at 3507 cm^{-1}, the conjugated C=O stretching at 1627 cm^{-1}, the aromatic C=C stretching at 1602 cm^{-1}, the C=O stretching at 1506 cm^{-1}, the olefinic C-H bending at 1427 cm^{-1}, the C-O-C stretching at 1026 cm^{-1}, and the C-H out of plane bending of the aromatic rings at 855 cm^{-1} [53], [102], [117]–[120].

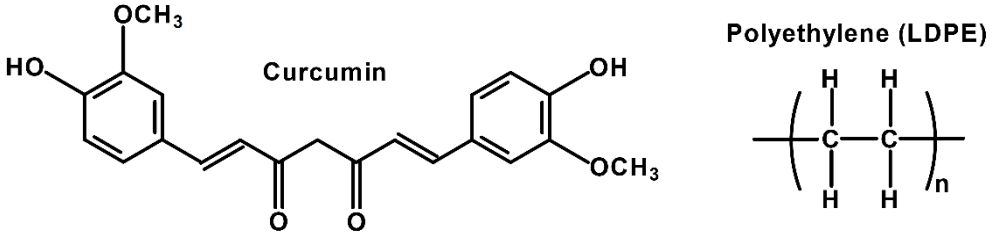

Figure 7. Chemical structure of curcumin and LDPE

On the other hand, at the spectrum of the LDPE, peaks assigned to the basic PE structure (Figure 7 and Figure8) are evident, such as asymmetric and symmetric CH_2 stretching at 2914 and 2849 cm^{-1} respectively, and CH_2 bending and rocking modes at 1470 $cm^{-1}$and 718 cm^{-1} respectively [121]–[125]. The Cur/LDPE film's spectrum presents the characteristic bands of both the LDPE and curcumin, without any kind of shifts or additional peaks, indicating no chemical interactions between the two components. However, some subtle modifications of the main LDPE bands (i.e., CH_2 stretching, bending, and rocking modes) are detected. To highlight these differences the subtraction of the LDPE spectrum form the 5% Cur/LDPE one is performed and the results are presented in Figure 8b,c,d. After subtraction, in the region associated with the asymmetric and symmetric CH_2 stretching modes, positive absorptions were observed at higher wavenumbers than the maxima of $\nu_a(CH_2)$ and $\nu_s(CH_2)$ of the LDPE spectrum, indicating a blue shift. A similar behavior was noticed for the CH_2 rocking mode. On the contrary, the CH_2 bending mode presented positive absorptions at lower wavenumbers, that is, a red shift. This type of slight shifts has been previously reported for LDPE as a function of the temperature and are ascribed to a bulk contraction and subsequent increase of van der Waal forces between polymer chains [126]. In this sense, the presence of curcumin clusters in the composite and the high pressure during extrusion molding can effectively induce a polymer shrinkage, decreasing the distances between LDPE chains.

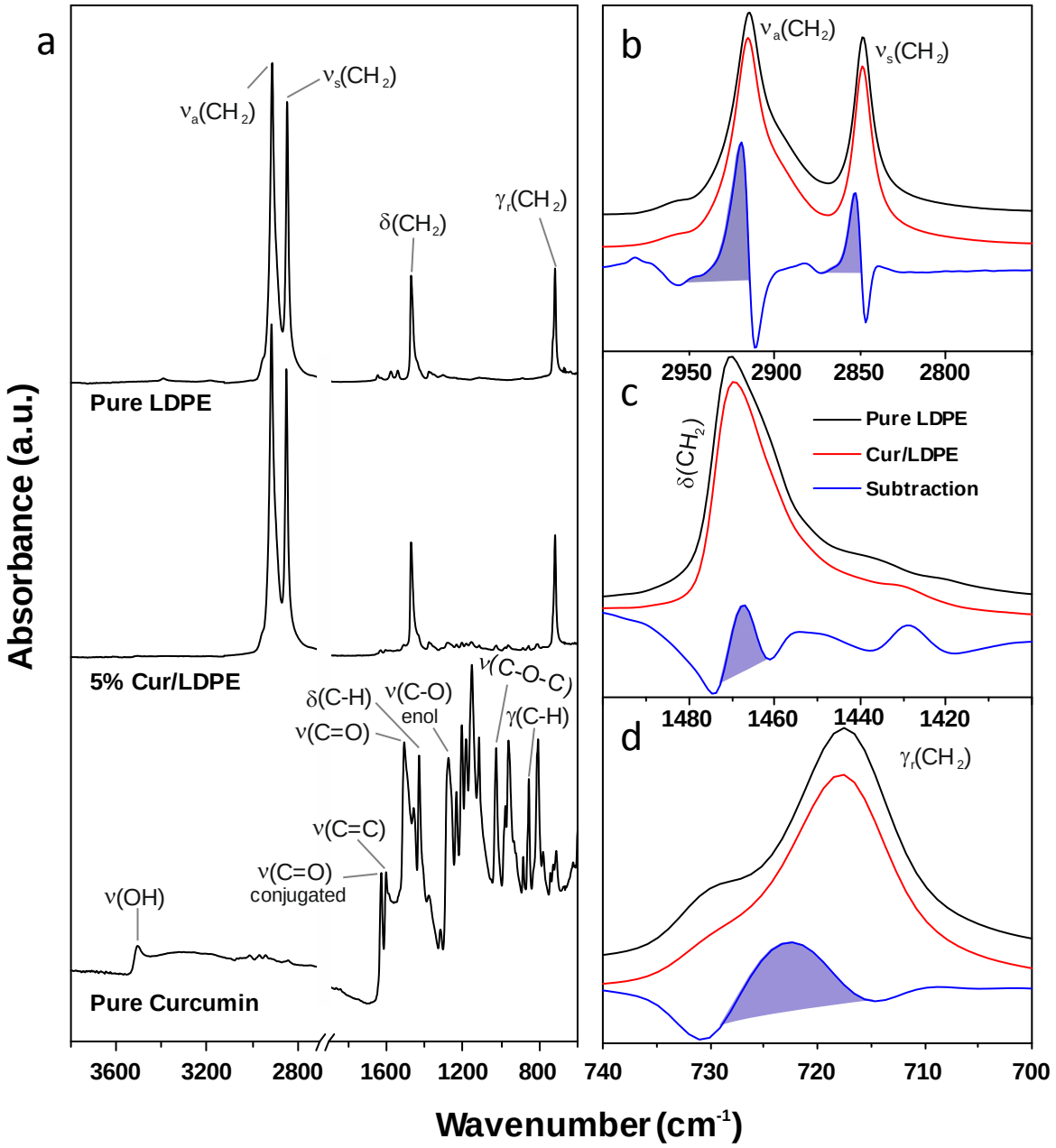

Figure 8. (a) FTIR spectra of pure curcumin, LDPE, and the 5% Cur/LDPE composite. (b,c,d) CH_2 stretching (3000-2750 cm^{-1}), bending (1500-1400 cm^{-1}), and rocking (740-700 cm^{-1}) modes, respectively, of pure LDPE and 5% Cur/LDPE composite. The corresponding subtraction spectra are included and the regions of interest are highlighted by filling the peaks in a light blue color.

2.3.3 Differential scanning calorimetry (DSC)

DSC analysis of the biocomposite films and of the pure LDPE was carried to determine their melting (T_m) and crystallization (T_c) temperatures and to investigate the presence of any possible thermal phase transitions. As evident from the Figure 9, the addition of the curcumin in the biocomposite does not cause any change to the melting or crystallization peaks (T_m and T_c are 113 °C and 92 °C

respectively, (complete details of DSC results are shown in Table 1)) and therefore causes minimal changes to the thermal properties of the polymer matrix indicating that the polymer chain mobility is preserved. Therefore, the Cur/LDPE composite films can be easily processed thermally, without changing the melt processing methods that are already well established and adopted in industrial scale for the LDPE polymers. This is also observed in another LDPE composite system (LDPE with 5%wt. of carvacrol), where the presence of the natural antioxidant did not have a significant effect on the melting and crystallization behavior of the LDPE films (T_m and T_c both are slightly modified from 113 °C to 110 °C and 95 °C to 98 °C respectively) [22].

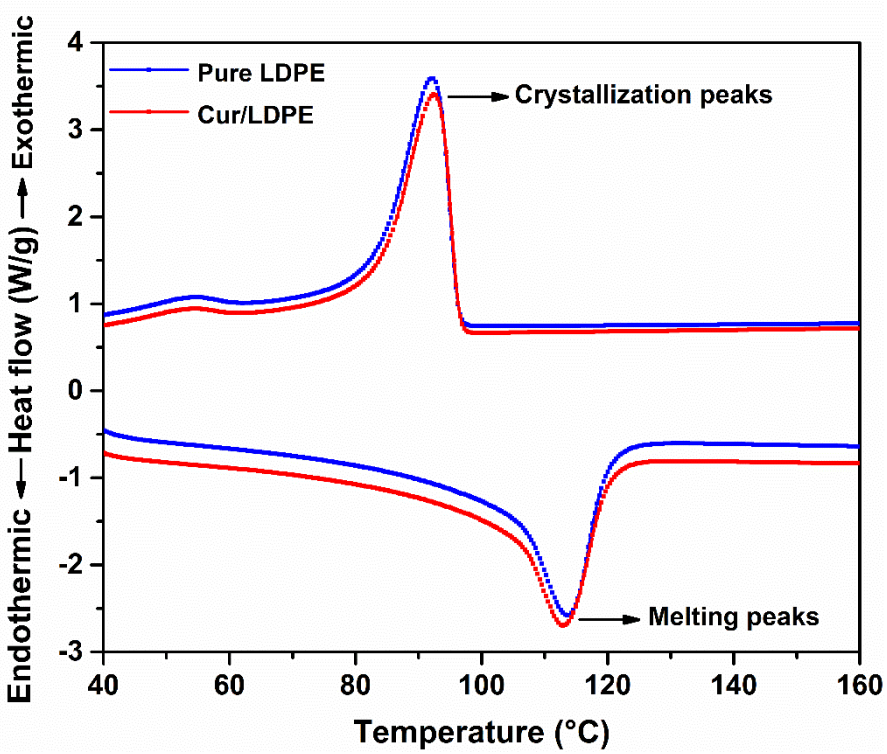

Figure 9. Normalized DSC thermograms, second heating cycle and first cooling cycle for pure LDPE and 5% Cur/LDPE films.

2.3.4 Thermo-gravimetric analysis (TGA)

The thermal stability of the pure curcumin, pure LDPE and Cur/LDPE films were evaluated by TGA analysis under the air atmosphere (Figure 10). As evident in the thermogram, the decomposition of curcumin takes place in two different steps [127]. After the evaporation of the adsorbed humidity at lower temperatures, the first degradation step takes place between 201 °C and 337 °C with a maximum rate of weight loss (T_{max}) at 290°C caused due to the decomposition of the substituent groups of curcumin [128]. The second degradation step occurs in between 337 °C and 587 °C with a T_{max} at 535°C attributed to the decomposition of the two benzene rings [128]. The degradation of pure LDPE occurs just in one step at the temperature range from 237 °C to 461 °C (T_{max}: 373°C) due to the random polymer chain scission and branching [129].

In the case of Cur/LDPE composite, thermal degradation takes place in two defined steps. The first one occurs at a very slow rate, between 224 °C and 387 °C (T_{max}: 345°C) with a weight loss of 4.3%, while the second degradation step takes place in between 387 °C and 459 °C with a rapid degradation rate and a T_{max} of 390°C. Compared to the pure LDPE, the Cur/LDPE composite films present higher thermal stability with a degradation temperature shifted by 17 °C (from 373°C to 390°C), attributed to the presence of curcumin, which is able to capture/hold the generated free radicals of the polymer during the thermal oxidation, decelerating the degradation process [75], [77].

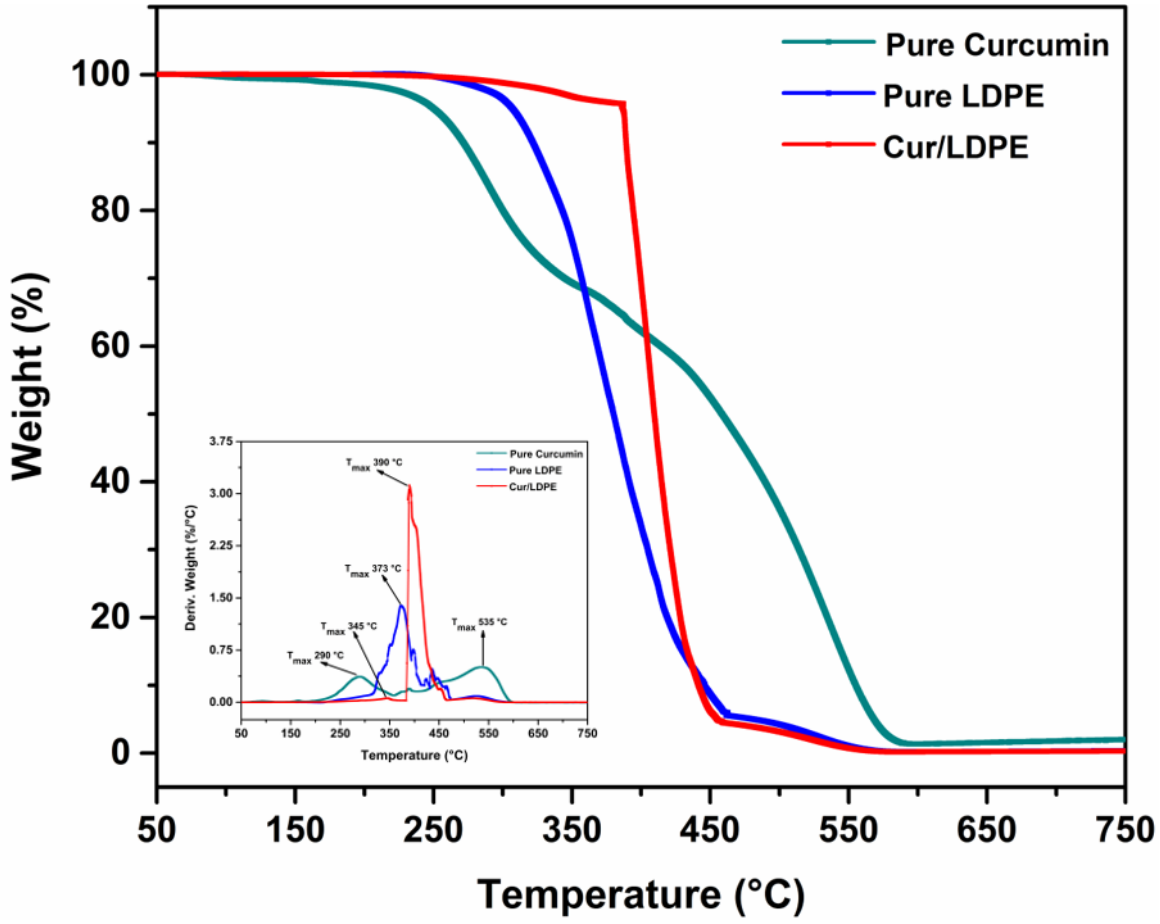

Figure 10. TGA curves of curcumin, pure LDPE and 5% Cur/LDPE films. The inset shows DTGA curves for the three samples.

Table 1**.** DSC and TGA parameters for pure curcumin powder, pure LDPE and 5% Cur/LDPE films

Sample type	**T_c (°C)**	**T_m (°C)**	**T_i (°C)**	**$T_{5\%}$ (°C)**	**$T_{10\%}$ (°C)**	**$T_{50\%}$ (°C)**	**$T_{90\%}$ (°C)**	**T_{max} (°C)**
Pure curcumin	N/A	N/A	201	250	271	458	555	290, 535
Pure LDPE	92	113.36	237	307	322	380	446	373

5% Cur/LDPE	92.37	112.89	224	387	389	409	442	345, 390

T_i = Initial degradation temperature

$T_{5\%}$ = Temperature at 5% degradation

$T_{10\%}$ = Temperature at 10% degradation

$T_{50\%}$ = Temperature at 50% degradation

$T_{90\%}$ = Temperature at 90% degradation

T_{max} = Temperature at maximum degradation

2.3.5 Interaction of the films with water

LDPE is extensively used in food packaging also because of its favorable water vapor barrier properties. Food packaging films with improved water vapor barrier properties contribute significantly to the enhancement of the shelf life of the food products, by preventing the migration of the water molecules in or out through the walls of the package [13], [101]. The water vapor permeability of the packaging films depends on the film's morphology, chemical structure and environmental temperature [12]. The water vapor transmission rate (WVTR) and water vapor permeability (WVP) of the pure LDPE and Cur/LDPE films are shown in Figure 11 and Table 2. It should be mentioned that the WVP of the developed pure LDPE films is significantly higher compared to the WVP of the commercial LDPE films (1.07×10^{-17} g.m/m^2.d.Pa) found in literature possibly due to the different polymer chain length and less volume of voids (free volume) [130]. Nonetheless, as shown in Figure 11, WVTR and WVP decrease significantly with the increase in the curcumin content in the polymer and is 73% and 51.5% lower for the 7% and 5% Cur/LDPE films respectively compared to pure LDPE film indicating significant improvement in the water vapor barrier performance in the presence of curcumin. This can be attributed to the hydrophobic nature of the curcumin filler which is uniformly distributed in the polymer matrix and act as a physical barrier in the path of the water vapors [131]. In fact, as shown in Figure 12 the water contact angle (WCA) of the 5% Cur/LDPE film is 10° higher (110.8° ± 1.6°) compared to the pure LDPE (101.2° ± 1.1°) resulting in the enhancement of the hydrophobicity of the composite films that in turn significantly improves the water vapor barrier performance.

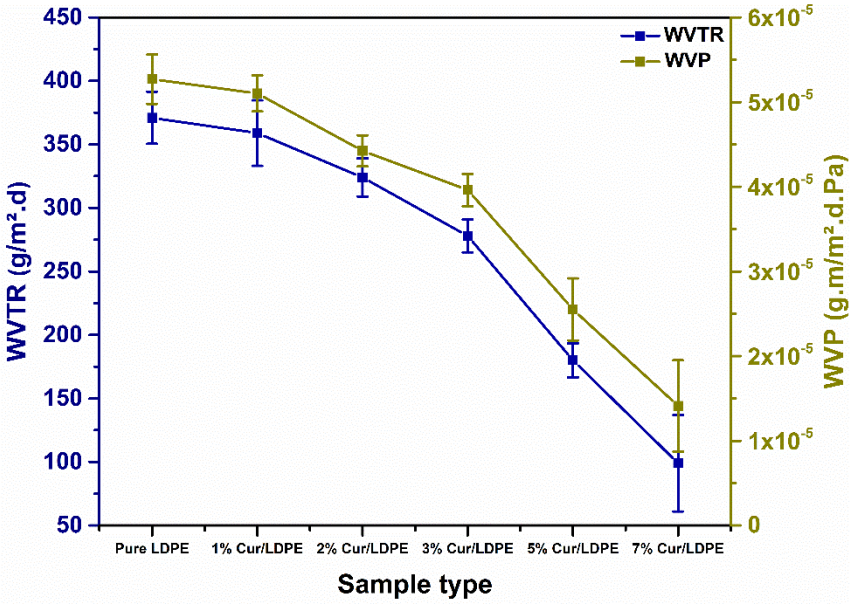

Figure 11. Water vapor transmission rate (WVTR) and water vapor permeability (WVP) for pure LDPE and Cur/LDPE films.

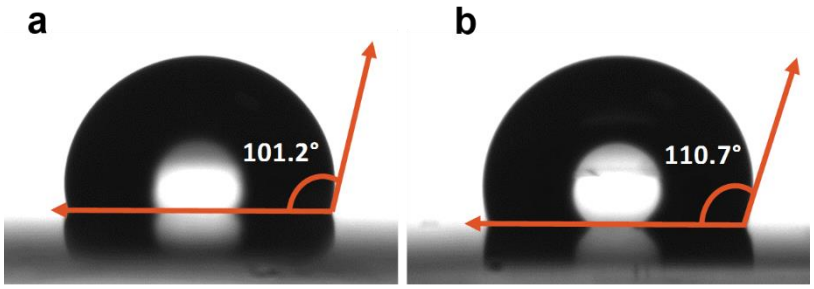

Figure 12. WCA of (a) pure LDPE and (b) 5% Cur/LDPE film.

Table 2. Water vapor barrier properties parameters. Mean values are reported with standard deviation in the same column. Mean ± standard deviation

Sample type	WVTR ($g/m^2.d$)	WVP ($g.m/m^2.d.Pa$)
Pure LDPE	371.18 ± 20.54	$5.26\times10^{-5} \pm 2.91\times10^{-6}$
1% Cur/LDPE	359.08 ± 25.79	$5.10\times10^{-5} \pm 2.14\times10^{-6}$
2% Cur/LDPE	324.34 ± 15.07	$4.42\times10^{-5} \pm 1.83\times10^{-6}$
3% Cur/LDPE	278.51 ± 12.89	$3.96\times10^{-5} \pm 1.89\times10^{-6}$
5% Cur/LDPE	180.29 ± 13.36	$2.55\times10^{-5} \pm 3.66\times10^{-6}$

7% Cur/LDPE	099.29 ± 38.79	$1.41\times10^{-5} \pm 5.39\times10^{-6}$

2.3.6 Oxygen permeability

The oxygen permeability is another important property of the food packaging materials that affect the quality and shelf life of the packaged food products [132]. The effect of the presence of curcumin on the oxygen transmission rate (OTR) and oxygen permeability (OP) of the LDPE films are presented in Figure 13 and Table 3. As shown, both parameters are slightly increased (c.a. 13.9% and 15.4% for 5% Cur/LDPE and 7% Cur/LDPE films respectively) indicating that there is a minimum contribution of the curcumin to the oxygen barrier performance of the composite films. This slight increase in the OTR and OP for Cur/LDPE films may be attributed to the polarity of the composite system, which is mostly determined by the low polar curcumin filler [53]. Its long carbon chain and benzene rings may cause the reduction of the polarity of the films making them slightly poorer barriers to non-polar substances, such as oxygen [53]. Additionally, the slight increase of the OP of the Cur/LDPE films might be attributed to the structural modification of the LDPE matrix due to the curcumin additive that reduces the resistance of the films to oxygen diffusion through them [14].

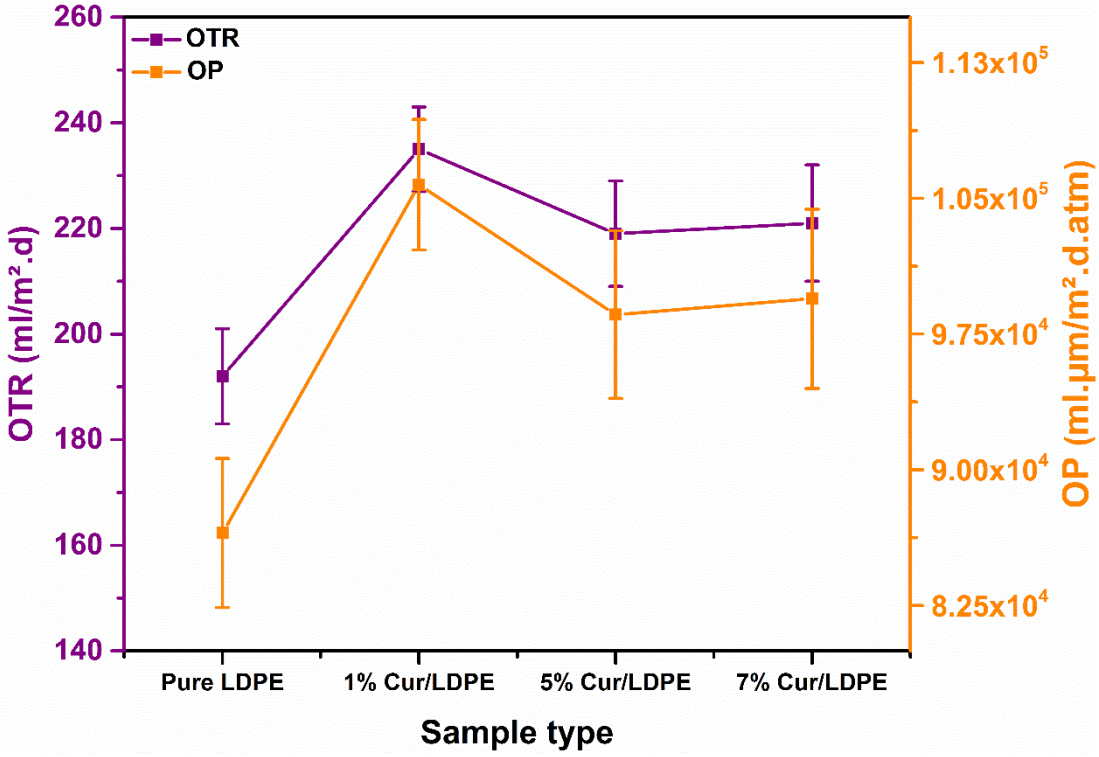

Figure 13. Oxygen transmission rate (OTR) and oxygen permeability (OP) for pure LDPE and Cur/LDPE films.

Table 3. Oxygen barrier properties parameters. Mean values are reported with standard deviation in the same column. Mean ± standard deviation.

Sample type	OTR ($ml/m^2.d$)	OP ($ml.\mu m/m^2.d.atm$)
Pure LDPE	192.25 ± 9.14	086511 ± 4116
1% Cur/LDPE	235.19 ± 8.74	105750 ± 3600
2% Cur/LDPE	NA	NA
3% Cur/LDPE	NA	NA
5% Cur/LDPE	219.06 ± 10.28	098576 ± 4630
7% Cur/LDPE	221.89 ± 11.26	099450 ± 4950

2.3.7 Mechanical properties

The effect of curcumin on the mechanical properties of the LDPE is presented in Figure 14 and Table 4. It is clear that the presence of the curcumin in the LDPE polymer causes the significant improvement of the tensile modulus, and the decrease of the elongation at break, reaching 47% and 68% respectively for the 7% Cur/LDPE film. Concerning the 5% Cur/LDPE films, the tensile modulus is 34% higher compared to the pure LDPE (361 ± 9 MPa and 269 ± 8 MPa respectively) while the elongation at break is 57% lower (75% ± 9% compared to the 175% ± 13% of the pure LDPE film). The increase in the tensile modulus with an increase in the curcumin content is attributed to the presence of the uniformly dispersed curcumin filler in the polymer matrix which, as also proved by the FTIR analysis previously presented, induces the bulk contraction by causing the increase of the van der Waals forces between the polymer chains and therefore, significantly reinforcing the material. The decrease in the elongation at break is caused by the increase in the stiffness and close packing of the polymeric chains of the composites that prevent the polymer to polymer chain slippage after the addition of the curcumin [133].

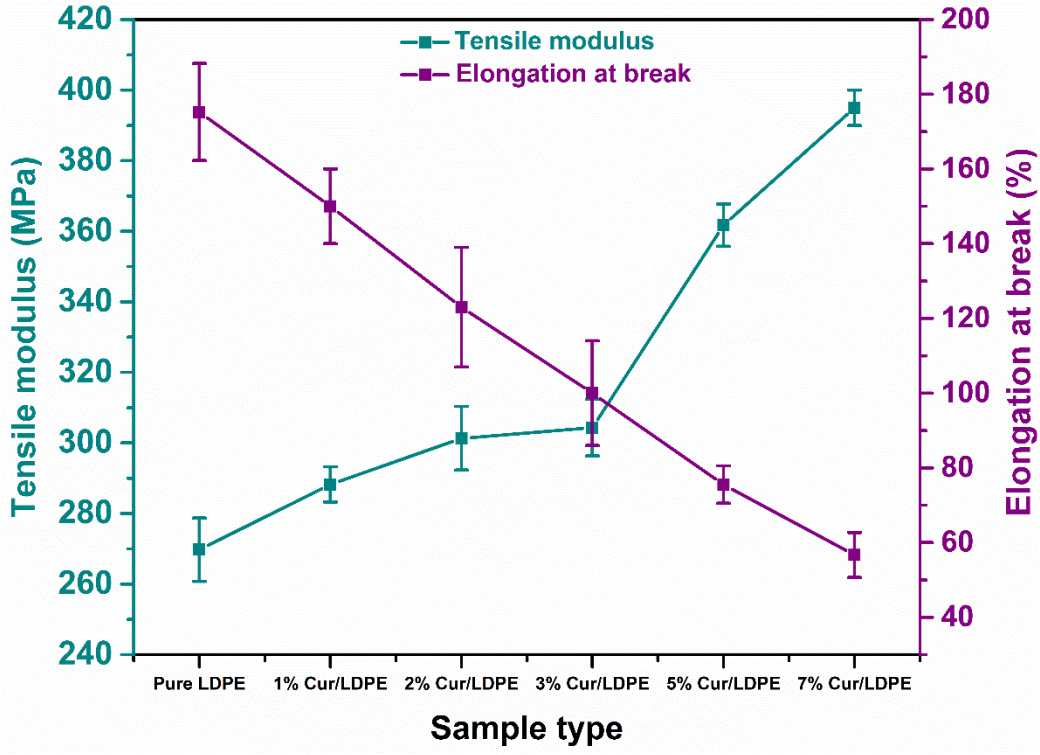

Figure 14**.** Tensile modulus and elongation at break for pure LDPE and Cur/LDPE films.

Table 4**.** Tensile modulus and elongation at break values for pure LDPE and Cur/LDPE films. Mean values are reported with standard deviation in the same column. Mean ± standard deviation

Sample type	Tensile modulus (MPa)	Elongation at break (%)
Pure LDPE	269 ± 08	175 ± 13
1% Cur/LDPE	288 ± 05	150 ± 10
2% Cur/LDPE	301 ± 09	123 ± 14
3% Cur/LDPE	304 ± 08	100 ± 16
5% Cur/LDPE	361 ± 09	075 ± 09
7% Cur/LDPE	395 ± 05	056 ± 06

2.3.8 Release kinetics

The release kinetics of the curcumin from the Cur/LDPE films in ethanol was studied by UV-vis absorption spectroscopy. It is clear from the Figure 15a that the intensity of the absorbance peak at 428 nm (characteristic of curcumin) increases with the increase in the curcumin content in the Cur/LDPE films and over contact time of each of the composite films with the solvent, due to the increase in the amount of released curcumin. During the first six hours, high release rate is observed for all Cur/LDPE films (2.518 µg/ml for 5% Cur/LDPE Figure 15b), possibly due to the release of the curcumin on the surface of the films, while afterwards there is a slow down, until a plateau is

reached after 24 hours (3.392 µg/ml for 5% Cur/LDPE). The continuous and controlled release of the curcumin from the films with time, will help to inhibit the oxidation of the food products by maintaining the critical concentration of the antioxidant at the surface that is essential for preventing the oxidative change with the passage of time [81], [134].

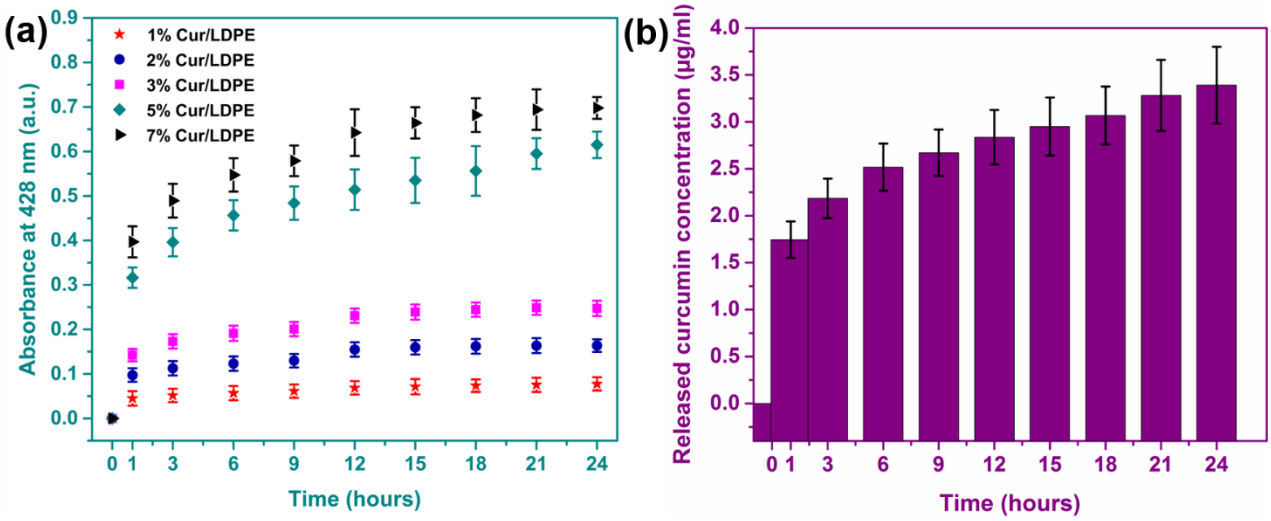

Figure 15. Release kinetics of Cur/LDPE films (a) absorbance profile and (b) released curcumin concentration for 5% Cur/LDPE as calculated by equation 4.

2.3.9 Antioxidant activity

In the active food packaging materials, it is necessary to use polymeric films with high antioxidant activity because this can significantly decrease the lipid oxidation and subsequently improve the quality and shelf life of the food products [13], [24], [116]. The DPPH• standard assay was used to determine the antioxidant activity of the Cur/LDPE films [13], [80], [101] as a representative method to determine the antioxidant activity towards lipid oxidation [101].

The antioxidant activity of the Cur/LDPE films was evaluated by monitoring the decrease in the absorbance peak of the DPPH• at 517 nm when in contact with the curcumin extract released by the composite films [135]. As evident in Figure 16, the antioxidant activity of Cur/LDPE films increases with the increase in the curcumin content in the composite films and time (7% Cur/LDPE: 27.8% to 55.2% for an observed time period of 1-24 hour) due to the higher amount of curcumin released in the solution.

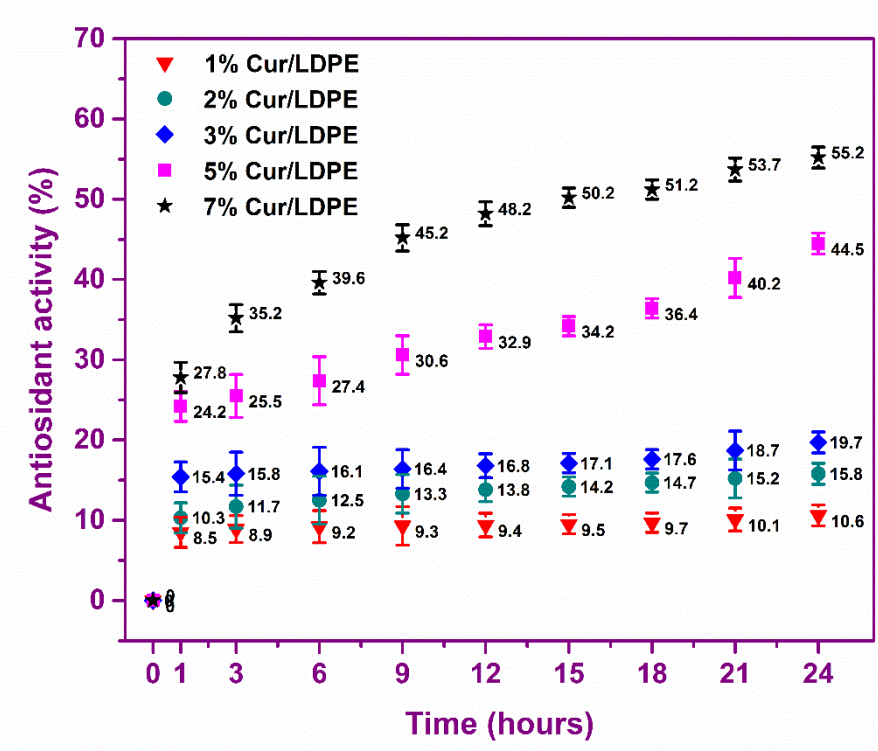

Figure 16. DPPH• free radical scavenging activity for Cur/LDPE films.

Consequently, the higher amount of released curcumin in the solution ensures the higher stabilization of more and more DPPH• free radicals, through the formation of DPPH-H compounds (Figure 17), as also observed optically by the solution color change from violet to yellow[12], [18], [135]. These results show that the Cur/LDPE films possess excellent antioxidant properties (5% Cur/LDPE: 44.5% after 24 hours at a minor release of 3.392 μg/ml of curcumin) due to the free radical scavenging activity of the curcumin molecules through hydrogen donation [135]. The antioxidant potential of the developed Cur/LDPE films is in accordance with the curcumin based polymer packaging systems reported in the literature [79].

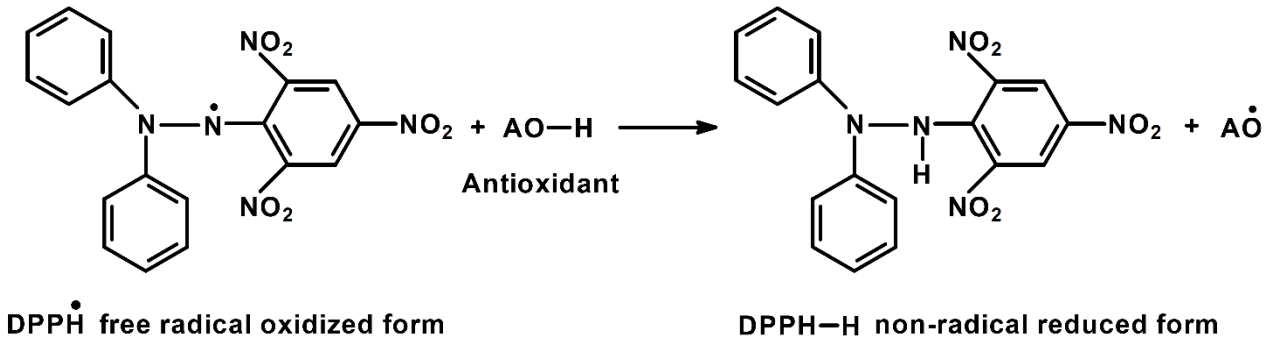

Figure 17. Mechanism of DPPH• free radical scavenging.

The results of this study prove that the higher the amount of curcumin in the LDPE matrix the better the antioxidant activity and the water vapor barrier performance of the composite films are. However,

the 7%wt. Cur/LDPE films present a poor elongation at break making difficult their application in food packaging. Thus, we conclude that the 5%wt. Cur/LDPE film possesses overall better properties and their slow scavenging process can be helpful in applications where the prolonged and sustained antioxidant effect is required such as in active food packaging.

2.4 Conclusion

The results of the present study suggest that the addition of curcumin in LDPE following industrially applied methods such as extrusion and compression molding results in the formation of uniform active packaging films. The presence of curcumin makes the composites more stable against the thermal degradation without altering their melting point and therefore their thermal processability. Furthermore, the presence of curcumin makes the LDPE much stronger. The incorporation of curcumin in the polymer significantly improves the water vapor barrier performance, and, as a result, active films prohibit the penetration of water molecules through them. The active films show the continuous and steady release of the active species to the surrounding environment with excellent antioxidant activity against the lipid oxidation. The LDPE is an extensively used polymer in food packaging, but it never has been functionalized with curcumin before for active food packaging applications. The use of LDPE will continue to grow due to its excellent properties e.g. low cost, easy processability and recyclability, but more recently the development of bio based LDPE by using renewable resources, the present biocomposites developed following a widely applied industrial method that makes the material feasible for using it in active food packaging.

Chapter 3: Multifunctional porous pH natural indicators for intelligent food packaging

Abstract

The aim of this study is to develop highly porous biocompatible colorimetric indicators for intelligent food packaging applications, able to rapidly respond to a wide range of pH changes caused by the food spoilage, and to be reused. This is succeeded by the combination of polyvinyl alcohol, polyvinylpyrrolidone and microcrystalline cellulose functionalized with red cabbage anthocyanins. The effect of the microcrystalline cellulose on the surface and cross-sectional morphologies, porosity, and pore size of the indicators was analyzed by scanning electron microscopy (SEM), Brunauer–Emmett–Teller (BET) analysis and mercury intrusion porosimetry (MIP). The fourier transform infrared spectroscopy (FTIR) and thermo-gravimetric analysis (TGA) was used to observe the possible chemical and thermal phase transitions induced to the polymer matrix after the addition of microcrystalline cellulose and red cabbage anthocyanins. The UV-Visible spectroscopy and CIELab analysis were used to observe the optical color changes of the anthocyanin solutions and colorimetric indicators when subjected to environments of different pH. Following the abovementioned characterization methods it can be concluded that the addition of microcrystalline cellulose at a defined weight percentage decreases the pore size, and increases the porosity and pore interconnectivity of the foams that in turn improve the responsiveness towards the acidic or basic environment. The indicator foams showed distinct color changes over a broad pH range (1-14) as proved by colorimetric analysis. The color changes are reversible, making possible the use of the developed porous indicators for several times. The colorimetric foams indicate efficiently the spoilage of chicken and prawns proving that they can be used for real time monitoring the food freshness in intelligent packaging applications.

3.1 Introduction

Meat and seafood products are highly perishable due to microbial and enzymatic reactions [36], [136], [137]. Microorganisms can degrade protein and fat present in these products, resulting in the formation of gases such as carbon dioxide (CO_2), hydrogen sulfide (H_2S) and ammonia (NH_3) [67]. Furthermore, the bacterial enzymatic reaction leads to the reduction of trimethylamine oxide (TMAO) that results in ammonium based compounds e.g. ammonia (NH_3), dimethylamine (DMA) and trimethylamine (TMA) mostly known as total volatile basic nitrogen (TVB-N) [30], [57], [138]. The determination of the presence of the TVB-N has been widely used as an important indicator of the meat and seafood freshness [30], [66], [67], [136].

To this aim, colorimetric indicators for real time monitoring the freshness of the food products have been developed, as they offer numerous advantages such as small size, sensitivity, safety, low cost, while they provide direct information just by optical/visual color changes [30]–[37]. In fact, their counterparts e.g. biological and chromatographic assays, although they provide precise results, require advanced instruments and highly skilled operators, and the detection of the biogenic gasses is generally time consuming, and expensive. These methods are not suitable for the real time monitoring [30], [34].

In general, for the sensing of biogenic gasses pH colorimetric indicators are used. To do so, materials containing dyes sensitive to pH changes have been developed and their majority is of synthetic nature. In particular, methyl yellow, methyl red, bromophenol blue, bromothymol blue, chlorophenol red, cresol red, bromocresol green, neutral red, chlorophenol red, phenol red, bromocresol purple, and hexamethoxy red, have been used for the sensing of the presence of CO_2, ammonia, biogenic amines/TVB-N and other byproducts of bacterial and enzymatic reactions [31], [139], [140]. For example, Geltmeyer et al. [35] developed colorimetric indicators by the combination of silicon oxide membranes, methyl yellow and methyl red that are capable of sensing NH_3 vapors, biogenic amines and pH changes in aqueous solutions. Rukchon et al. [67] developed pH indicators for food packaging applications by the combination of cellulose based coating with bromothymol blue, methyl red, bromocresol green and phenol red. Although the developed materials present distinct color changes in different environments, the use of such synthetic colorimetric pH dyes in food applications are not considered safe due to their possible toxicity and health hazards [31].

For this reason, recently, the research has been focused on the utilization of pH-sensitive dyes extracted from natural resources such as alizarin, curcumin and anthocyanins extracted from red cabbage, blueberry, mulberry, black rice, grape skin, black carrot and purple sweet potato because they are expected to be biocompatible, environment friendly, making possible their use in food based applications [35], [37], [54], [57], [65], [67], [137], [139]–[145]. However, replacing synthetic dyes with natural colorants is challenging, mainly due to the dependence and stability of the color change to different environmental factors e.g. humidity, light, oxidation, temperature and pH [145].

Anthocyanins (Figure 18) are natural occurring water soluble and non-toxic pigments that are responsible for the red, purple and blue color of many plants [37], [146]. Among natural colorants, anthocyanins from red cabbage possess preferable properties such as stability upon the chemical structure, good water solubility, broad color spectrum at an extended pH range, stability against photodegradation and excellent color stability at high temperatures [31], [145]. The stability of the chemical structure of the red cabbage anthocyanins is attributed to the acyl protection of the hydroxyl groups [145]. Acylated anthocyanins are generally less prone to color fading compared to non-

acylated analogs [145]. For these reasons, anthocyanins deriving from red cabbage are widely studied for the development of food indicators. For example, Pereira et al. [60] fabricated chitosan/polyvinyl alcohol films with red cabbage anthocyanins for intelligent food packaging applications. Prietto el al. [142] developed pH-sensitive films from corn, starch and anthocyanins extracted from the black bean seed coat and red cabbage that are capable of sensing pH changes in aqueous solutions and intelligent food packaging applications. Liang et al. [147] developed intelligent biocomposite films by Artemisia sphaerocephala Krasch. gum/ carboxymethyl cellulose sodium and red cabbage anthocyanins for intelligent packaging and gas sensing (NH_3) applications. However, these studies did not address the response kinetics (sensitivity) and reversibility of the pH sensing films that are also important parameters in order to find out the responsiveness/effectiveness and reusability of the intelligent films. Additionally, most of the work that has been performed so far is based on the development of pH indicator films. Due to the highly compact structure of the films, their responsiveness against different media apart from liquids, e.g. gases and vapors, significantly important for the food-based indicators, is questionable and not addressed adequately.

The aim of this research is to give answers to some of the gaps referred above. In particular, the scope is to develop biocompatible colorimetric indicators that can rapidly respond to acidic and basic vapors and gasses, and that can show reversibility and reusability. Specifically, herein we develop highly porous colorimetric indicator foams, based on polyvinyl alcohol, polyvinylpyrrolidone and microcrystalline cellulose functionalized with red cabbage anthocyanins. The indicator foams are fabricated through the freeze drying method and the effect of microcrystalline cellulose on the porosity, responsiveness and sensitivity of the pH indicators is studied. The developed indicator foams are then subjected to different pH solutions ranging from 1-14, to hydrochloric acid and to ammonia vapors in order to evaluate the usability of the indicator foams for multiple applications. In the end, indicator foams were exposed to meat and seafood products to check the versatility of the indicators towards biogenic amines or TVB-N. The results of the present study reveal that the developed indicator foams can be used for the sensing of acidic and basic vapors for different applications e.g. intelligent food packaging, industrial plants and environmental protection.

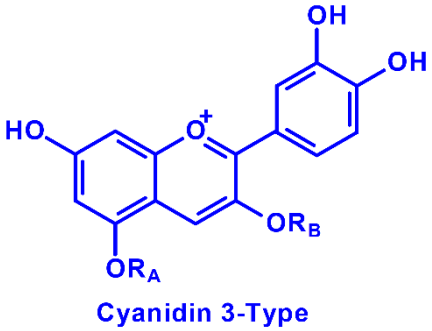

Figure 18. The basic structure of RCA.

3.2 Materials and methods

3.2.1 Materials

Polyvinyl alcohol (PVA) with Mw 89 000–98 000 and 99% hydrolyzed, polyvinylpyrrolidone (PVP) with Mw 40 000, microcrystalline cellulose (MCC) powder (51 μm particle mean size), ethanol with 96% purity, sodium hydroxide (NaOH) with 98% purity, hydrochloric acid (HCl) with 37% (w/w) concentration and ammonium hydroxide (NH_4OH) solution with 30% purity were purchased from Sigma Aldrich and were used without further purification. Fresh red cabbage and sugar crystal were purchased from a local supermarket. Ultrapure MilliQ water was used in all the experiments presented.

3.2.2 Extraction of anthocyanins from red cabbage

Anthocyanins were extracted from red cabbage according to Pereira et al. [60] method with slight modifications. First 150 g sample of red cabbage was chopped and dipped in 80 ml ethanol/water solution (7:3). After that pH of the mixture was adjusted to 2 with the appropriate amount of 1M HCl solution. The mixture was stored in the fridge at 5 °C for 24 hours. Then, the mixture was filtered and the extracted solution was centrifuged at 2000 rpm for 10 minutes. Subsequently, the supernatant was filtered on Whatman filter paper #1 with a pore diameter of 11μm. After that, the pH of the resulted red cabbage anthocyanins (RCAs) solution was adjusted to 6 with the appropriate amount of 2.5 M NaOH solution.

3.2.3 Fabrication of the foams

First of all 1g PVA and 0.2g PVP was dissolved in 10 ml of water with the assistance of microwave oven (Panasonic NN-K101WM) at a power of 360 W. After the solution was poured on a petri dish and manually mixed with 20g of sugar crystals and 0, 0.5, 1, 2 and 3 g of MCC powder. Then the mixture was placed in the freezer for 8 hours and subsequently placed under the fume hood at ambient temperature for 8 hours to promote the cross linking between the PVA and PVP matrix [148], [149]. The resulting gel was washed three times with the MilliQ water at 50 °C for 6 hours to remove the

sugar traces and cutted with the help of dye cutting press to make small circular shaped samples. The circular shaped samples were freezed inside the freeze dryer (CHRIST Epsilon 2-4 LSCplus Germany) at a temperature of -20°C and an atmospheric pressure of 1 bar, followed by drying at 10 °C under vacuum pressure (1.14 mbar). The foams without RCAs were named as F_0, $F_{0.5}$, F_1, F_2 and F_3 respectively according to the amount of cellulose in each foam. Subsequently, the 2g foams were immersed in 25 ml of anthocyanin solution for 24 hours then again subjected to freeze drying in order to acquire anthocyanin treated foams. After the addition of the RCAs, foams were named as F_{0R}, $F_{0.5R}$, F_{1R}, F_{2R} and F_{3R}.

3.2.4 Scanning electron microscopy (SEM)

The surface and cross-sectional (cryo-fractured) morphologies of the foams were studied by scanning electron microscopy (SEM, JEOL JSM-6490AL). For that purpose first specimens were attached to the metallic stubs with carbon tape then coated with 10 nm thin gold layer using a high-resolution sputter coater Cressington 208HR (Cressington Scientific Instrument Ltd., UK).

3.2.5 Water absorption capacity and amount of RCA retained by the foams

First, dried foams were immersed in the 10 ml distilled water for 24 hours. After that, the foams were removed from the water and placed on a wet tissue paper to remove the free water on the surface of the foams. Then, the wet weight of the samples was noted. The water absorption capacity was calculated according to the Equation 6 and values of eight different samples are reported as average along with their standard deviation.

$$\text{Water absorption capacity (\%)} = \frac{\text{wet weight} - \text{dry weight}}{\text{dry weight}} \times 100 \qquad \text{Equation 6}$$

The amount of the RCA retained by the foams was determined by measuring the dry weight of the foams before and after 24 hours immersion to RCA solution. The wt% amount of RCA in the treated foams was noted with respect to the final weight of the composite foams and average values of eight different samples are reported along with their standard deviation.

$$\text{wt\% of RCA} = \frac{\text{final weight} - \text{initial weight}}{\text{final weight}} \times 100 \qquad \text{Equation 7}$$

3.2.6 Brunauer–Emmett–Teller (BET) analysis

BET and Barrette Joynere Halenda (BJH) analyses were used to characterize the specific surface area and pore size distribution of the foams. For that purpose, first, the samples were degassed at 90 °C under vacuum for 3 hours to remove the weakly adsorbed water molecules. After that nitrogen physiosorption measurements were carried out by using a gas sorption analyzer Autosorb-iQ (Quantachrome Instruments) at a temperature of 77 K. The multipoint BET model was used to

measure the specific surface areas of the samples by considering 20 equally spaced points in the P/P_0 range from 0.05 to 0.3. Where P/P_0 (relative pressure) is the pressure of the adsorbate (P) divided by its saturation pressure (P_0). The pore size distribution was evaluated from the desorption isotherms with the help of the BJH model, taking into account 13 points.

3.2.7 Skeletal density and mercury intrusion porosimetry (MIP)

The skeletal density of the foams was evaluated by helium pycnometry (Pycnomatic Evo, Thermo Fisher Scientific) equipped with a 4 cm^3 chamber, at 20 °C. The skeletal volume of the sample (volume of the sample without considering open pores) was measured by monitoring the change in pressure due to the volume of helium that is displaced by the sample inside the sealed and pressure-equilibrated chamber. The skeletal density is obtained by dividing the sample mass by the skeletal volume assuming that all the open pores of the sample are accessible by the helium atoms. Average values of ten measurements of the same sample are reported along with their standard deviation (Table 5).

Table 5. Skeletal density values of the foams. Mean values are reported together with the standard deviation. Mean ± standard deviation.

Sample	Skeletal density (g/cm^3)
F_{0R}	1.328 ± 0.003
$F_{0.5R}$	1.339 ± 0.003
F_{1R}	1.371 ± 0.002
F_{2R}	1.470 ± 0.002
F_{3R}	1.496 ± 0.004

The pore size distribution of the macropores of the foams and their porosity were defined using the mercury intrusion porosimetry (MIP) (Thermo Fisher Scientific). To evaluate the pore size distribution of the foams, measurements were performed using both, low-pressure (Pascal 140 Evo) and high-pressure (Pascal 240 Evo) modules with a standard dilatometer. During the measurements, using the low-pressure module (Pascal 140 Evo), the mercury intrusion starts from vacuum pressure and the pressure was continuously increasing up to 400 kPa, with a rate of 6 kPa min^{-1}. In the case of the high-pressure module (Pascal 240 Evo), the mercury intrusion starts from atmospheric pressure and continuously increased up to 200 MPa, with a rate of 6 kPa min^{-1}. In both cases, the mercury contact angle and the surface tension of pure mercury were assumed to be 140° and 0.48 Nm^{-1} respectively, while the Washburn equation is used to calculate the pore size from the applied pressure, assuming that the pores are of cylindrical shape. After the experiments, data from both modules, low-pressure (Pascal 140 Evo) and high-pressure (Pascal 240 Evo) were combined together in order to

determine the porosity and pore size distribution of the foams in the range of (0.1 µm - 100 µm). The porosity of the foams was evaluated by the SOL.I.D Evo software and for this, the skeletal density values, previously measured, are considered. In this way, the closed pores (or sample compressed effects) that have no access to external fluid and can contribute to the final porosity data are not included. In order to explore the pore size greater than 100 µm, experiments were performed with an ultramacropore kit (dilatometer) in the low-pressure module (Pascal 140 Evo) by maintaining the same experimental conditions as above-mentioned.

3.2.8 Fourier transform infrared spectroscopy (FTIR)

Fourier Transform Infrared Spectroscopy (FTIR) analysis was used to study the possible chemical interactions between the different polymers before and after RCA inclusion. Infrared spectra were acquired with an FTIR spectrometer (Vertex 70v FT-IR, Bruker) coupled with the diamond crystal. All spectra were recorded in the range from 3800 to 600 cm^{-1} with a resolution of 4 cm^{-1}, accumulating 128 scans.

3.2.9 Thermo-gravimetric analysis (TGA)

Thermal stability of the developed foams before and after RCA treatment, pure polymers and pure RCA powder, was evaluated by thermo-gravimetric analysis using a TGA Q500 system (TA Instruments USA). The measurements were performed on 5 mg samples weighed in aluminum pans and heated from 30 °C to 800 °C with a heating rate of 10 °C/min under the air of a constant flow rate of 50 ml/min.

3.2.10 Response of the foams upon exposure to vapors

UV-Vis spectroscopy was used to see the color changes of the pure RCA (baseline correction: Ultrapure MilliQ water) and of the indicator foams against different pH solutions and vapors. Absorption spectra of the foams before exposure is considered as baseline correction.

To do so, the indicator foams with thickness (3.0 mm ± 0.2 mm, diameter:14 mm) were dipped for 3 minutes in different pH solutions (range 1-14), prepared by adding the appropriate amounts of 0.1 M HCl or 0.1 M NaOH solutions. The indicator foams were dried completely before acquiring their UV-Vis absorption spectra. The response kinetics of the indicator foams to acidic or basic vapors were evaluated by subjecting the foams (thickness: 1.00 mm ± 0.05 mm, diameter:14 mm) to HCl and NH_3 vapors for 120 seconds, generated in a closed petri dish with dimensions 100 mm × 20 mm diameter (D) x height (H) respectively, by adding HCl or NH_4OH solution drops (100 µl and 50 µl respectively) and the UV-Vis spectra were recorded after every 10 seconds.

The adsorption kinetics study of the indicator foams in presence of the HCl vapors was performed by applying the pseudo second-order (Equation 8) kinetics model on the graphs presenting the variation of the maximum absorption intensity of the foams at 524 nm during time.

$$I_t = \frac{k I_e t}{1 + k I_e t} \qquad \text{Equation 8}$$

Where I_t (au) is the absorption intensity in time (t), I_e (au) is the absorption intensity at equilibrium and k (au s^{-1}) is the rate constant.

3.2.11 Response of the indicator foams against chicken and seafood

The response of the indicator foams against fresh prawns and chicken was investigated to demonstrate their potential use in intelligent food packaging. First the indicator foams were mounted on the inner side of the lid of the petri dish with size (petri dish 100 mm × 20 mm) and subjected to 30g and 40g of fresh prawns and chicken respectively. The color variations of the indicator foams were monitored for three days.

3.2.12 Color analysis of indicator foams

The CIELab color space analysis has been done in collaboration with Matteo Bustreo currently working as a senior technician in the department of "Pattern Analysis and Computer Vision", Istituto Italiano di Tecnologia, Genova, Italy.

Porous indicators' color evolution has been recorded using a reflex camera (Canon EOS 5D Mark II). One frame per second of the videos was analyzed and converting the acquired images to CIELab color coordinates. CIELab color space has been designed for producing a color representation that mimic the human color perception [150] and it consists of three components related to the brightness of the color (L) and its hue (a and b). During color conversion, CIE standard illuminant D65 as reference white point (theoretically corresponding to a color temperature of 6504 K) was used. The Euclidian distance (dE) of the CIELab sample coordinates, obtained from different videos or photos provide a quantitative measure to the human perceived color difference and it can be calculated from the following equation [151]:

$$dE = \sqrt{[(L_1 - L_2)^2 + (a_1 - a_2)^2 + (b_1 - b_2)^2]} \qquad \text{Equation 9}$$

When dE > 3.5, the color difference is clearly perceivable by experienced and unexperienced observers [151].

The indicator foams with (thickness: 1.00 mm ± 0.05 mm, diameter:14 mm) were exposed to HCl and NH_3 vapors for 5 and 12 minutes respectively, generated in a closed petri dish (dimensions: 60 mm × 15 mm, DxH respectively) with the appropriate amounts of HCl and NH_4OH solution drops

(100 µl and 50 µl respectively). Porous pH indicators' color evolution has been recorded using a reflex camera (Canon EOS 5D Mark II). In the case of video, one frame per second was analyzed converting the acquired images to CIELab color coordinates.

For the kinetics study, the CIELab color analysis was performed on foams exposed under the same conditions as the ones used for the kinetics study through UV-Vis spectroscopy previously described. In particular, photographs of the indicator foams (thickness: 1.00 mm ± 0.05 mm, diameter: 14 mm) were acquired after every 10 seconds of exposure to acidic or basic vapors. The foams were exposed to HCl and NH_3 vapors for a total time of 120 seconds, generated in a closed petri dish (dimensions: 100 mm × 20 mm, DxH respectively) with the appropriate amounts of HCl and NH_4OH solution drops (100 µl and 50 µl respectively).

3.3 Results and discussion

3.3.1 Scanning electron microscopy (SEM)

The surface and cryo-fractured morphologies of the developed foams are shown in Figure 19 and Figure 20. As shown in Figure 19, the surface morphology is greatly influenced by the presence of RCA in the structure of the foams. The surface of the foams without the presence of RCA presents more pores and after the addition of RCA, pores are not any more evident in the magnification that the SEM analysis permits, from their surface due to the presence of RCA molecules. However, a highly porous structure is formed under the surface (cross-section) in the presence of RCA (Figure 20) in which pores become smaller with the presence of MCC and are well connected to each other.

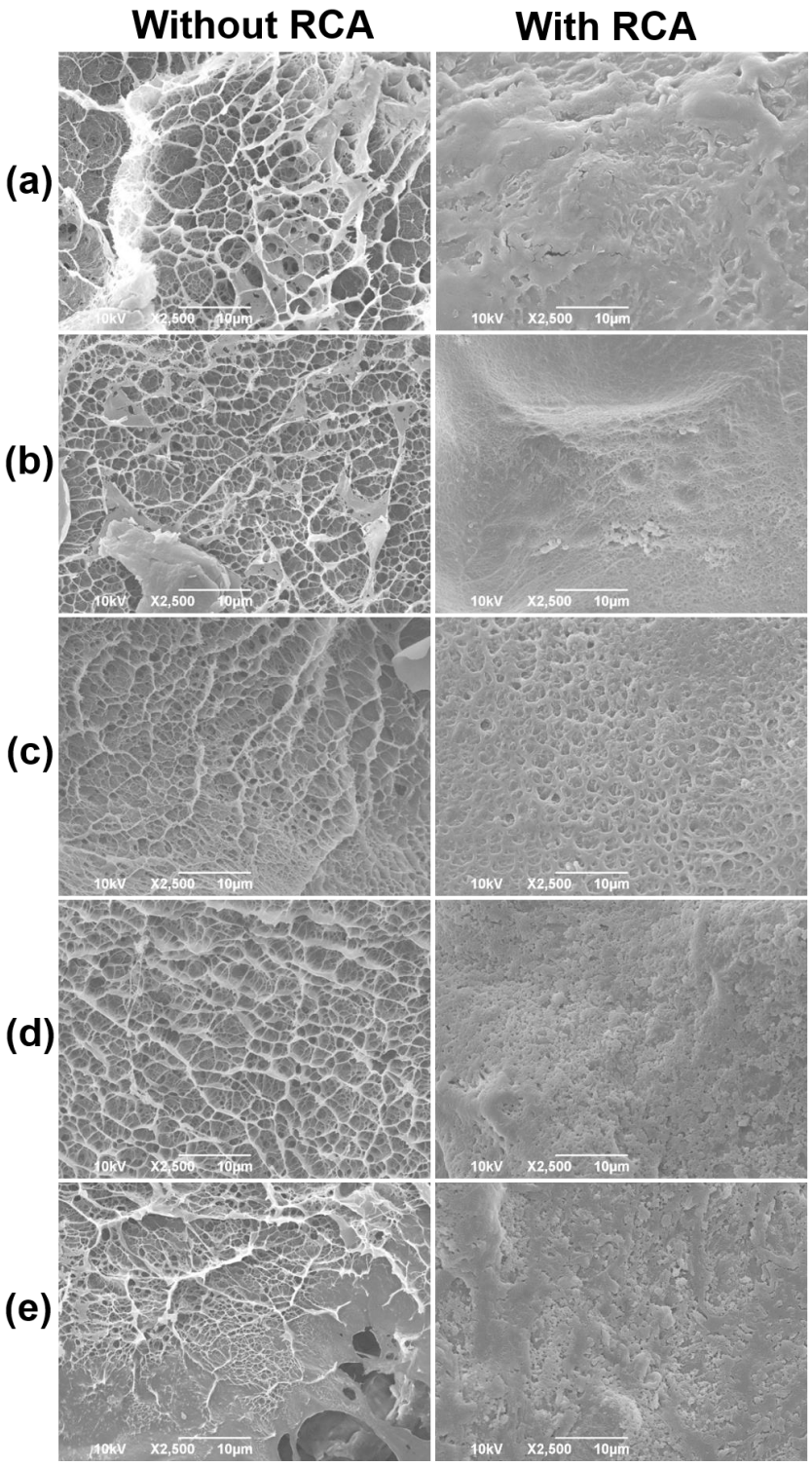

Figure 19. Surface morphologies of the (a) F_0 and F_{0R}, (b) $F_{0.5}$ and $F_{0.5R}$, (c) F_1 and F_{1R}, (d) F_2 and F_{2R} and (e) F_3 and F_{3R} foams.

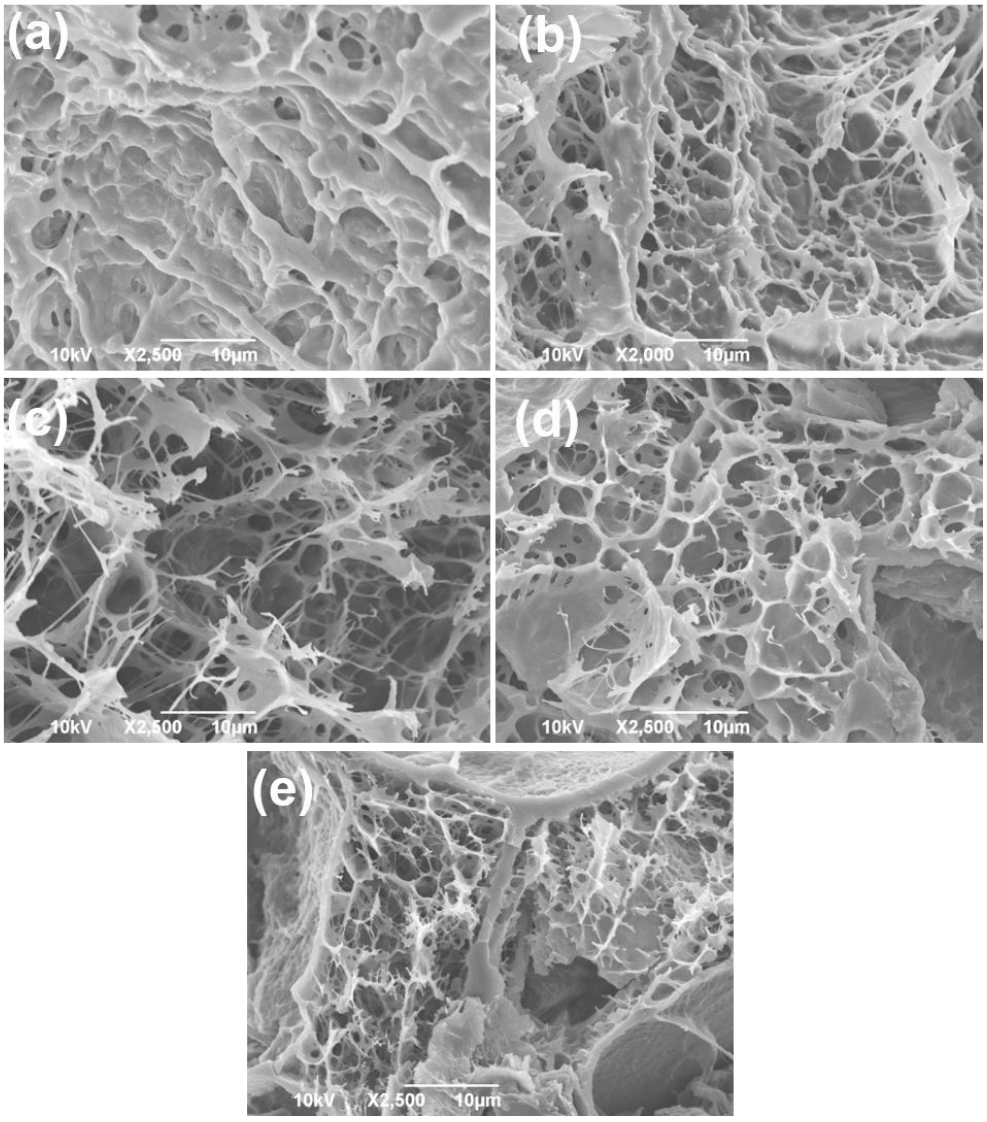

Figure 20. Cross sectional SEM images of the (a) F_{0R}, (b) $F_{0.5R}$, (c) F_{1R}, (d) F_{2R} and (e) F_{3R} foams.

3.3.2 Water absorption capacity and amount of RCA retained by the foams

The effect of the MCC content on the water absorption capacity and RCA retained by the foams is shown in Figure 21 and Table 6. As evident from the Figure 21 and Table 6 the water absorption capacity significantly decreases (from 11.34g/g ± 0.97g/g for F_{0R} to 3.42g/g ± 0.14g/g for F_{3R}) with the increase in the MCC content, and as a result, RCA% retained by the foams also decreases significantly (from 50.26% ± 3.09% for F_{0R} to 19.13% ± 0.99% for F_{3R}). This behavior can be explained by the fact that the crosslinked polymeric chains lose their mobility after the addition of MCC particles [60] thus, the access and interaction of all chains with water is reduced, as well as the water absorption capacity of the foams, and therefore the amount of RCA entrapped together with the water and retained by the foams. Another thing that might contribute to this behavior is the possible hydrogen bonding interaction (see section 3.3.6 FTIR studies) between the MCC and PVA that

restricts the availability of the free hydroxyl groups of PVA to water molecules thus, the interactions with the water [60] decreasing the water absorption capacity and therefore the amount of RCA present in water retained by the foams.

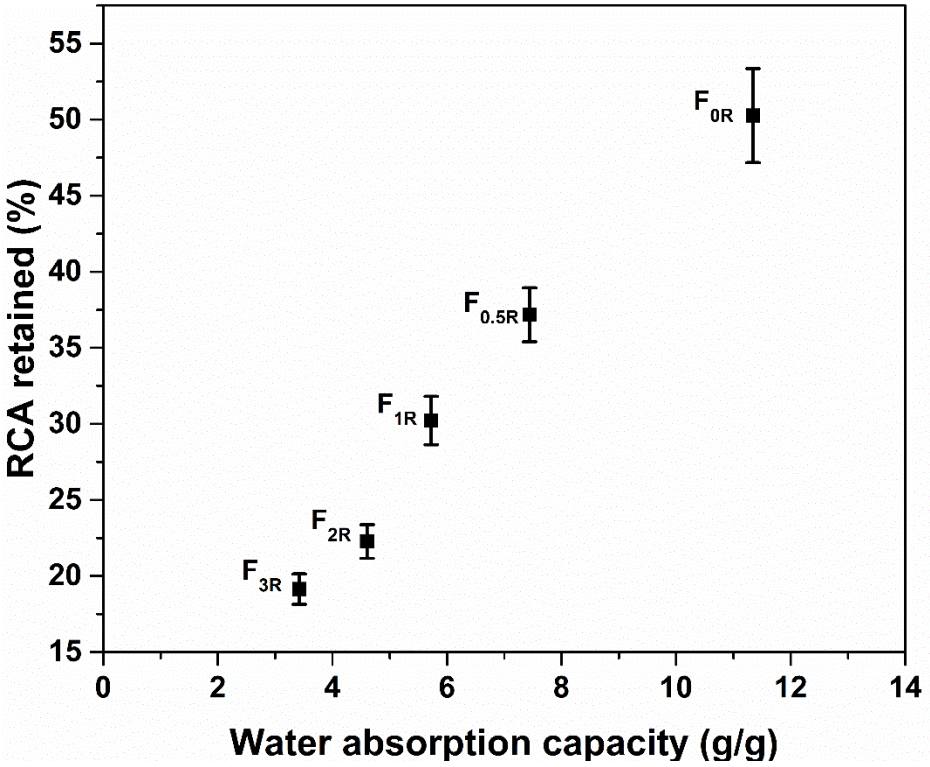

Figure 21. RCA retained vs water absorption capacity for F_{0R}, $F_{0.5R}$, F_{1R}, F_{2R} and F_{3R} indicator foams.

Table 6. Water absorption capacity (g/g) and wt.% amount of RCA retained by each of the foams. Mean values are reported together with the standard deviation. Mean ± standard deviation.

Sample type	Water absorption capacity (g/g)	Weight of RCAs retained (%)
F_0	11.34 ± 0.97	50.26 ± 3.09
$F_{0.5}$	07.44 ± 0.36	37.16 ± 1.77
F_1	05.72 ± 0.18	30.21 ± 1.58
F_2	04.60 ± 0.24	22.26 ± 1.10
F_3	03.42 ± 0.14	19.13 ± 0.99

3.3.3 Brunauer–Emmett–Teller (BET) analysis

The BET analysis was carried out to determine the specific surface area and pore size distribution of the foams. The Brunauer–Emmett–Teller (BET) N_2 adsorption/desorption isotherms and the corresponding Barret–Joyner–Halenda (BJH) pore size distribution graphs of the RCA treated foams are presented in Figure 22-26 and Figure 27-31. According to the IUPAC classification, all isotherms

(Figure 22-26) are classified as Type IV isotherm, characteristic of the materials containing mesopores (2 nm - 50 nm) and macropores (> 50 nm) [152], [153]. In particular, the narrow hysteresis loops observed in all isotherms are classified as H_3 type by the IUPAC classification, characteristics of the N_2 condensation in the mesopore region associated with the mixed shaped pores (cylindrical, wedge and slit shaped) created by the fabrication method adopted [152]–[155]. Furthermore, the absence of the plateau in the N_2 adsorption/desorption isotherms at the higher relative pressure (P/P_0) confirmed the presence of pores in the macropore region [152], [153]. As far as the effect of MCC on the BET specific surface area (S_{BET}) of the foams is concerned (Figure 27-31), it decreases with increase in the concentration of MCC in the foams from 40.60 $m^2.g^{-1}$ (F_{0R}) to 5.99 $m^2.g^{-1}$ (F_{3R}) while the total pore volume (V_P) remain practically the same (0.009 $cm^3.g^{-1}$ - 0.006 $cm^3.g^{-1}$). Therefore, the presence of MCC particles makes the foams less porous in the nanometric range, possibly by reducing the number of the open nanopores The pore size distribution calculated from the adsorption branch of the isotherm by BJH model is appeared to be broad for all samples and the addition of MCC does not have a great impact on it, in the nanometric range, with an average pore size diameter (D_P) centered at 4.3 nm - 3.4 nm for all samples.

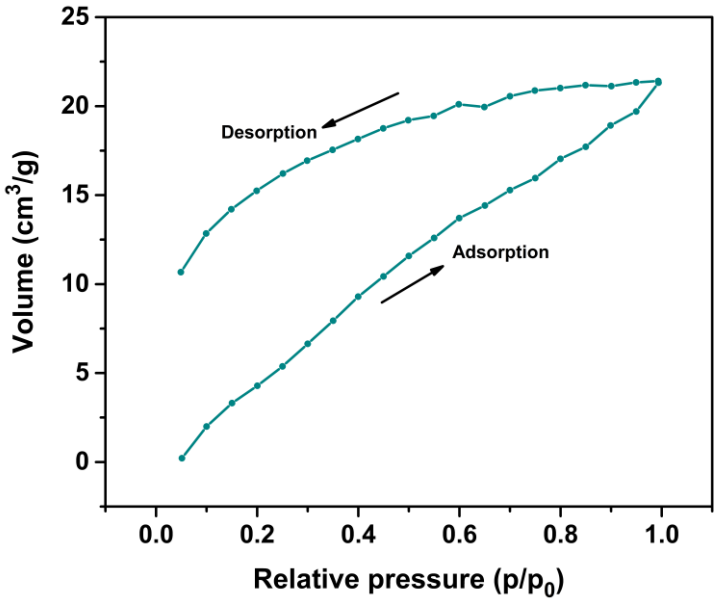

Figure 22. BET N_2 adsorption/desorption isotherms for F_{0R}.

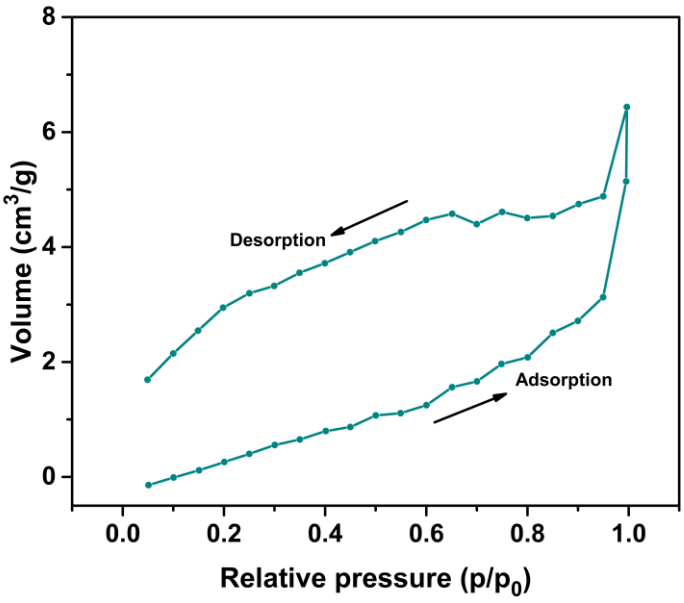

Figure 23. BET N_2 adsorption/desorption isotherms for $F_{0.5R}$.

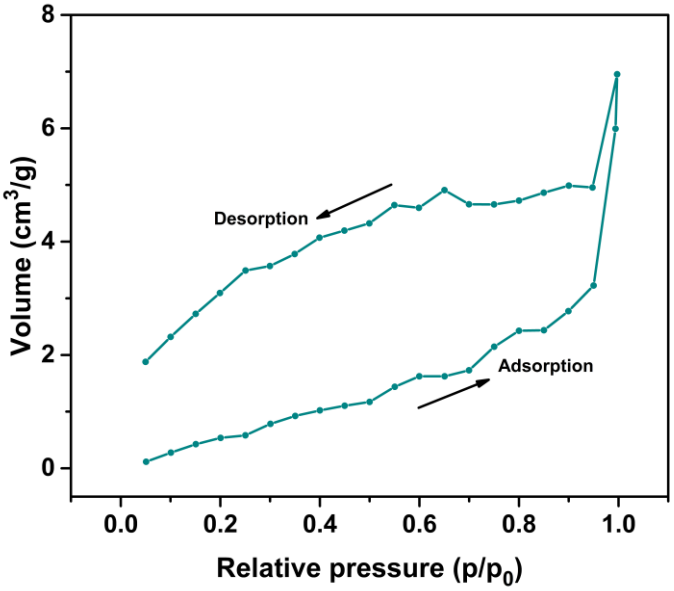

Figure 24. BET N_2 adsorption/desorption isotherms for F_{1R}.

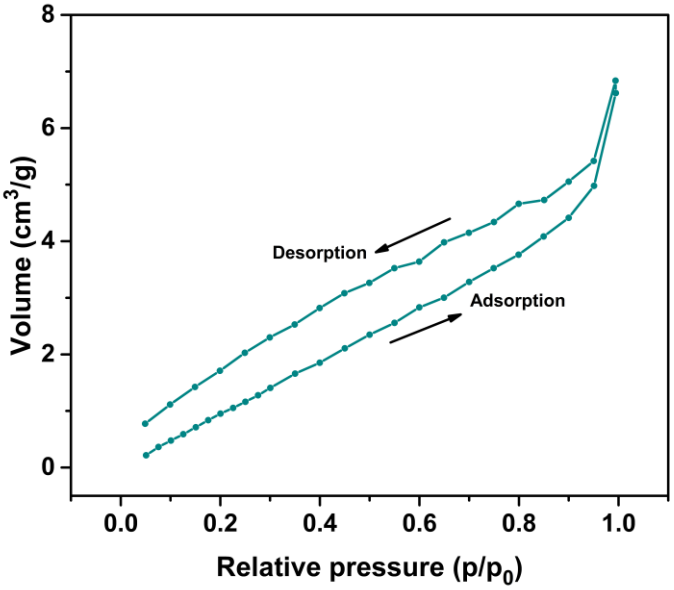

Figure 25. BET N_2 adsorption/desorption isotherms for F_{2R}.

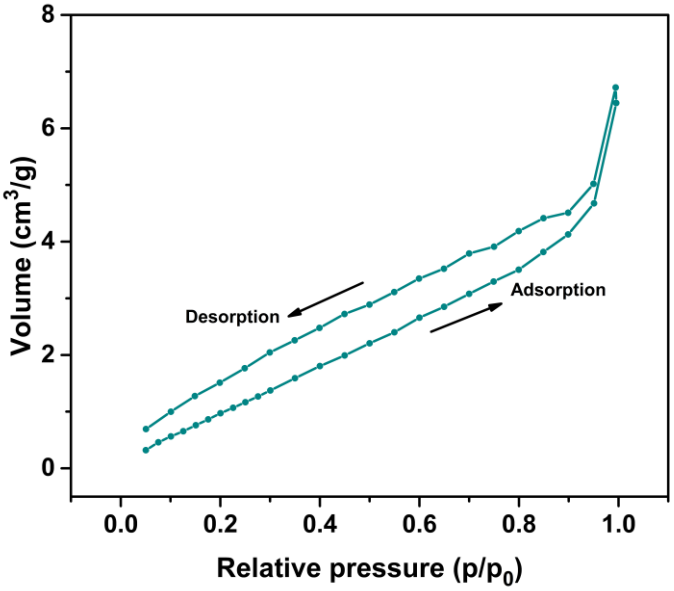

Figure 26. BET N_2 adsorption/desorption isotherms for F_{3R}.

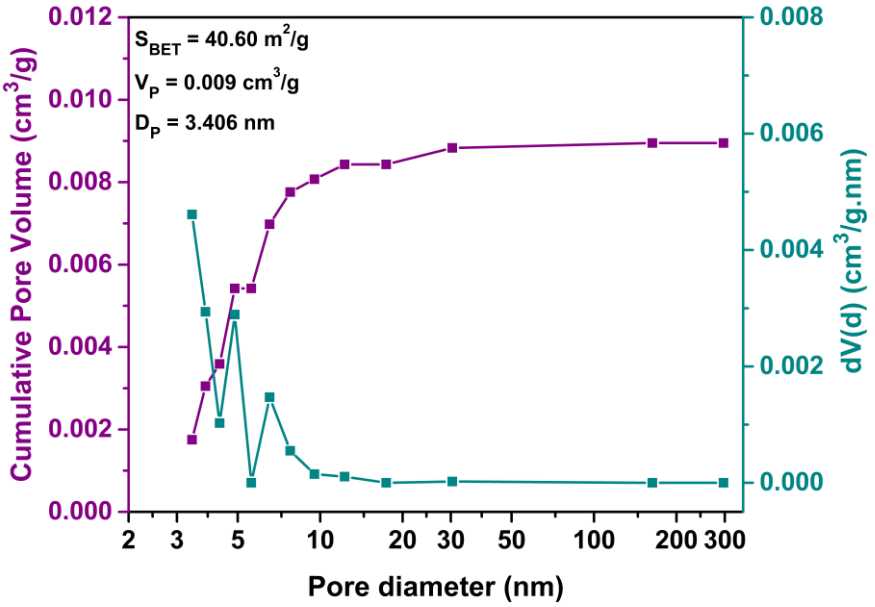

Figure 27. BJH pore size distribution for F_{0R}.

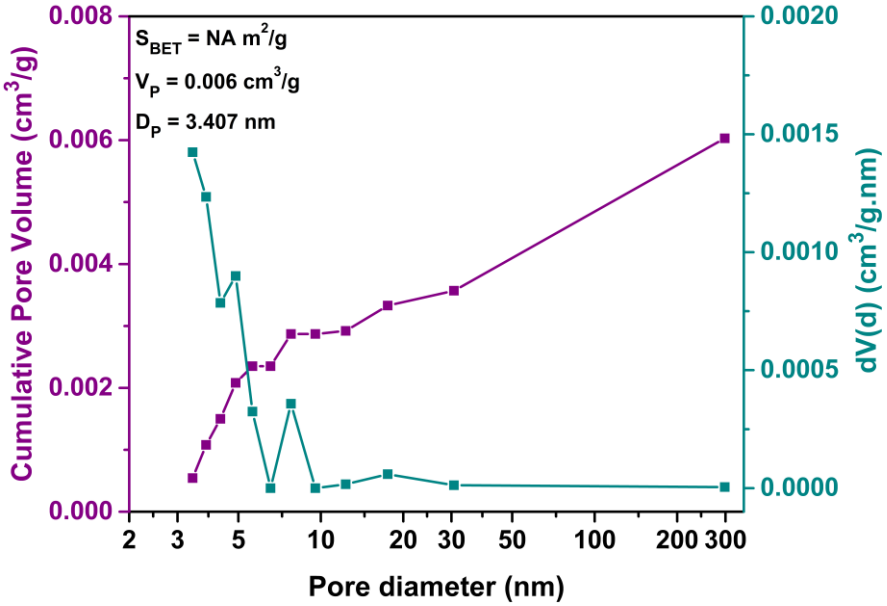

Figure 28. BJH pore size distribution for $F_{0.5R}$.

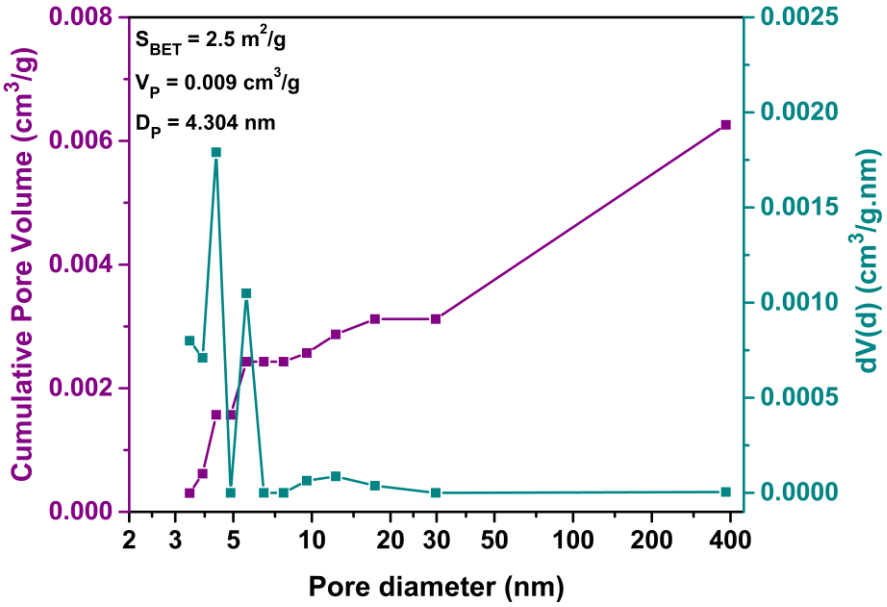

Figure 29. BJH pore size distribution for F_{1R}.

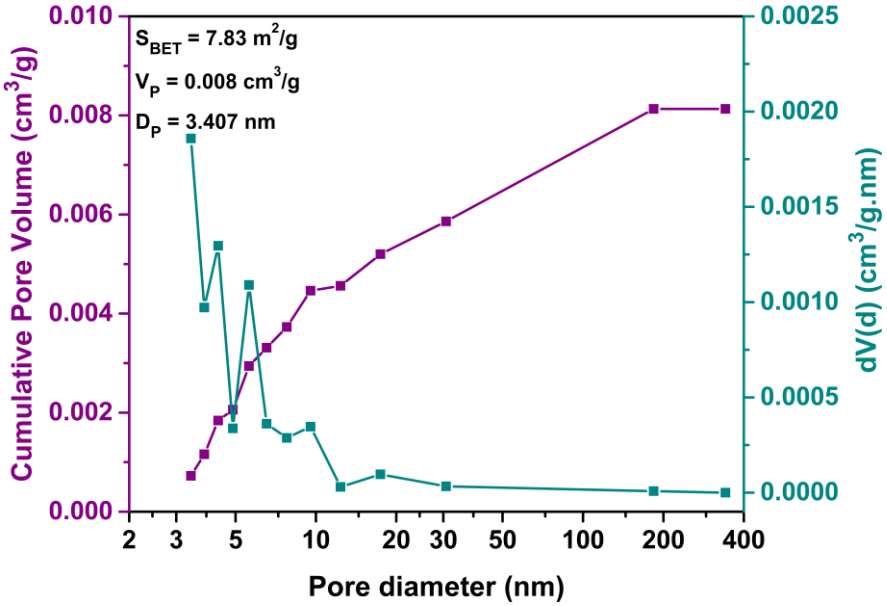

Figure 30. BJH pore size distribution for F_{2R}.

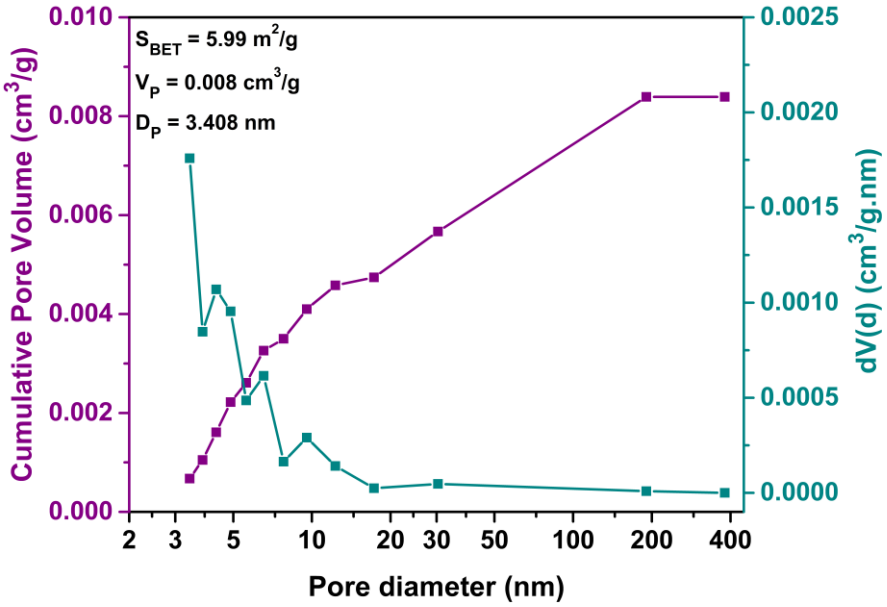

Figure 31. BJH pore size distribution for F_{3R}.

3.3.4 Mercury intrusion porosimetry (MIP)

The porosity and the pores size distribution of the foams in the macropore range were evaluated by the mercury intrusion porosimetry (MIP) measurements. The great volume of mercury entrapped during the intrusion and extrusion process confirms the presence of interconnected pores as shown in the respective isotherms (Figure 32-36). The increase in the concentration of MCC in the formulation increases the porosity of the RCA-treated foams (64%, 70.7%, 72.3%, 77.2% and 79.6% for the F_{0R}, $F_{0.5R}$, F_{1R} F_{2R}, and F_{3R} respectively). The effect of MCC content on the pore size distribution of the foams is presented in Figure 37 and Figure 38. As shown in figures, the presence of MCC has a prominent effect on the pore size distribution of the foams in agreement with the SEM analysis. Specifically, the increase in the MCC amount causes the increase in the pores population with sizes in the range of 1-10 µm (Figure 37), decrease the population of the pores with sizes greater than 300 µm (Figure 38). The MIP analysis confirms that the presence of MCC in the formulation of the foams is necessary for the fabrication of foams with high porosity and small pore sizes.

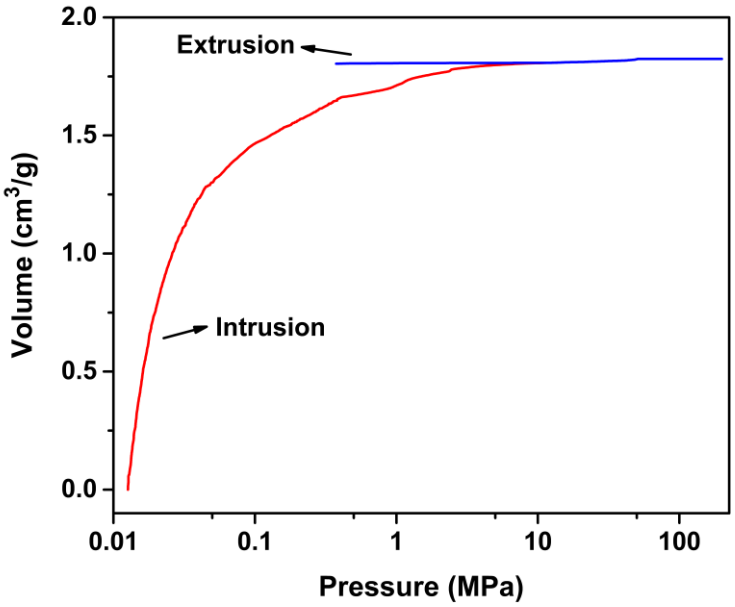

Figure 32. Mercury intrusion/extrusion isotherms for $F_{0R.}$

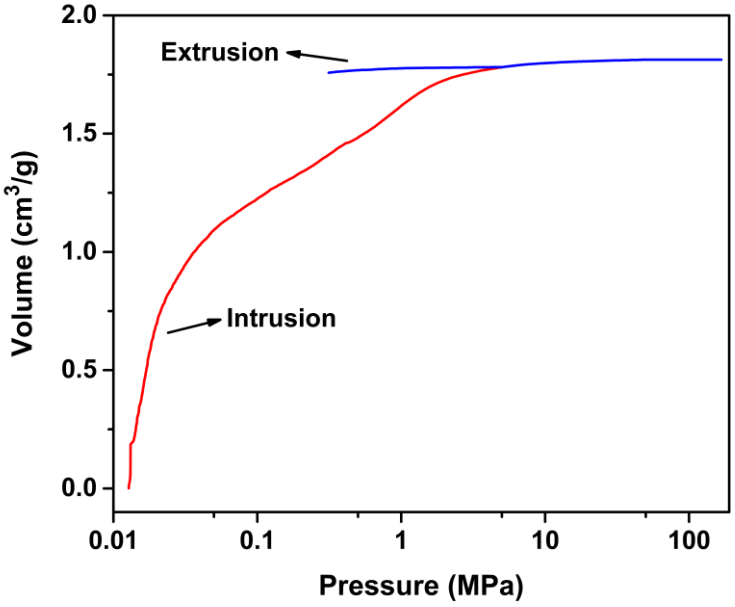

Figure 33. Mercury intrusion/extrusion isotherms for $F_{0.5R.}$

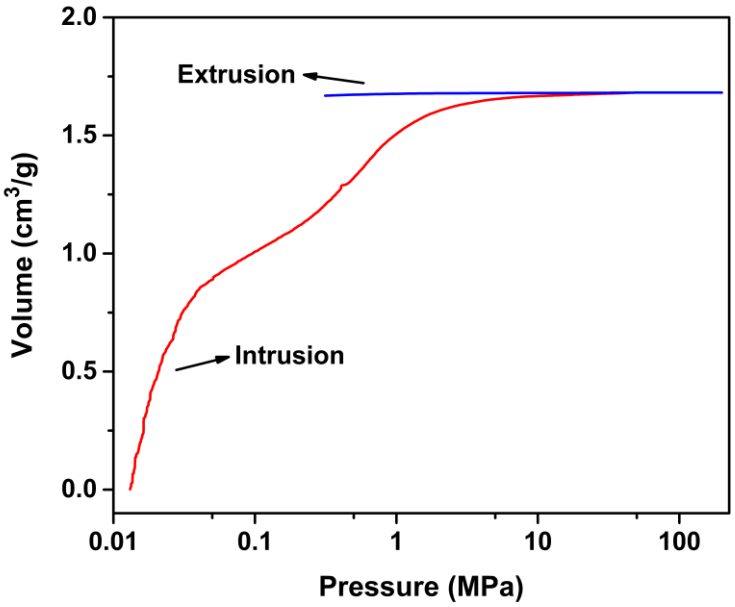

Figure 34. Mercury intrusion/extrusion isotherms for $F_{1R.}$

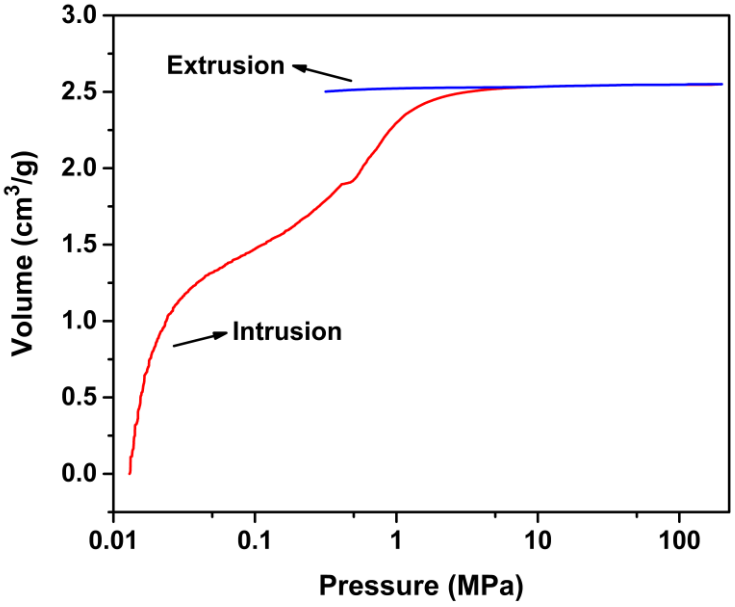

Figure 35. Mercury intrusion/extrusion isotherms for $F_{2R.}$

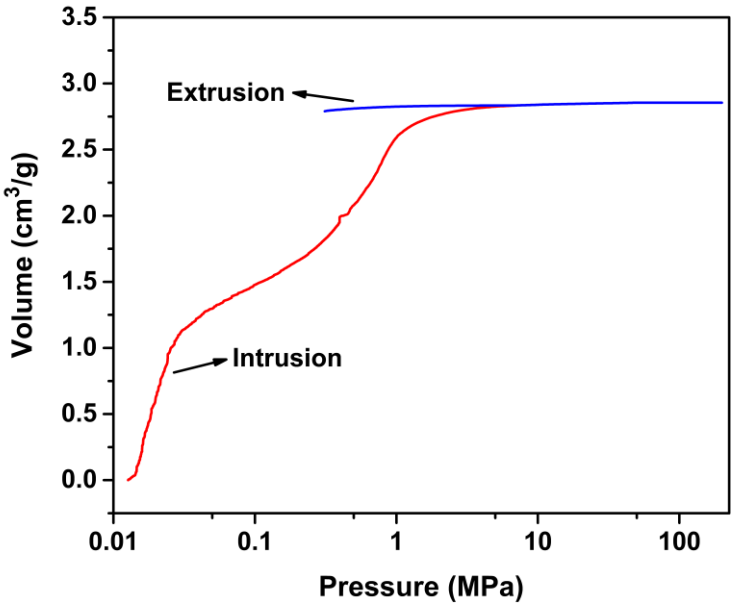

Figure 36. Mercury intrusion/extrusion isotherms for F_{3R}.

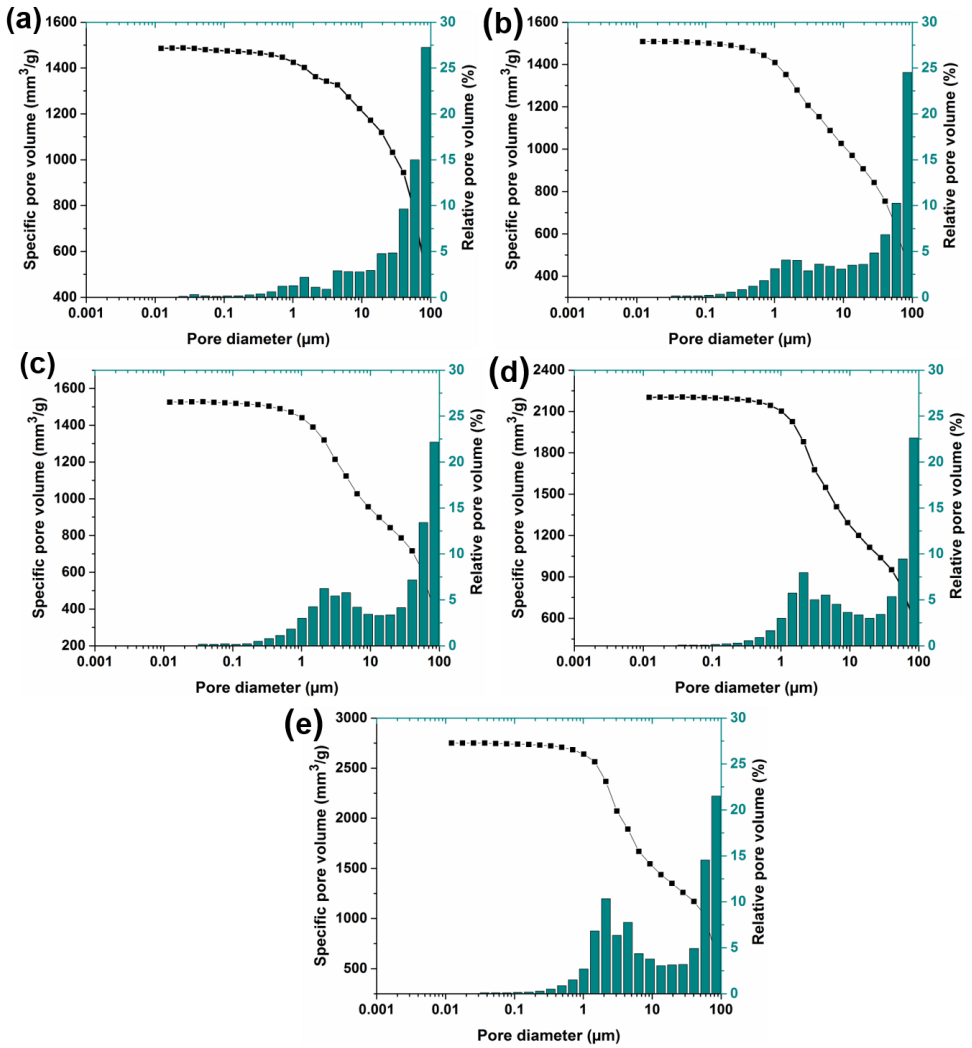

Figure 37. Pore size distribution of the foams as calculated by the MIP for pore sizes below 100 μm.

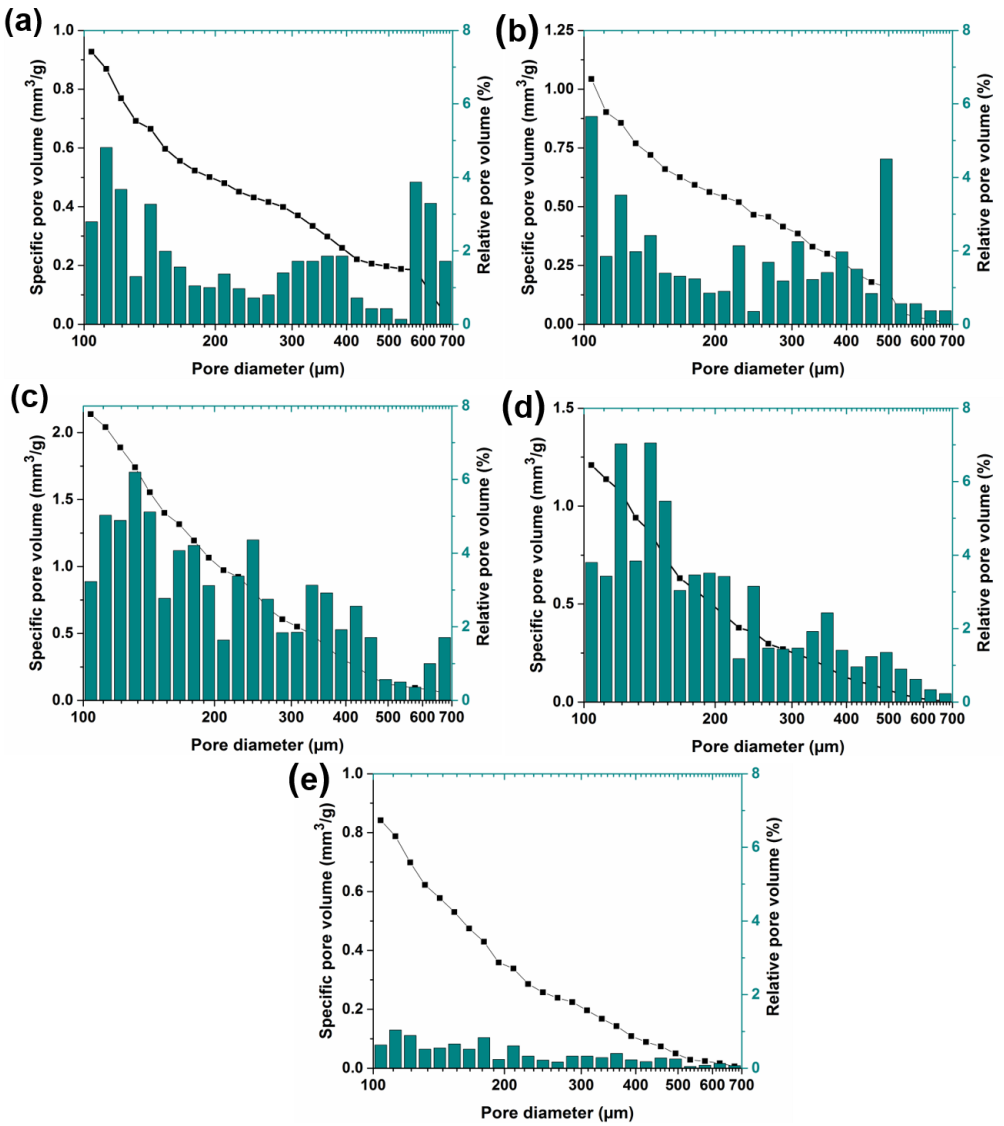

Figure 38. Pore size distribution of the foams as calculated by the MIP for pore sizes above 100 μm

3.3.6 Fourier transform infrared-attenuated total reflection spectroscopy (FTIR-ATR)

The FTIR spectra of pure PVA, PVP, MCC, RCA and composite foams were analyzed to investigate the possible chemical interactions between the polymers and RCA (Figure 39 and Figure 40 and Table 7). The FTIR spectra of pure RCA shows its characteristic peaks at 3268 cm^{-1} attributed to OH stretching, C-H stretching at 2984 cm^{-1}, mixed C=O and C=C stretching at 1642 cm^{-1} and C-O stretching at 1084 cm^{-1} [30], [56], [60], [64]. FTIR spectra of the F_0 (PVA/PVP) shows most of the characteristic peaks of pure PVA and PVP powder with some shifts e.g. OH stretching from 3272 cm^{-1} to 3309 cm^{-1}, symmetric CH stretching from 2907 cm^{-1} to 2911 cm^{-1} and C-O stretching from 1088 cm^{-1} to 1092 cm^{-1}, confirming the crosslinking between the PVA and PVP through hydrogen bonding [156], [157]. The spectra of F_0 foam shows its characteristic peaks at 3309 cm^{-1} attributed to OH stretching, asymmetric and symmetric CH stretching at 2941 cm^{-1} and 2911 cm^{-1}, respectively, C=O stretching of PVP at 1660 cm^{-1}, CH bending at 1423 cm^{-1} and C-O stretching at 1092 cm^{-1} [156]–

[159]. In the case of the F_{0R} spectrum all the characteristic peaks of F_0 are shifted e.g. the OH stretching is shifted from 3309 cm^{-1} to 3272 cm^{-1}, asymmetric and symmetric CH stretching from 2941 cm^{-1} and 2911 cm^{-1} to 2937 cm^{-1} and 2917 cm^{-1}, respectively, C=O stretching from 1660 cm^{-1} to 1614 cm^{-1}, CH bending from 1423 cm^{-1} to 1414 cm^{-1}, C-O stretching from 1092 cm^{-1} to 1029 cm^{-1} indicating strong hydrogen bonding interactions between the polymers and RCA molecules. Furthermore, F_2 represents the main assignments of both the F_0 matrix and MCC with the shift of few peaks e.g. OH stretching from 3309 cm^{-1} to 3296 cm^{-1}, intensified C=O stretching of PVP from 1660 cm^{-1} to 1654 cm^{-1}, C-O stretching from 1092 cm^{-1} to 1096 cm^{-1} showing strong molecular interaction among the PVA, PVP and MCC polymers. In case of the F_{2R} spectrum, all the characteristic peaks of F_2 are shifted similarly as happened in case of F_{0R} e.g. OH stretching from 3296 cm^{-1} to 3272 cm^{-1}, asymmetric and symmetric CH stretching from 2941 cm^{-1} and 2910 cm^{-1} to 2937 cm^{-1} and 2915 cm^{-1} respectively, mixed C=O and C=C stretching peak from 1654 cm^{-1} to 1632 cm^{-1}, CH bending from 1423 cm^{-1} to 1415 cm^{-1} and C-O stretching from 1096 cm^{-1} to 1029 cm^{-1}. All these observations indicate the presence of strong hydrogen bonding and van der Waals interactions between the polymers and RCA [160] essential for the immobilization of the dye molecule in the polymers matrix and the prevention of the leaching/migration of dye in aqueous solutions.

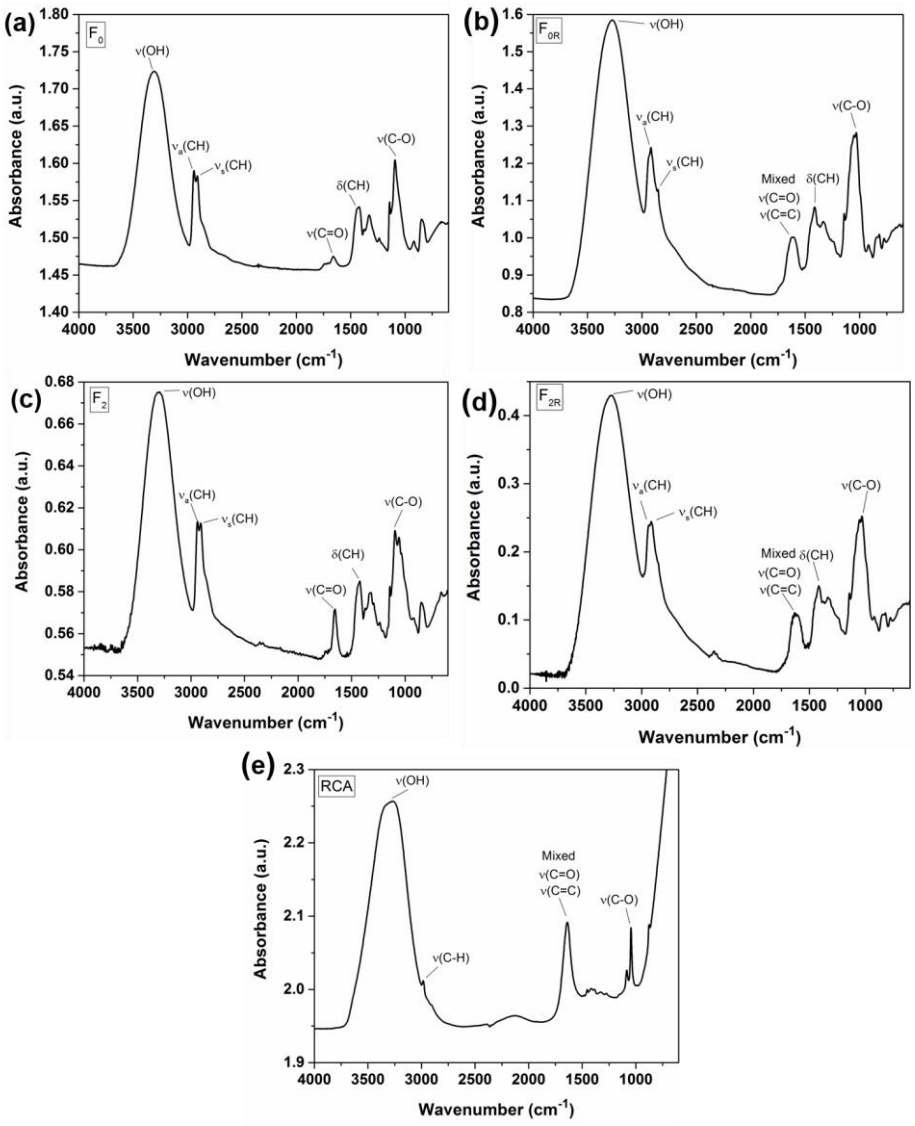

Figure 39. FTIR spectra of (a) F_0, (b) F_{0R}, (c) F_2, (d) F_{2R} and (e) pure RCA

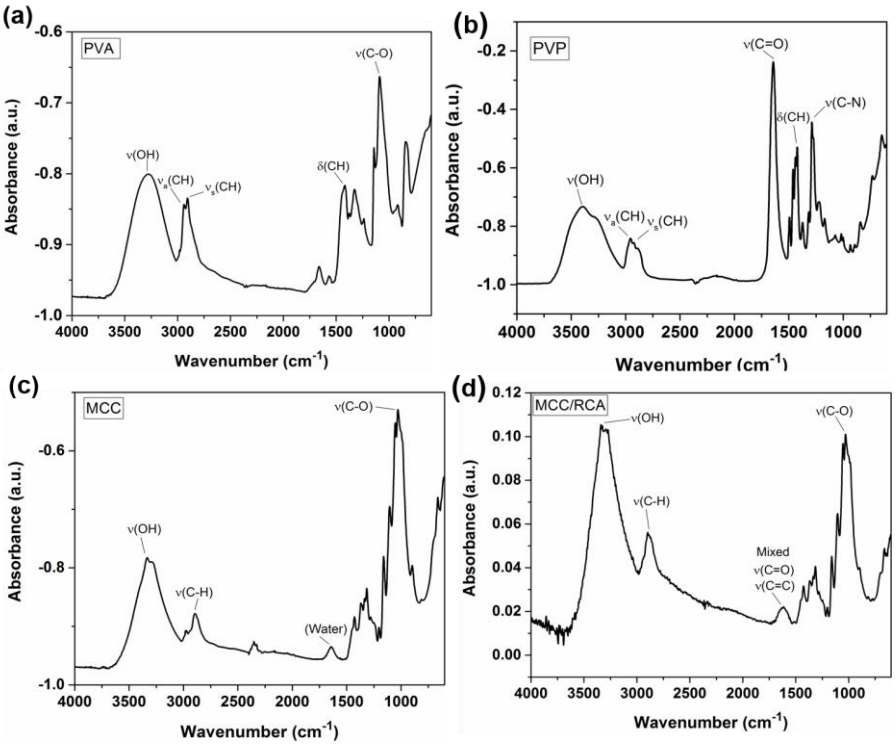

Figure 40. (a) FTIR spectra for (a) pure PVA, (b) pure PVP, (c) pure MCC and (d) MCC/RCA.

Table 7. Characteristic wavenumbers and groups of pure PVA, PVP, MCC, RCA, MCC/RCA and composite foams

Sample type	Bands (cm^{-1})	Chemical Associated groups
PVA	3272	OH Stretching
	2940	C-H Asymmetric Stretching
	2907	C-H Symmetric Stretching
	1418	C-H Bending
	1088	C-O Stretching
PVP	3393	OH Stretching
	2955	C-H Asymmetric Stretching
	2892	C-H Symmetric Stretching
	1424	C-H Bending
	1289	C-N Stretching
MCC	3335	OH Stretching
	2893	C-H Stretching
	1643	Absorbed H_2O
	1028	C-O Stretching
RCA	3268	OH Stretching

	2984	C-H Stretching
	1642	Mixed C=C and C=O Stretching
	1084	C-O Stretching
	1044	C-H Aromatic
MCC/RCA	3392	OH Stretching
	2897	C-H Stretching
	1614	C=C and C=O Stretching of RCA
	1030	C-O Stretching
F_0	3309	OH Stretching
	2941	C-H Asymmetric Stretching
	2911	C-H Symmetric Stretching
	1660	C=O Stretching
	1423	C-H Bending
	1092	C-O Stretching
F_{0R}	3272	OH Stretching
	2937	C-H Asymmetric Stretching
	2917	C-H Symmetric Stretching
	1614	Mixed C=C and C=O Stretching
	1414	C-H Bending
	1029	C-O Stretching
F_2	3296	OH Stretching
	2941	C-H Asymmetric Stretching
	2910	C-H Symmetric Stretching
	1654	C=O Stretching
	1423	C-H Bending
	1096	C-O Stretching
F_{2R}	3272	O-H Stretching
	2937	C-H Asymmetric Stretching
	2915	C-H Symmetric Stretching
	1632	Mixed C=C and C=O Stretching
	1415	C-H Bending
	1029	C-O Stretching

3.3.5 Thermo-gravimetric analysis (TGA)

The effect of MCC and RCA on the thermal stability of the foams was further investigated by TGA analysis in air atmosphere (Figure 41 and Figure 42). As explained by the isotherm, the degradation of the MCC takes place in two steps: the first degradation step takes place at temperatures lower than 100 °C, and is associated to the thermal elimination of the absorbed moisture. The second degradation step of MCC takes place between 235 °C to 335 °C due to the decarboxylation, depolymerization and decomposition of the saccharide rings and of the macromolecular chains [161], [162].

Concerning the F_0 the first degradation step takes place below 90 °C due to the evaporation of water. The second step takes place from 227 °C to 432°C due to the chain-striping elimination of water from the PVA structure leading to polyenes [163]. The third step of degradation takes place between 432 °C to 586 °C and it is attributed to the disintegration of the carbon skeleton of the polymeric chains (carbonation) [164], [165]. The degradation of the cellulose containing foams e.g. $F_{0.5}$, F_1, F_2 and F_3 take place in three steps with the thermal stability of the foams to decrease with the increase in the concentration of MCC (Figure 41). This decrease in the thermal stability is due to the lower degradation temperature of cellulose (MCC) as compared to the PVA and PVP polymers.

The degradation of Pure RCA takes place in five steps. The first step involves the loss of tightly bonded moisture up to 100 °C. The second degradation step takes place from 110 °C to 190 °C. The third step takes place from 190 °C to 304 °C. The fourth step happens between 304 °C to 473 °C and the fifth degradation step of pure RCA takes place from 473 °C onwards. After the addition of RCA in the foams, the degradation process of RCA treated foams e.g. F_{0R}, $F_{0.5R}$, F_{1R}, F_{2R} and F_{3R} splits into multiple steps due to the RCA (Figure 42). However, the addition of RCA improves the thermal stability of the MCC foams possibly due to the hydrogen bonding interactions between the RCA and the polymers. The DTGA curves (Figure 43), proved these interactions as the second degradation step of the pure RCA shifts 13 °C towards higher temperatures when it is embedded in the polymer matrix. The increase in the MCC content leads to the decrease in the thermal stability of the RCA treated foams at temperatures greater than 300 °C due to the overall lower degradation temperature of MCC.

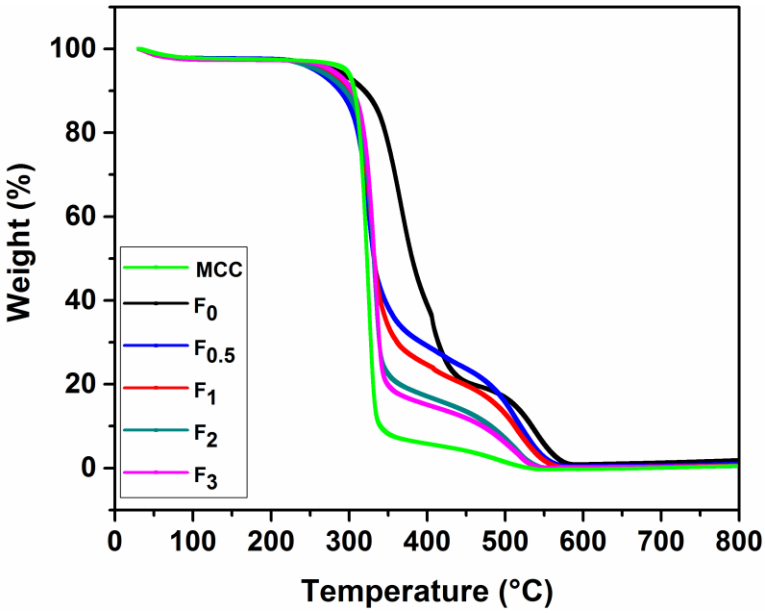

Figure 41. TGA curves for MCC and foams before RCA treatment.

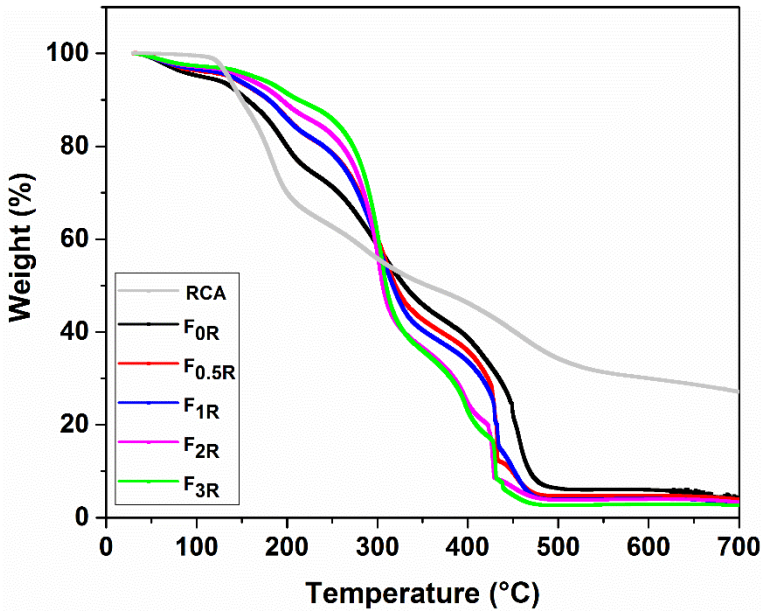

Figure 42. TGA curves for pure RCA and RCA treated foams.

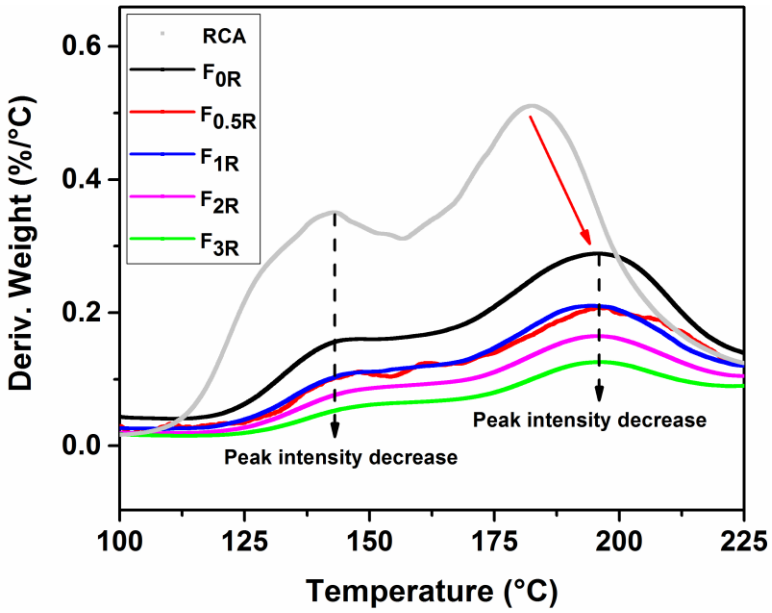

Figure 43. Zoom in DTGA curves for pure RCA and RCA treated foams.

3.3.7 Response of the RCA and RCA treated foams to solutions

RCAs undergo structural changes (Figure 44) when subjected to different pH environments due to the protonation and deprotonation of their molecules, resulting in color variations of the materials where they are embedded [30], [147], [166], [167].

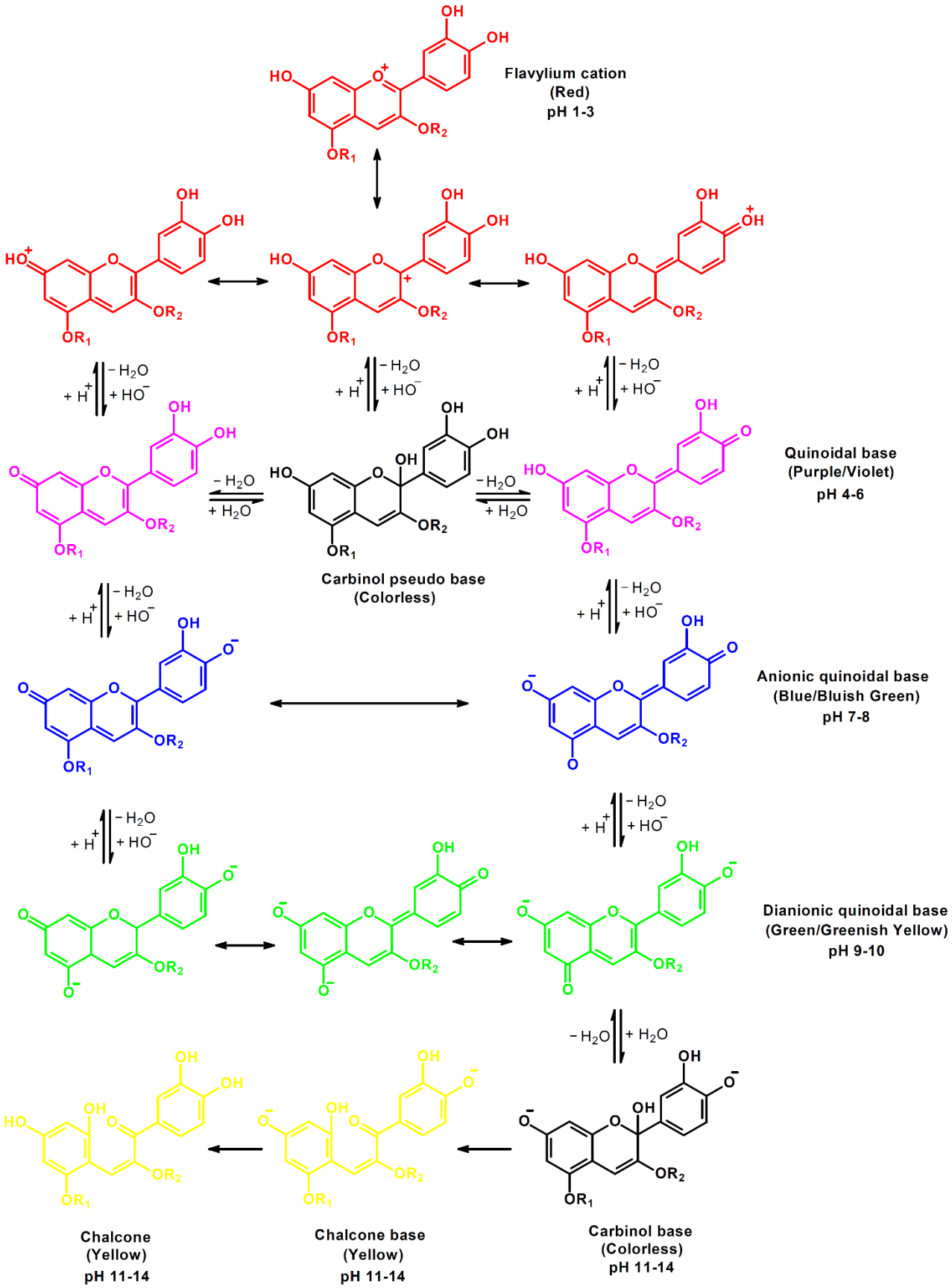

Figure 44. Chemical modifications of RCA upon pH variations adopted from [166][168].

The color variations of the RCA solutions and indicator foams (F_{2R} foam will be of focus as it will be proved below has the better response kinetics) against different pH solutions in the range of 1-14 are presented in Figure 45 and Figure 46. As evident from the figures, RCA produces different colors almost at every pH. The color of the RCA solutions and indicator foams (Figure 45) is red at pH (1-3) due to the presence of the predominant flavylium cations [56], [130], [142], [169] caused by the protonation of the RCA. The color changes gradually to purple/violet at pH 4-6, due to the deprotonation of the RCA that leads to the formation of quinoidal base [56], [130], [142], [169] and carbinol pseudo base [130], [169]. At pH 7-8 the color changes to blue/bluish green due to the formation of anionic quinoidal base [56], [130], [142], [169], while it becomes green/yellowish green at pH 9-10 due to the formation of dianionic quinoidal base [56], [130], [142], [169] and yellow at pH > 10 due to the further deprotonation and formation of carbinol base [56], [130], [142], [169], chalcone and chalcone base [56], [130], [142], [169]. Furthermore, CIELab analysis of the indicator foams was conducted as scientific proof of the optical color changes upon exposure to different pH values. The CEILab analysis assigned a dE value (Figure 46) to every indicator foam at a particular pH. As shown in Figure 46, at every pH, the indicator foams possess unique dE values greater than 3.5 indicating that the foams distinct color change at every specific pH, perceivable by the human naked eye.

Figure 45. RCA solution response upon pH changes for F_{2R}.

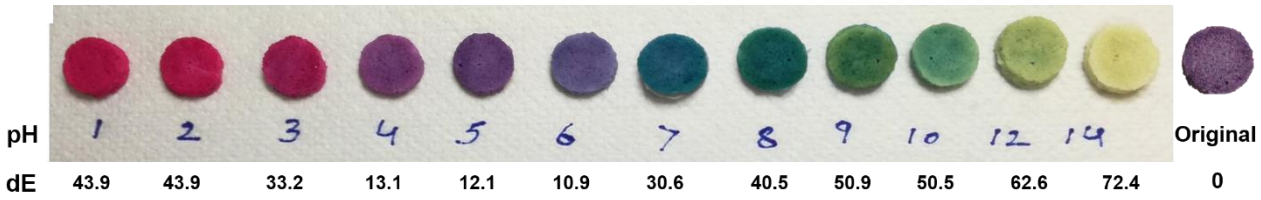

Figure 46. F_{2R} foam response to pH changes. The corresponding dE values, obtained by CIELab color space analysis are also presented. The photo of the reference sample is a non-exposed F_{2R} foam (original).

Additionally, the color changes of RCA upon pH variations were observed by the UV-Vis spectroscopy. As shown in (Figure 47a), the differences between the maximum absorption peaks of the RCA solutions and RCA treated foams exposed at different pH values are not significant which means that the RCA produces similar kind of changes in both forms (RCA in solution form and RCA

in the indicator foams). In particular, as can be seen from the Figure 47b,c which corresponds to the UV-Vis absorption spectra of RCA solutions and of the indicator foams respectively, when the environment is highly acidic (1-3) there is a small hypochromic shift of the main RCA peak from 524 nm to 529 nm. When the pH of the medium is increased to (4-8) a bathochromic shift (red shift) is observed in the absorbance from 539 nm to 608 nm. After that, when the pH of the medium further increases (9-14) a hypsochromic shift (blue shift) is observed with the peak shifting from 384 nm to 355 nm. Similar behavior is observed in the UV-Vis spectra of agar/starch films functionalized with anthocyanin extracts from purple sweet potato [56]. In particular, both the anthocyanin solutions and anthocyanin treated films produce similar colors at the specific pH values and the color changes are perceivable over the broad pH range (in between 4-10) [56].

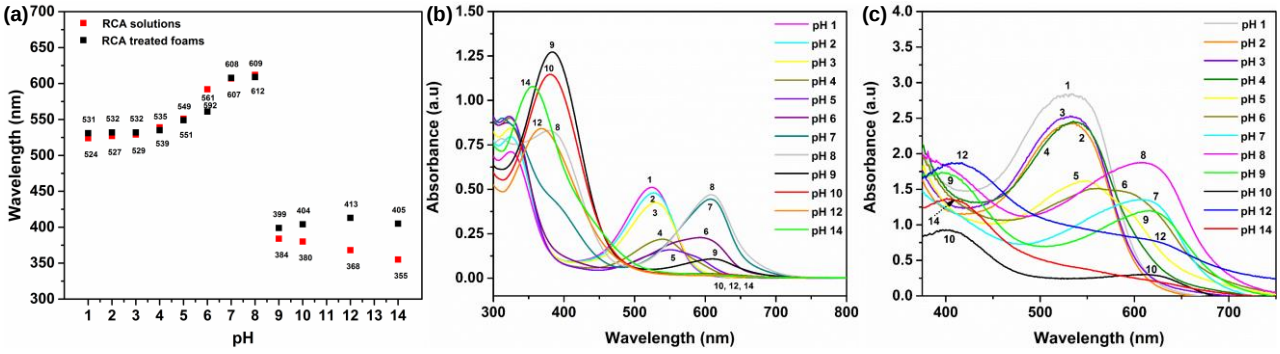

Figure 47. (a) Wavelength at maximum absorbance obtained by UV- visible absorption spectra of RCA solution and RCA treated foams upon pH changes, (b) UV- visible absorption spectra of RCA solution and (c) UV- visible absorption spectra of RCA treated foams upon different pH values: The absorption spectra is cut short to 375 nm due to the saturation of the signal beyond that range.

3.3.8 Response of the foams against vapors

The effect of MCC on the response kinetics of the indicator foams were evaluated by CIELab color analysis. For that purpose, first, the indicator foams (F_{0R} and F_{2R}) were exposed to HCl and NH_4OH vapors separately in closed petri dishes. Afterwards, a video was recorded for the analysis purpose and one frame per second was analyzed. As shown in Figure 48 and Figure 49, the F_{2R} foam changes the color more faster as compared to the F_{0R} foam. Particularly, in the case of HCl exposure (Figure 48), the value of the dE reaches the perceivable limit (3.5) just after 17 seconds whereas F_{0R} took 200 seconds to reach that limit. In the case of NH_3 exposure (Figure 49), F_{2R} foam took 122 seconds to reach the perceivable limit whereas this limit is not reached for F_{0R} even after 700 seconds.

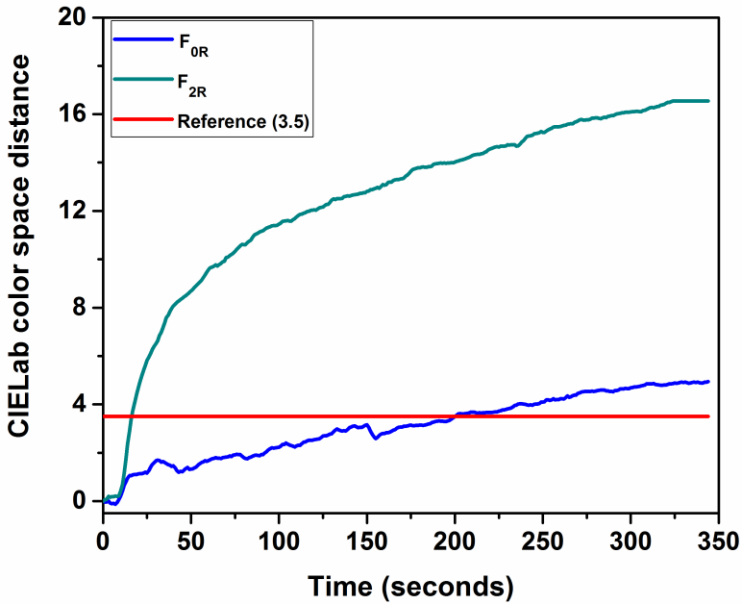

Figure 48. CIELab color space coordinates of the F_{2R} and F_{0R} foams when exposed to HCl vapors.

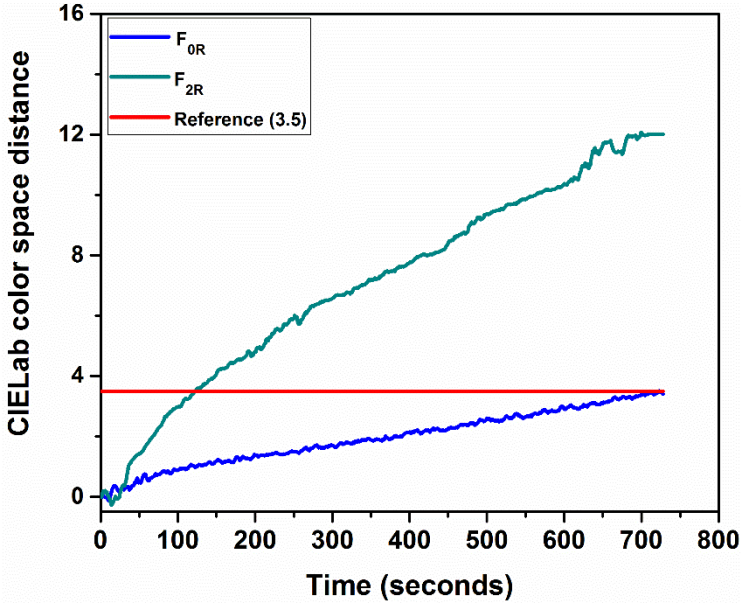

Figure 49. CIELab color space coordinates of the F_{2R} and F_{0R} foams when exposed to NH_3 vapors.

The CIELab analysis confirmed that the presence of MCC in the foams structure is necessary for faster response kinetics. Additionally, the effect of MCC on the response kinetics of the indicator foams is further evaluated by the UV-Vis spectroscopy. For that reason, the indicator foams were subjected to HCl vapors in a closed environment and the increase in the intensity of the absorption peak at 524 nm was plotted with time in each case (Figure 50-54). To determine how fast is the change in the absorption intensity takes place, the obtained data is subjected to a pseudo second-order non-linear kinetic model analysis. As shown in Table 8, all foams have R^2 value higher than 0.982 and the indicator foams with higher MCC amount (higher porosity) show higher rate constants values (k: 0.010 au s^{-1}, 0.019 au s^{-1}, 0.028 au s^{-1}, 0.059 au s^{-1} and 0.063 au s^{-1} for F_{0R}, $F_{0.5R}$, F_{1R}, F_{2R} and F_{3R}

respectively) proving the importance of the MCC component on the responsiveness of the indictors. However, there is no significant difference observed between the rate constants of F_{2R} and F_{3R} foams (7% more for F_{3R}) even if the MCC amount in the F_{3R} is 50% higher. Considering that, we selected the F_{2R} indicator foams for further experiments, since it provides a fair balance between the performance and the fabrication costs.

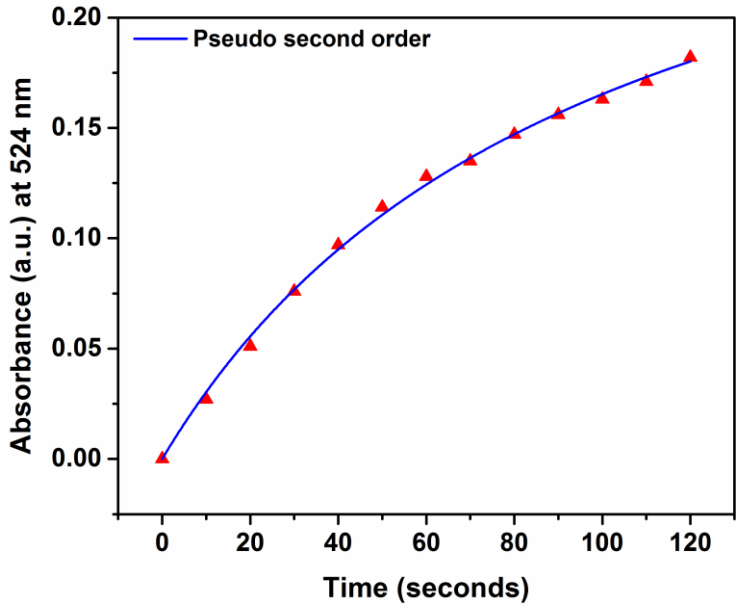

Figure 50. Absorption intensity variation of the peak at 524 nm over time upon exposure of the foams to HCl vapors and the non-linear fitting curve of F_{0R}.

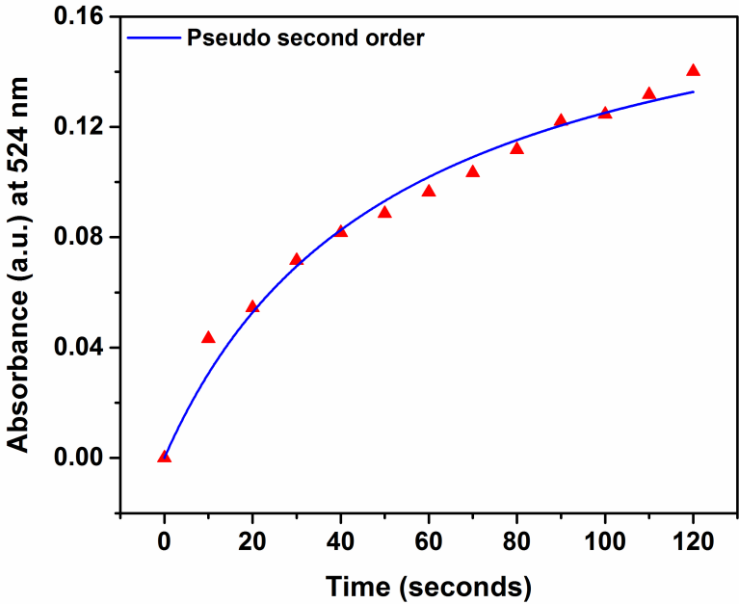

Figure 51. Absorption intensity variation of the peak at 524 nm over time upon exposure of the foams to HCl vapors and the non-linear fitting curve of the $F_{0.5R}$.

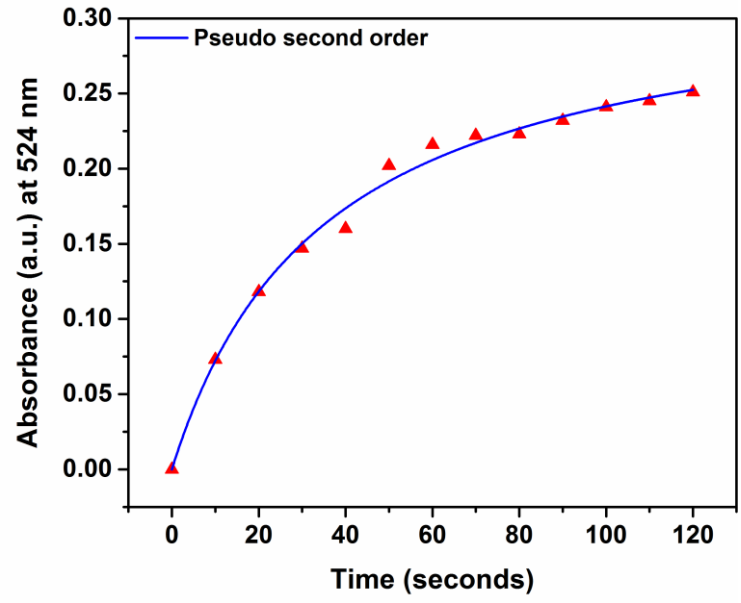

Figure 52. Absorption intensity variation of the peak at 524 nm over time upon exposure of the foams to HCl vapors and the non-linear fitting curve of the F_{1R}.

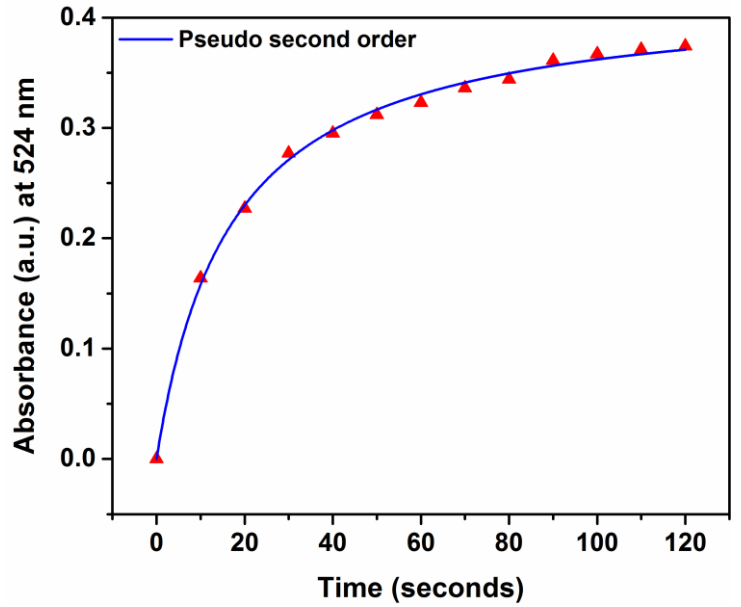

Figure 53. Absorption intensity variation of the peak at 524 nm over time upon exposure of the foams to HCl vapors and the non-linear fitting curve of the F_{2R}.

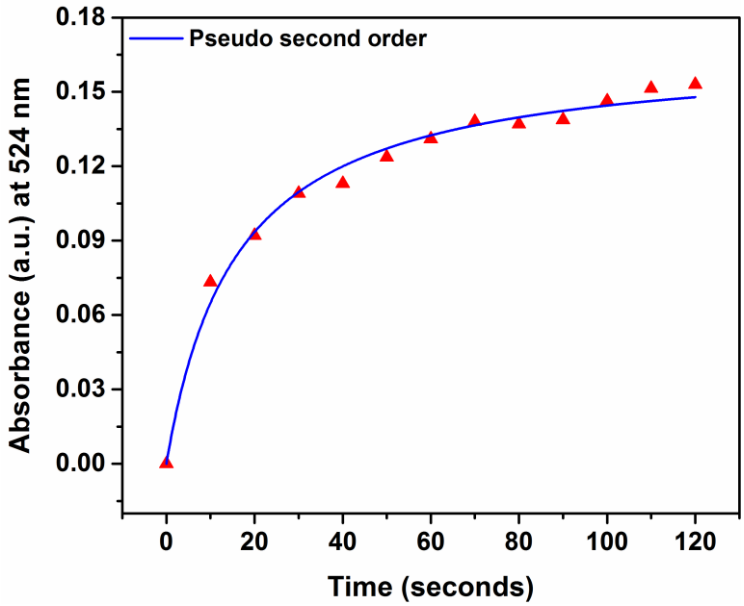

Figure 54. Absorption intensity variation of the peak at 524 nm over time upon exposure of the foams to HCl vapors and the non-linear fitting curve of the F_{3R}.

Table 8. Data obtained from the pseudo second-order non-linear fitting.

Sample	I_e (au)	k_2 (au s^{-1})	R^2
F_{0R}	0.32689	0.01022	0.99808
$F_{0.5R}$	0.19043	0.01914	0.98295
F_{1R}	0.32651	0.02836	0.99342
F_{2R}	0.42268	0.05958	0.99784
F_{3R}	0.16733	0.06321	0.98985

In order to have more detailed investigation and to demonstrate the versatility of the F_{2R} pH indicator, first, the indicator foam was exposed to HCl and NH_3 vapors, and the changes were recorded by UV-Vis spectroscopy and CIELab color analysis (Figure 55-58). As shown in Figure 55 and Figure 56, the indicator foam changes its color to red from purple due to protonation of the RCA and the formation of flavylium cations, just after 10 seconds of exposure to HCl vapors. The intensity of the red component (524 nm) keeps growing with increase in the exposure time to acidic vapors and stabilizes after 90 seconds indicating the HCl sensing ability of the indicator. This is also proved by the CIELab analysis (Figure 56) which shows a continuous increase in the dE value with the passage of time for the specific foam. In cases of NH_3 sensing (Figure 57 and Figure 58), a clear color change (green from purple) is produced just after 10 seconds of exposure time due to deprotonation of the RCA and the formation of the anionic quinoidal base. The intensity of the absorption peaks around

418 nm and 644 nm keeps growing with increase in the reaction time to the NH_3 vapors. Additionally, the NH_3 vapor sensing is also proved by the CIELab analysis (Figure 58 that shows a continuous increase in the dE value with the reaction time. Similar changes were observed in the case of starch/PVA films functionalized with roselle anthocyanin by Zhai et al. [30] but the films took 2 minutes to produce the color change.

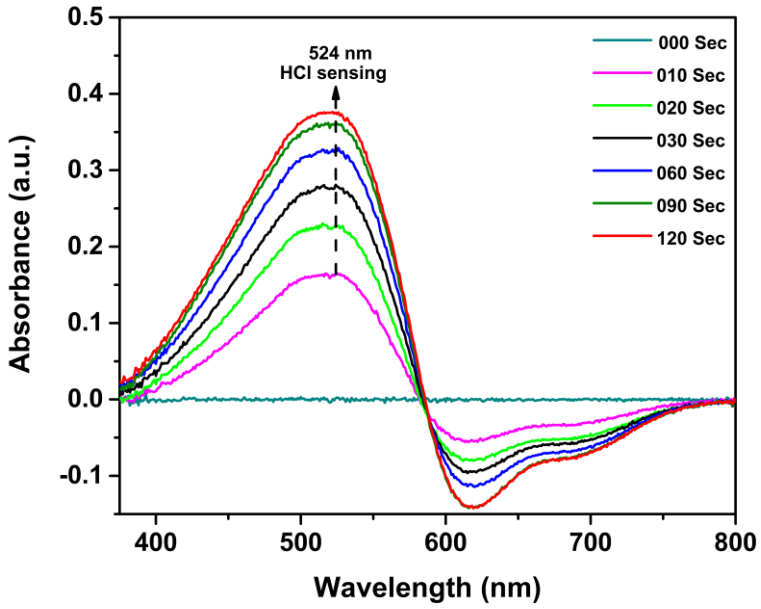

Figure 55. Absorption spectra of the F_{2R} upon exposure to HCl vapors up to 120 seconds.

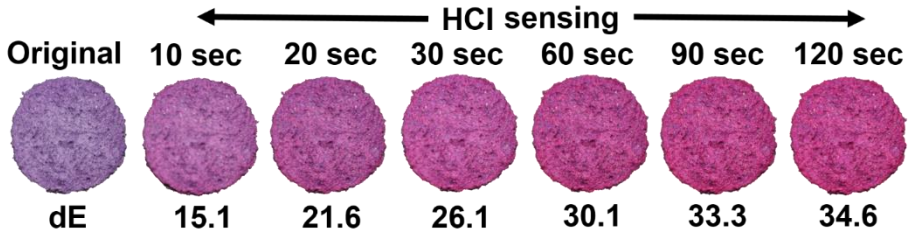

Figure 56. Corresponding color changes of the F_{2R} foam upon exposure to HCl vapors with the dE values compared to the original foam.

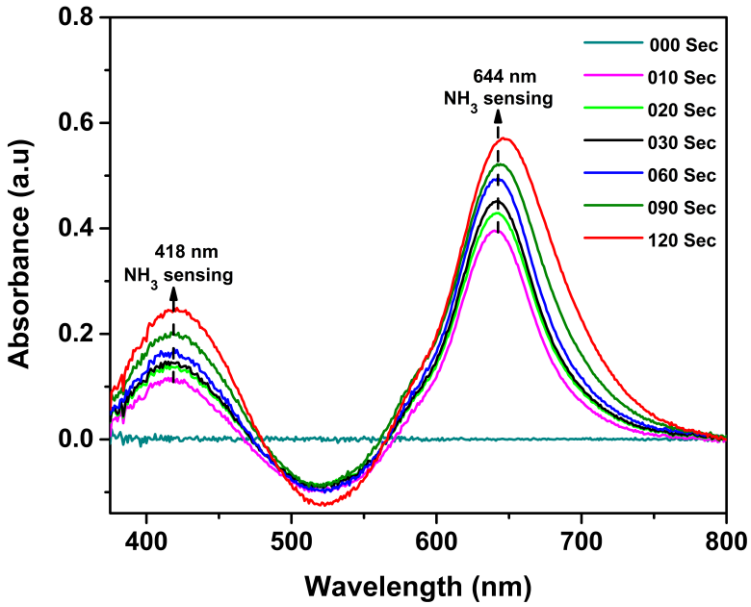

Figure 57. Absorption spectra of the F_{2R} foam upon exposure to NH_3 vapors up to 120 seconds.

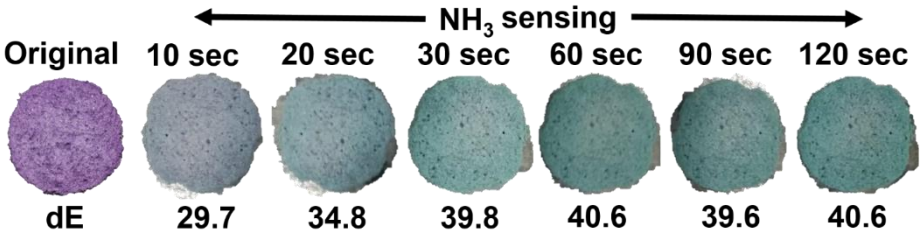

Figure 58. Corresponding color changes of the F_{2R} foam upon exposure to NH_3 vapors with the dE values compared to the original foam.

3.3.9 Reversibility test

The results for the reversibility and reusability of the indicator foam (F_{2R}) are presented in Figure 59-61. For that purpose, the F_{2R} foam was exposed to HCl and NH_3 vapors alternatively up to 15 cycles. As evident in Figure 59 and Figure 60, the indicator color becomes red after exposure to HCl vapors due to protonation of the RCA and the formation of flavylium cations, with the absorption spectrum to present a peak at 524 nm. The intensity of that peak decreases gradually with the increase in the exposure time to NH_3 vapors. Almost after 60 seconds of reaction with the NH_3 vapors, a new peak (634 nm) is appeared corresponding to the green color indicating an increase in the alkalinity of the indicator foam. However, the indicator color becomes green with exposure time greater than 120 seconds which is characteristic of the interaction of the RCAs with the basic environment due to deprotonation and formation of the anionic quinoidal base. However, the interaction with NH_3 vapors for less than 2 minutes, under the specific experimental conditions, favors the partial deprotonation of the RCA and the absorption intensity of the peak at 524 nm seems to stabilize after 90-120 seconds of exposure to a minimum value. Furthermore, the CIELab analysis (Figure 60) also confirmed the

reversibility of the indicator by showing a continuous decrease in the dE value upon exposure to NH_3 vapors.

This process is repeatable for diverse cycles producing the purple-red-purple color change upon sequential exposure to HCl and NH_3 vapors confirming the reversibility, reusability, and stability of the developed pH colorimetric porous indicators under specific conditions. In fact, as presented in Figure 61, after the HCl exposure, the exposure to NH_3 vapors for less than 2 minutes causes the partial deprotonation of the cations, inducing thus the recovery of the original color of the indicators, and the decrease of the absorption intensity of the peak to a minimum value. The subsequent exposure to HCl, results in the further protonation of the deprotonated species, while the NH_3 exposure that follows, induces their partial deprotonation. This process continues for more than 15 cycles. As seen in Figure 61 in each cycle not all the deprotonated, of the previous cycle, species protonate and in the same way, not all the protonated species deprotonate upon NH_3 exposure, however the color change of the foam indicators is still evident.

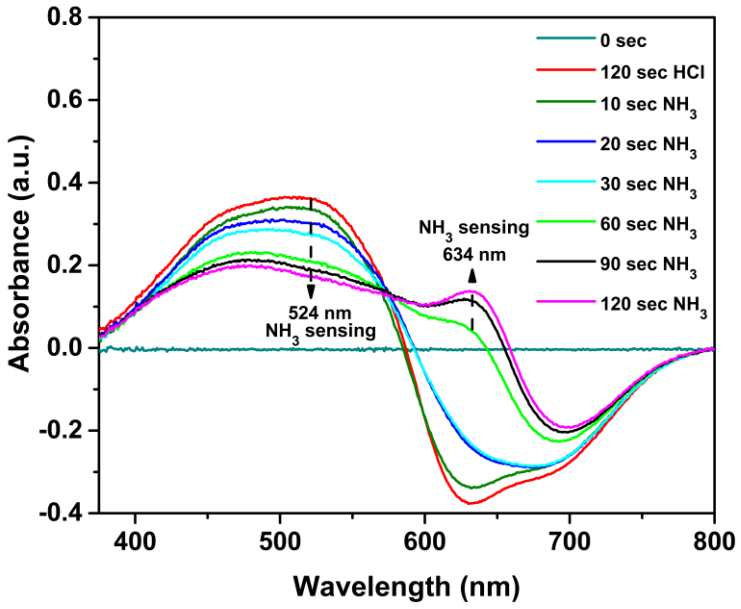

Figure 59. Absorption spectra for one complete recovery cycle of the F_{2R} foams upon consecutive exposure to HCl for 120 seconds and to NH_3 vapors for 120 seconds. The negative absorption spectra is due to the background subtraction as colored foam (F_{2R}) before exposure to vapors was used to acquire baseline correction.

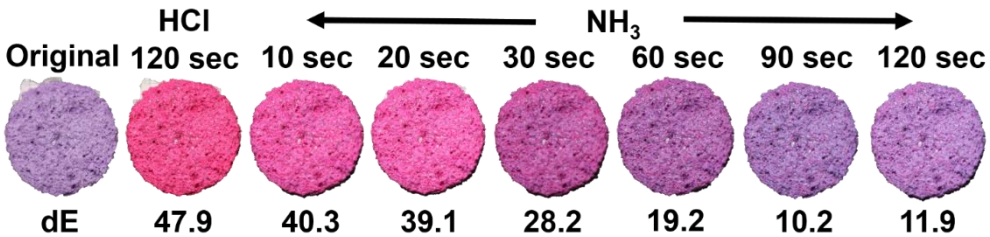

Figure 60. Corresponding color changes of the F_{2R} foams upon consecutive exposure to HCl for 120 seconds and to NH_3 vapors for 120 seconds and calculated dE values with respect to the original foam.

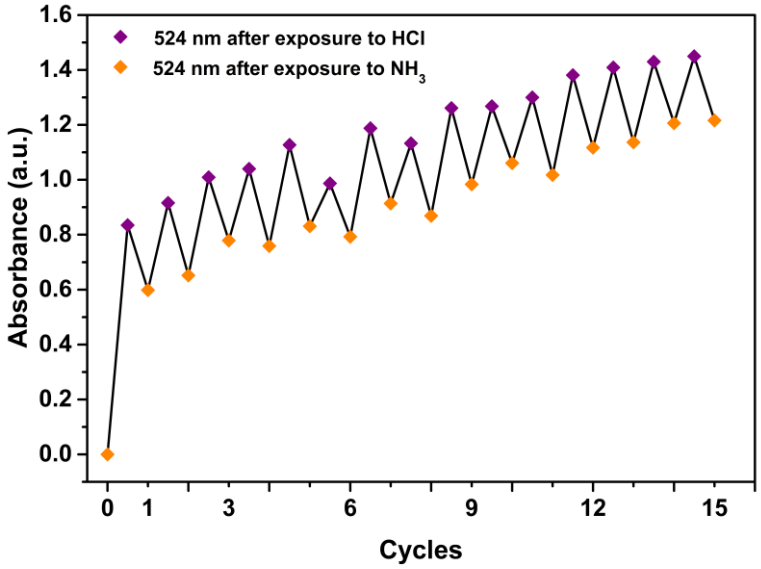

Figure 61. Absorption intensity of the F_{2R} at 524 nm upon 15 alternating HCl and NH_3 exposure cycles.

3.3.10 Interaction of the foams with meat products

In the end, the response of the indicator foam (F_{2R}) against fresh chicken and prawns was evaluated at ambient conditions in closed petri dishes. In the case of chicken (Figure 62), the indicator produces a clear color change just after one day of exposure, turning from purple (dE = 0 original sample) to violet (dE = 9.1) due to the generation of TVB-N [30], [65], [168] demonstrating the spoilage of the food product. On the second day, the change in violet color becomes intensified as confirmed by a slight increase in the dE = 10.2. The indicator produces greenish color after three days of exposure with a remarkable increase in the dE = 30.6 showing the effectiveness of the indicator as the pH of the surrounding environment becomes highly alkaline due to the severe bacterial growth [30], [65], [168].

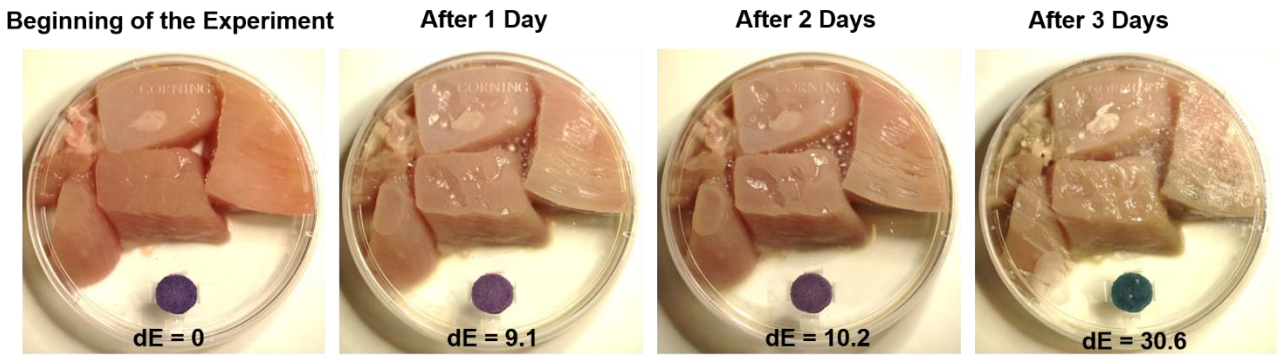

Figure 62. Application of the indicator for the evaluation of chicken freshness.

Likewise, in the case of the fresh prawns (Figure 63), the indicator color was purple (dE = 0) at the beginning of the experiment and changed to blueishgrey (dE = 17.6) just after one day of exposure followed by the change in the intensity of the color at the second day with a slight increase in dE = 21.3. The indicator turns greenish grey after three days of storage with a remarkable increase in the dE = 36.9. The indicator foams performance is significantly better compared to other studies presented so far, in fact, PVA/chitosan films combined with mulberry anthocyanin show minimum changes after 1 day of exposure to meat dE = 2.7 as also tara gum/cellulose films functionalized with anthocyanin extracted from vitis amurensis husk (dE = 1) [166], [170]. Hence, the developed indicator foams can be efficiently used to indicate the food spoilage of the meat products with perceivable color changes and therefore can potentially be used in intelligent food packaging applications.

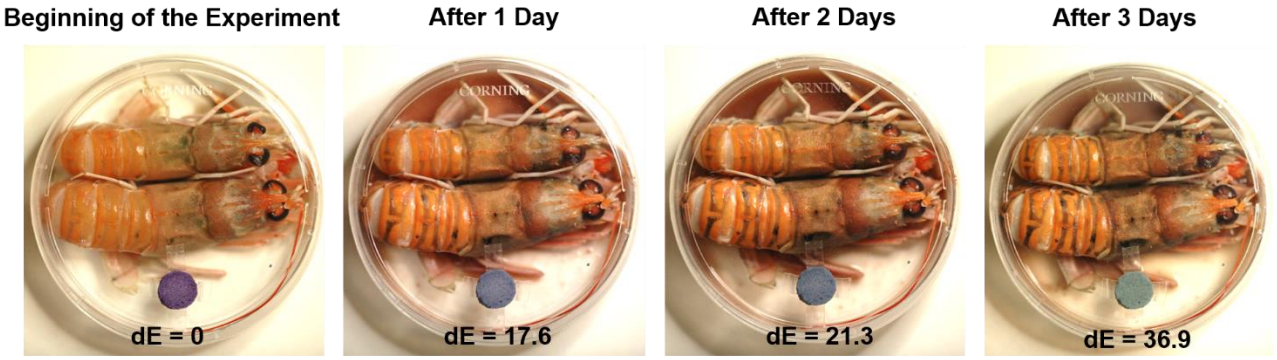

Figure 63. Application of the indicator for the evaluation of prawns freshness

3.4 Conclusions

In the present study, multifunctional and reusable colorimetric pH indicator foams based on biodegradable materials e.g. PVA, MCC and RCA were prepared. The SEM, BET and mercury intrusion porosimetry analysis revealed that the indicator foams have highly porous interconnected structure in the mesopores and macropores range and the addition of MCC to the PVA/PVP matrix increases significantly the porosity of the indicator foams that in turn improve the responsiveness of the indicator foams. Furthermore, the polymer matrix shows strong hydrogen bonding interactions with the MCC and RCA. The pH indicator foams show distinct color changes against different aqueous solutions in a broad pH range and also respond promptly within seconds against HCl and NH_3 vapors. Moreover, during the food spoilage test indicator foams efficiently respond to biogenic amines/TVB-N by producing a clear color change just after one day of exposure to meat or fish products that can be easily perceived by the human eye. These results suggest that the newly developed pH indicators can be employed in different sensing application especially intelligent food packaging, industrial chemical plants and environmental protection.

Chapter 4. Biodegradable smart food packaging films based on renewable resources

Abstract

This study aims to develop bioplastic films based on renewable resources by the combination of red cabbage powder and chitosan for smart food packaging applications. The effect of the chitosan concentration on the morphology of the smart packaging films was observed by scanning electron microscopy (SEM), and on their mechanical properties by universal testing machine (UTM). The chemical interactions between the components was explored by fourier transform infrared spectroscopy (FTIR), while the films' stability in water by solubility studies and water contact angle (WCA) measurements. The performance of the developed films in smart food packaging applications was evaluated by studying their water vapor permeability (WVP), their antioxidant activity and their optical color changes upon exposure to acidic or basic vapors through UV-Visible spectroscopy. Finally, the biological oxygen demand (BOD) characterization was employed to evaluate the biodegradability of the bioplastic films. Following such methodology, it can be concluded that the chitosan and the red cabbage powder interact via hydrogen bonding which results in the formation of films with good mechanical and water vapor barrier properties. On the top, the developed films have excellent antioxidant activity against DPPH• free radicals, and are biodegradable in sea water. Such features, in combination with their distinct color changes in the presence of acidic or basic environments, make the herein presented bioplastic films feasible for smart packaging applications.

4.1 Introduction

Plastic is one of the most consumed materials in daily life and their consumption is growing worldwide day by day. The production of plastics reached 407 million metric tons worldwide in 2015, owing to their excellent physical properties, easy processing and low cost [78], [171]. Unfortunately, they have a significantly negative impact on the environment as most of the plastic materials are disposed in non appropriate ways and due to the fact that their majority is non biodegradable and therefore remains in the environment as persistent wastes (Table 9). Not only they do not biodegrade but also release small toxic fragments e.g. phthalates, bisphenol A and polychlorinated biphenyls that further pollute the ecosystem [171]. A great source of such plastic pollution are the packaging plastic materials. Additionally, the depletion of the nonrenewable resources of petroleum, source of the synthetic plastic materials, is a fact, indicating that in the near future will be faced scarcity of resources for the production of such widely used materials. Therefore, it is necessary to focus research on the development of innovative plastic materials for food packaging, from renewable resources with minimal environmental impact.

Table 9. Global plastic production and waste generation in 2015 [78].

Polymer type	**Production (Million metric tons)**	**Waste (Million metric tons)**
Packaging	146	141
Transportation	27	17
Building and Construction	65	13
Electrical and Electronics	18	13
Consumer and Institutional Products	42	37
Industrial Machinery	3	1
Textiles	59	42
Others	47	38
Total	**407**	**302**

To address the aforementioned issue, the production of bioplastics from naturally occurring biopolymers and agro-waste as alternative feedstocks is attracting the attention of researchers [172]. Cellulose is the most abundant naturally occurring biodegradable polymer on earth with an annual production of about 1.5×10^{12} tons [158], [172], and it is considered as one of the most promising renewable resources for replacing the petroleum-based plastics [172]. Cellulose is a basic component of plants, vegetable and fruit peels. Considering the fact that every year around 1.3 billion tons of food is wasted worldwide, with fruits and vegetables to have the highest wastage ratios [132], it is considered the utilization of such waste as a new source of raw materials for cellulose based bioplastics. Their valorization can minimize the problems related to fossil fuel plastics, since it could significantly improve the sustainability of our economy [132], [173].

So far, different strategies that involve the utilization of diverse solvents e.g. trifluoroacetic acid (TFA), NaOH, N-Methylmorpholine N-oxide (NMMO), lithium chloride with N,N'-dimethyl acetamide (LiCl/DMAc), 1-alkyl-3-methylimidazolium chloride and 1-butyl-3-methylimidazolium chloride [132], [172], [174] are used to convert the agro wastes into value added cellulose based products (bioplastics) with excellent mechanical properties and full biodegradability [175], [176]. For example, Bayer et al. [171] developed bioplastics from edible vegetable waste (e.g. parsley and spinach stems, rice hulls and cocoa pod husks). The process adopted directly converts the cellulose based plant waste into bioplastic in the presence of a solvent trifluoroacetic acid (TFA). This process induces the amorphization of cellulose in the presence of TFA that allows the production of bioplastic entirely made from vegetable or biomass. In a similar but more sustainable route, Perotto et al. [132] developed bioplastic from unusable vegetable waste (e.g. parsley, carrot, cauliflower and radicchio) by partially hydrolyzing the cellulose in HCl based solutions. The above mentioned fabrication methods require huge amounts of toxic ionic and organic solvents that need to be recycled in order to prevent the environmental pollution. However, most of the ionic liquids are non volatile (e.g. 1-

alkyl-3-methylimidazolium chloride and 1-butyl-3-methylimidazolium chloride) and non recyclable, restricting thus their use at in large scale applications [172].

In the present study, smart packaging films were developed by processing red cabbage powder with a water based solution without the need of utilization of organic and ionic solvents. To improve the properties and the usability of the developed films chitosan is introduced in the formulation, and its concentration effect on the properties of the red cabbage bioplastic is evaluated.

The results of this study showed that the presence of chitosan to the red cabbage bioplastic improves its stability to water. The presence of chitosan enhances the tensile modulus and water vapor barrier performance of the developed films due to the formation of hydrogen bonds between the chitosan and red cabbage matrix. The developed bioplastic films showed excellent antioxidant activity (90%) and biodegradability when immersed in seawater for 10 days. Moreover, distinct color changes are produced under acidic or basic vapor environments. Considering all these properties, we propose the utilization of the developed biocomposite films in smart food packaging applications.

4.2 Materials and methods

4.2.1 Materials

The fresh red cabbage was purchased from the local supermarket. Chitosan with medium molecular weight, 2, 2-diphenyl-1-picrylhydrazyl (DPPH), re-agent grade 37% hydrochloric acid (HCl) and ammonium hydroxide (NH_4OH) solution (30%) were purchased from Sigma Aldrich and were used without further purification. In all experiments, ultrapure MilliQ water was used.

4.2.2 Process for making red cabbage powder

The red cabbage was crushed with the home chopper and then dried in the oven at 40°C. Then, the dried red cabbage was converted into very fine powder by using 0.12 mm sieve in the dry milling machine IKA Pilotina MC.

4.2.3 Fabrication of the bioplastic films

5% w/v red cabbage powder was added in water along with different chitosan quantities such that the final concentration of the chitosan in the biocomposites remains as 0, 9, 23, 33, 41 and 50 wt%. The biocomposite solutions were subjected to vigorous stirring on the hotplate at 40 °C for 48 hours to ensure the complete dissolution of the chitosan. Followed by pouring on the petri dishes and the water was allowed to evaporate until the complete drying of the biocomposite films. After drying, uniform freestanding films with thickness of 115µm ± 5µm were obtained. The films are named as PRC, 9% CRC, 23% CRC, 33% CRC, 41% CRC and 50% CRC with respect to the wt% of chitosan present inside the structure.

4.2.4 Scanning electron microscopy (SEM)

To study the surface and cryo-fractured cross-sectional morphologies of the pure RC bioplastic and CRC biocomposites, scanning electron microscopy imaging was performed (SEM, JEOL JSM-6490AL) after coating the specimens with 10 nm thin gold layer using a Cressington 208HR high-resolution sputter coater (Cressington Scientific Instrument Ltd., UK).

4.2.5 Fourier Transform Infrared Spectroscopy (FTIR)

The chemical composition of pure RC powder, pure RC bioplastic and CRC biocomposites and the potential intermolecular interactions between the RC matrix and chitosan were characterized by Fourier Transform Infrared Spectroscopy (FTIR) analysis. The single-reflection attenuated total reflection (ATR) infrared spectra were obtained with a Fourier Transform Infrared (FTIR) spectrometer (Vertex 70v FT-IR, Bruker) coupled with the diamond crystal. All spectra were recorded in the range from 3800 to 600 cm^{-1} with a resolution of 4 cm^{-1}, accumulating 128 scans.

4.2.6 Water solubility

The weight loss of the PRC and CRC composite films were recorded by immersing the 50 mg samples of bioplastics in 20 ml of water. The bioplastic films were vacuum dried before and after immersion in water. The weight loss was calculated according to the following equation.

$$\text{Water solubility} = \frac{\text{dry weight before immersion} - \text{dry weight after immersion}}{\text{dry weight before immersion}} \times 100\% \quad \text{Equation 10}$$

For each sample the data acquisition was performed after 5, 15, 30, 45 and 60 minutes and each data corresponds to the average of three different samples.

4.2.7 Moisture regain

The moisture regain of the vacuum dried PRC and CRC composite films were characterized under 100% relative humidity environment for 24 hours. The moisture regain was calculated according to the following equation and the average values of three different samples are reported.

$$\text{Moisture regain} = \frac{\text{final weight} - \text{initial weight}}{\text{initial weight}} \times 100\% \quad \text{Equation 11}$$

4.2.8 Water contact angle

The static water contact angle of the films was obtained by an optical contact angle measurement instrument (Data Physics OCAH 200, Germany). A droplet volume of 5µl and droplet age of 30 seconds was used for all water contact angle experiments. Three different films of each type were used for experiments, for each film five measurements were recorded at different places and the average values are reported for each type of film.

4.2.9 Water vapor permeability

The water vapor permeability (WVP) of the PRC and CRC composite films was determined gravimetrically according to the ASTM E96/E96M standard method [111], [112], [177]. The tests were carried out at ambient temperature under 100% relative humidity gradient (ΔRH%). 400 µl of distilled water (which provides 100% RH inside the permeation cell) was placed in each of the permeation cells with a 10 mm inner depth and an inner diameter of 7 mm. The test films were cut in circular form using a dye cutting press, and then were mounted on the top of the permeation cells. The permeation cells were placed in a desiccator, which contained anhydrous silica gel as a desiccant in order to maintain 0% RH [49]. The water transferred through the test films and absorbed by the desiccant was determined from the weight loss of the permeation cell after every hour for an 8 hour period using an electronic weighing balance (0.0001 g accuracy). The weight loss of the permeation cells was plotted as a function of time. Then, the water vapor transmission rate (WVTR) was

determined from the slope of each line obtained from the linear regression, as shown by the following expression.

$$WVTR = \frac{Slope}{Area\ of\ the\ film} \qquad \text{Equation 12}$$

The WVP of the films was calculated as follows [111], [112], [177].

$$WVP = \frac{WVTR \times L \times 100}{P_S \times \Delta RH} \qquad \text{Equation 13}$$

Where, L (m) is the film thickness, ΔRH (%) is the relative humidity gradient and P_s (Pa) is the saturation water vapor pressure at 25 °C. The results are reported as a mean of 5 repetitions from different films with their standard deviation.

4.2.10 UV-visible spectroscopy

UV-visible (UV-Vis) spectroscopy was used to determine the absorption of solutions, PRC and CRC films. All the solutions were kept in a quartz cuvette (3.5 ml capacity) that was placed in the sample holder of Varian CARY UV–Vis spectrophotometer (CARY 6000i, USA). The release kinetics, response kinetics of the PRC and CRC composite films and the antioxidant tests were performed by UV-visible (UV-Vis) spectroscopy in the wavelength range of 200-800 nm.

4.2.11 Release kinetics of the films

For the release kinetics, 10 mg of the developed films were placed in water such that the sample concentration in the solution to be 0.10% (w/v). The absorbance of the extracted material in the solution was recorded after 1, 3, 5, 10 and 15 minutes intervals, using pure MilliQ water for the baseline correction. Following this process, three different samples were tested, and the average absorbance value of the characteristic peak of the anthocyanin (278 nm), was calculated for each time interval.

4.2.12 Antioxidant activity

To investigate the antioxidant activity of PRC and CRC composite films, the extracts from different vials containing 0.1% (w/v) PRC and CRC composite films were collected after time intervals of 1, 3, 5, 10 and 15 minutes. The antioxidant activity of the PRC and CRC composite films was determined by using a slightly modified standard DPPH• free radical scavenging method [177]. In particular, 2 ml of the extract solution was mixed with 2 ml of 0.1 mM solution of DPPH• in ethanol and kept in the dark. After 30 minutes, the absorbance of this solution was measured. The absorbance of a second solution was measured by mixing 2 ml of extract solution with 2 ml of ethanol. Finally, the spectrum of the absorbance was obtained by mixing 2 ml of 0.1 mM solution of DPPH• in ethanol

with 2 ml of water. The percentage of DPPH• scavenging activity was calculated according to the following equation.

$$\text{Radical scavenging activity (\%)} = \left[1 - \frac{A_1 - A_2}{A_3}\right] \times 100 \qquad \text{Equation 14}$$

Where A_1 is the absorbance value at 517 nm of the solution containing the curcumin extract and the DPPH• radical, A_2 is the absorbance at 517 nm of the curcumin extract with ethanol and A_3 refers to the absorbance of DPPH• control solution at the same wavelength. All the results are reported as an average of three repetitions of different samples.

4.2.13 Biological oxygen demand (BOD)

Biodegradability of the samples was assessed by means of Biochemical Oxygen Demand (BOD), which can be easily determined by monitoring the oxygen consumption in a closed respirometer. In detail, about 20 mg of bioplastic films were added to 432 ml of seawater as the single carbon source. The seawater was chosen in order to mimic real environmental conditions, and it already contains microbial consortia and the saline nutrients needed for such a process.

4.2.14 Interaction of the bioplastic films against vapors

The response kinetics of the bioplastic films to acidic or basic vapors were evaluated by exposing them to HCl and NH_3 vapors for a total time of 10 minutes, generated in a closed environment (petri dish dimensions: 100 mm × 20 mm diameter (D) x height (H) respectively) with the help of HCl and NH_4OH solution drops (800 μl and 400 μl respectively) and the UV-Vis spectra were recorded after every 1, 3, 5, 7 and 10 minutes.

4.3 Results and discussion

4.3.1 PRC and CRC bioplastic films

Red cabbage contains considerable amounts of cellulose, hemicellulose, lignin, waxes (cutin), pectins and a rich source of the great variety of minerals, vitamins, sugars and, antioxidants (anthocyanins) [178]–[181]. The fresh red cabbage was chopped, dried and pulverized in the laboratory and used without further processing. The 5% w/v red cabbage powder was added in water and processed on the hotplate at 40 °C for 48 hours under vigorous stirring. The viscosity of the solution increases after few minutes possibly due to the dissolution of sugars, pectins and waxes present in the red cabbage [132]. After a few hours, a more homogeneous dispersion of the red cabbage mixture with significant swelling (thickening of the mixture) was observed. The freestanding flexible edible bioplastic films were obtained after casting the mixture and drying. It is believed that the crystalline cellulose and the non-soluble portion of the red cabbage are responsible for the film formation while the soluble sugars, waxes and pectins act as plasticizers that offer flexibility to the films [132]. Usually, acid from the external source is added to facilitate the dissolution/hydrolysis of sugars, waxes, pectins [132] and other soluble portion of the vegetables but here, the inherent acidity of the red cabbage is utilized for the dissolution purpose as the pH of the mixture decreases 6 to 3 after two days of processing. Similarly, chitosan is blended with other water soluble polymers e.g. PVA and PVP under acidic pH achieved by adding acid [182] but herein, it is presented a novel method for blending the chitosan with red cabbage powder without using acid from an external source. Homogeneous freestanding biocomposite films of chitosan/red cabbage powder were obtained up to the weight ratio of 1:1.

4.3.2 Scanning electron microscopy (SEM)

The effect of the presence of chitosan on the surface and cross-sectional morphologies of the PRC bioplastic is shown in Figure 64. The surface and cross-sectional morphologies suggest that the dispersion of the red cabbage powder is homogeneous. However, with the presence of chitosan, some cracks can be observed in the cross-sectional images that become more evident at higher chitosan concentrations. The presence of cracks in the CRC films is due to the increase in the brittleness/stiffness of the material [183], [184]. In addition to this, cracks could also be the result of the increased amount of undissolved matter in the mixture that increases with an increase in the chitosan concentration as pH of the castable mixture increases from 3 to 4 for PRC and 50% CRC mixture respectively.

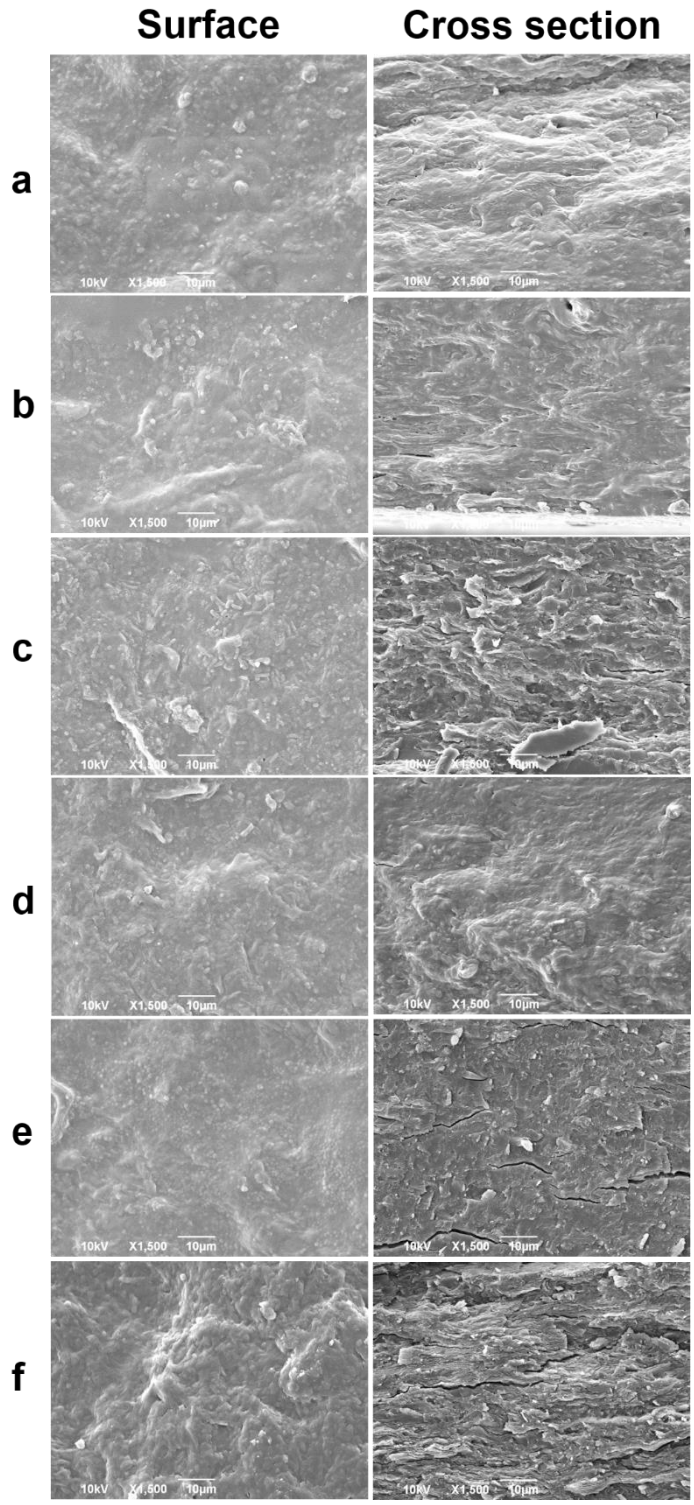

Figure 64. Surface and cross-sectional SEM images for (a) PRC, (b) 9% CRC, (c) 23%CRC, (d) 33% CRC, (e) 41% CRC and (f) 50% CRC bioplastic films.

4.3.3 Fourier Transform Infrared Spectroscopy (FTIR)

To study the possible chemical interactions between the polymer and the red cabbage powder, FTIR spectra of the components were analyzed (Figure 65 and Figure 66). As evident by the spectra (Figure 65) no difference is observed between the pure red cabbage powder and PRC bioplastic with the main

assignments of PRC at 3269 cm^{-1} (OH stretching), C-H stretching at 2924 cm^{-1}, C=C stretching at 1591 cm^{-1}, C-O stretching at 1024 cm^{-1}. On the other hand, in the presence of chitosan some shifts of the main peaks of both the chitosan and PRC bioplastic are observed. For example, in the case of 23% CRC (chosen as a representative sample), the OH stretching band shifted to 3256 cm^{-1} from 3269 cm^{-1} symmetric CH_2 stretching to 2974 cm^{-1} from 2924 cm^{-1} and C=C stretching to 1568 cm^{-1} from 1591 cm^{-1} showing powerful hydrogen bonding interactions. Moreover, with the increase in the chitosan content OH stretching and C=C stretching peaks shifted towards lower wavenumbers showing increases in the hydrogen bonding (indicated by the red dotted line in Figure 66). Figure 67 explains the effect of chitosan concentration on the wavenumbers of OH and C=C stretching peaks. As evident in figure wavenumbers of both the stretching peaks decrease gradually with the increase in the chitosan concentration indicating strong molecular interactions.

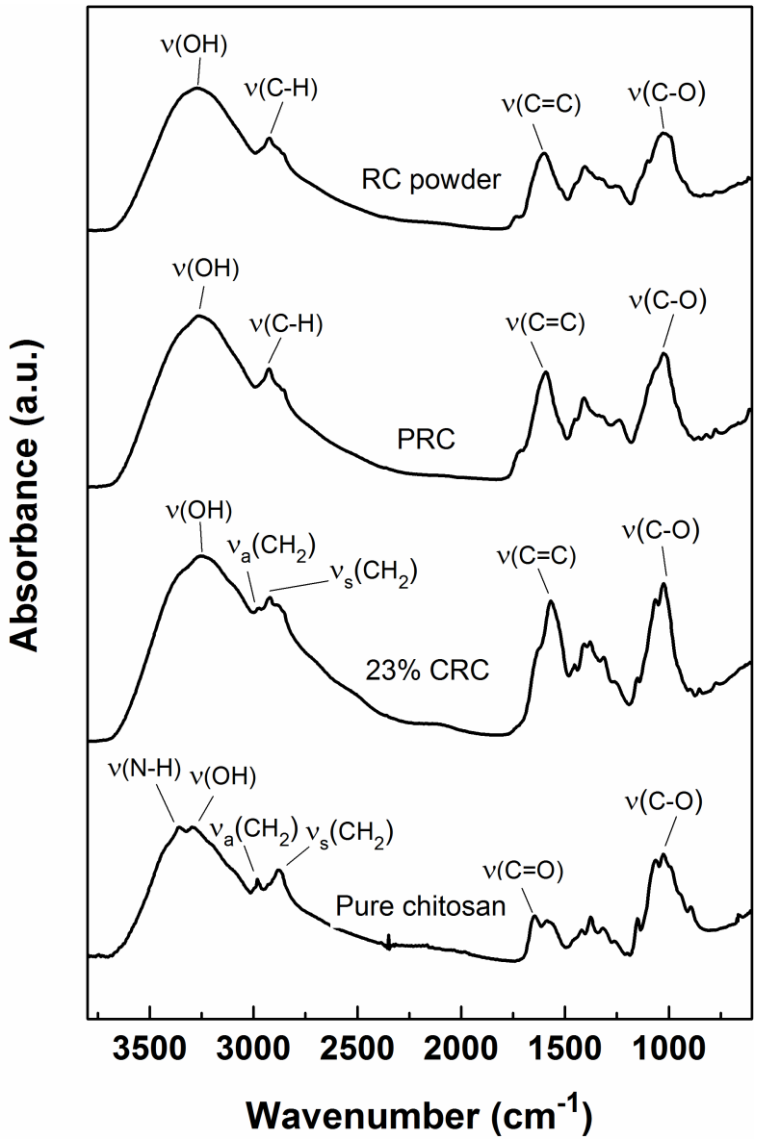

Figure 65. FTIR spectra for pure RC powder, pure chitosan, PRC, 23% CRC bioplastic films.

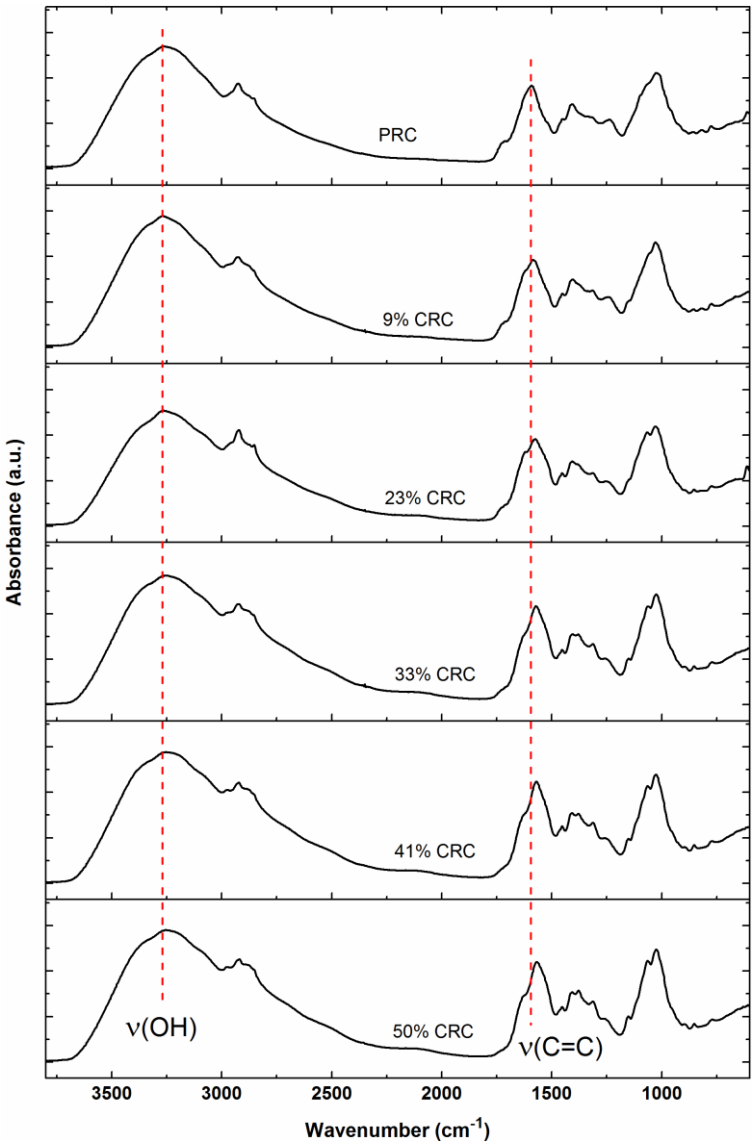

Figure 66. FTIR spectra for bioplastic films.

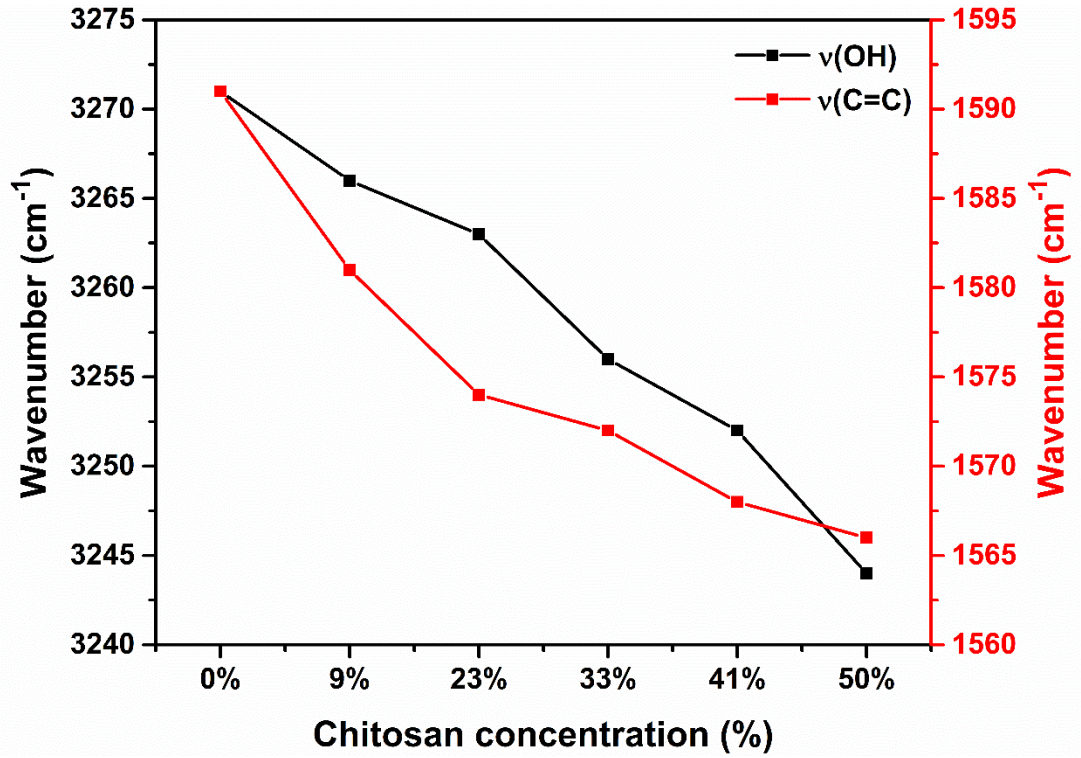

Figure 67. Changes in the wavenumber of OH and C=C stretching with chitosan concentration.

4.3.4 Interaction with water

One of the disadvantages of bioplastics is their unfavorable interaction with water. In this study, the interaction of bioplastics with water is characterized in terms of weight loss in water, moisture regain, water contact angle and water vapor permeability.

4.3.4.1 Water solubility

The water solubility is an important property of the packaging films. In general, packaging films with higher water solubility tend to dissolve easily in water due to the hydrogen bonding interactions between the absorbed water molecules and the packaging material [185]. For general packaging and food packaging applications, less water solubility is desired but in the case of edible films and coatings medium to high water solubility is of great interest [186]. The effect of the chitosan content on the water solubility is presented in Figure 68. As shown, all bioplastic films containing chitosan show similar kind of behavior with a weight loss of almost 50% just after 5 minutes of exposure to water which reaches up to 70% after 60 minutes. The higher solubility of the bioplastic films is attributed to their hydrophilic character and therefore to their strong molecular interaction with the water molecules [185]. In the absence of chitosan, and therefore for the pure PRC, after 60 minutes it is observed the complete disintegration of the films in the water. This is not the case for the CRC composite films which maintain their integrity/shape possibly due to the presence of strong hydrogen bonding interactions between the components as proved by the FTIR analysis.

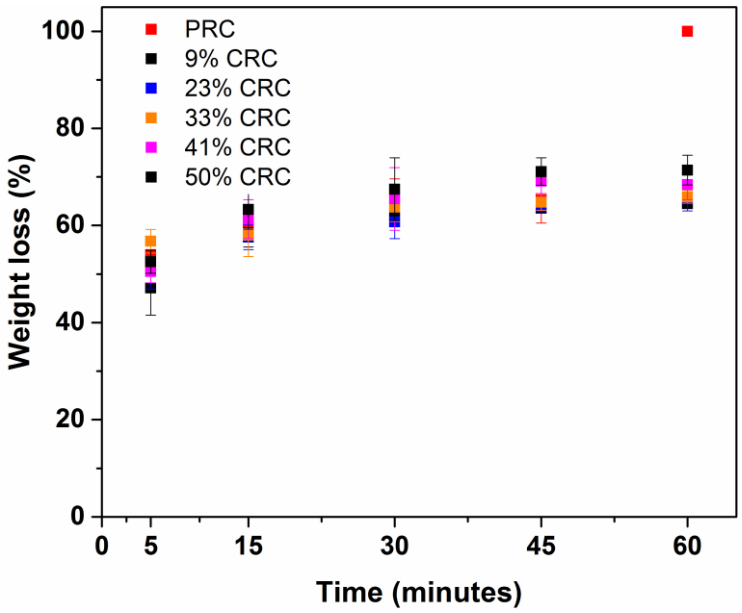

Figure 68. Water solubility results for bioplastic films.

4.3.4.2 Moisture regain

The moisture regain is the ability of a material to absorb moisture from its surrounding environment [187]. It is important to study the moisture regain of the bioplastic films, particularly, for packaging applications because of their high sensitivity towards water molecules [185]. The effect of the chitosan on the moisture adsorption of the bioplastic films was observed under 100% relative humidity for 24 hours. As clearly shown in Figure 69 all CRC composite films show less moisture regain (72% - 77%) compared to the PRC bioplastic (moisture regain 90%). This decrease in the moisture regain is explained by the formation of hydrogen bonds between the chitosan and red cabbage matrix, which in turn reduces the availability of free hydroxyl groups able to interact with the water molecules [187]. These results are in accordance with the literature where the addition of citric acid decreased the moisture absorption of starch based bioplastic films due to the presence of strong molecular interactions between them as a result decreased the availability of free hydroxyl groups to water [187].

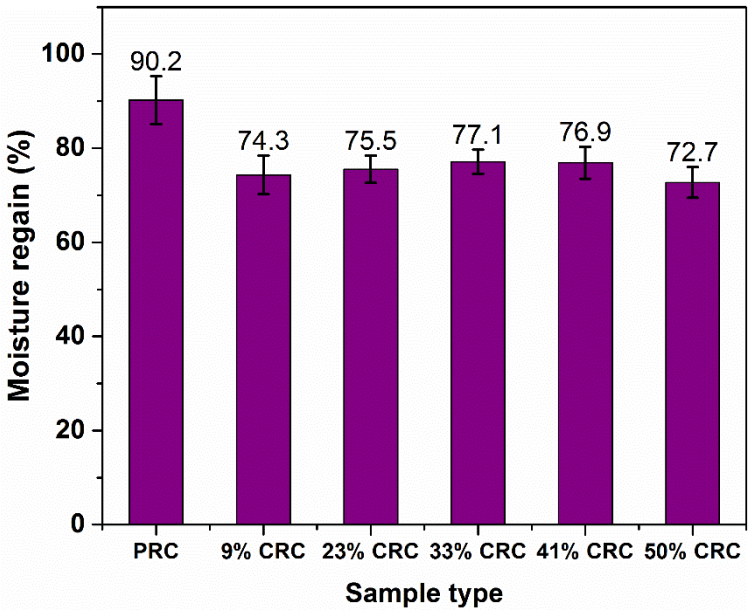

Figure 69. Moisture regain for bioplastic films.

4.3.4.3 Water contact angle and water vapor permeability

The water vapor barrier property is an important parameter that determines the effectiveness of a food packaging material [183]. Water vapor permeability plays an important role to minimize the exchange of moisture between the packaged goods and the surrounding environment [188], [189]. So, the water vapor permeability should be as low as possible [183]. The effect of the presence of chitosan on the water contact angle and water vapor barrier properties is presented in Figure 70. As shown in Figure 70a the PRC film presents the most hydrophilic character while the hydrophilicity of the composite films decreases with the increase in the chitosan concentration (27.4° for PRC and 62.1° for 50% CRC) due to the hydrophobic character of the chitosan and improved molecular interactions among the polymers [190]. This finding is also supported by the Dang et al. [190] study where the increase in the chitosan content increased the water contact angle of the starch/chitosan bioplastic films due to molecular interactions between them. Similarly, the water vapor transmission rate (WVTR) and water vapor permeability (WVP) both decrease gradually (Figure 70b) with the increase in the chitosan content (34% reduction for 50% CRC compared to PRC) due to the increase in the hydrophobicity of the composite films and formation of the hydrogen bonding interactions between the two matrices as proved by the FTIR studies. The higher WVP of the PRC film is due to the higher number of free hydroxyl groups available to water molecules that tend to enhance the molecular interaction with water and increases the WVP through the film [189], [191]. As the chitosan content in the biocomposite film increases the number of free hydroxyl groups available to water decreases due to hydrogen bonding interactions between the polymers. As a result, the water vapor barrier property of the CRC films are improved [188]. The results are in agreement with the Ren et al.[189] study where the increase in the chitosan content decreases the WVP of the corn starch/chitosan bioplastic films by

restricting the availability of hydrophilic groups to the water molecules due to the increase in the hydrogen bonding interaction between the two polymers.

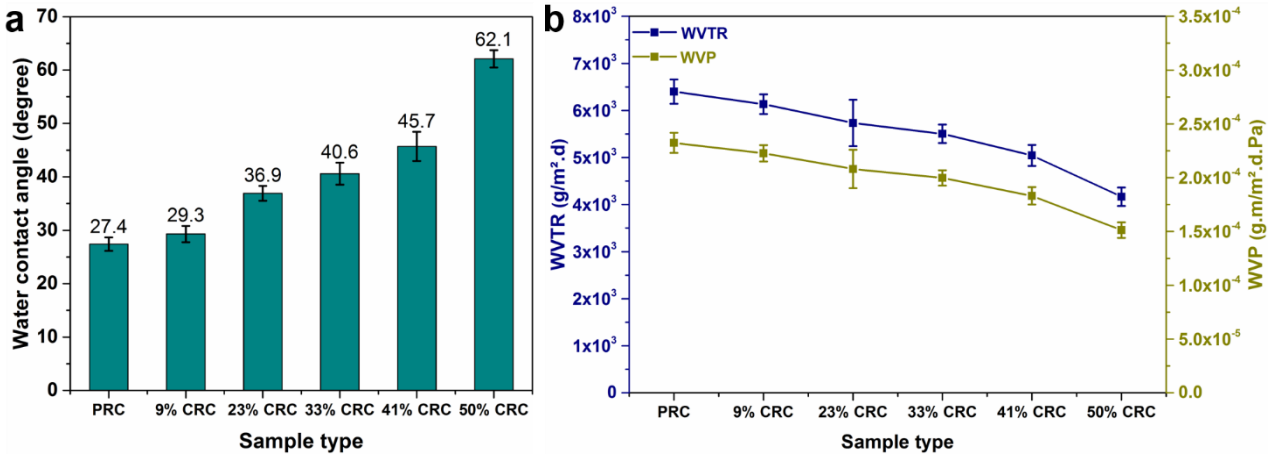

Figure 70. (a) Water contact angle and (b) water vapor barrier properties for bioplastic films.

4.3.5 Mechanical properties

A packaging film should possess adequate mechanical strength and flexibility to maintain the package integrity during handling [189]. The tensile modulus and elongation at break are important parameters that reflect the rigidity/stiffness and flexibility of the packaging films respectively [183], [189], [192]. Usually, higher tensile modulus with higher flexibility is required for packaging applications [183], [189], [192]. The effect of the presence of chitosan on the mechanical properties is shown in Figure 71. It is clear from the Figure 71 that the tensile modulus increases with the increase of the chitosan content and after 9% chitosan addition, a significant increase is observed (355 MPa to 1167 MPa for PRC and 50% CRC respectively), and this is attributed to the presence of hydrogen bonds between the components as proved by the FTIR studies. It is proved that the formation of the strong intermolecular bonding between the two natural polymers increases the tensile modulus [191][192], [193]. On the other hand, elongation at break significantly decreases (10.5% to 1.1% for PRC and 50% CRC respectively) with the increase in the chitosan concentration due to the increase in the stiffness of the material and reduction of the polymeric chain slippage [192], [193]. Nonetheless, the 9% CRC bioplastic showed a slight increase in the elongation at break (11.9%). This increase is attributed to the molecular interaction of the polymeric chains (chitosan) with the plasticizing component of red cabbage (sugars, waxes and pectins) at low chitosan concentration that facilitates the polymeric chain slippage and improves the overall flexibility of the 9% CRC film [189]. Therefore, the mechanical properties of the red cabbage matrix can be tailored just by controlling the amount of chitosan depending on the end application.

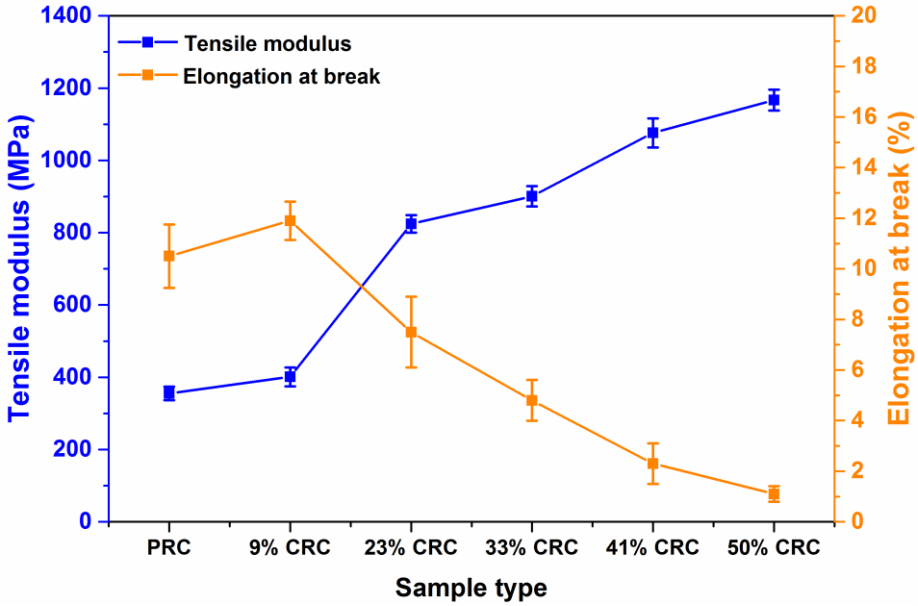

Figure 71. Tensile modulus and elongation at break for bioplastic films.

4.3.6 Release kinetics and antioxidant activity

The effect of the addition of chitosan on the release kinetics and antioxidant activity of the bioplastic films is shown in Figure 72. Specifically, Figure 72a presents the increase of the absorbance peak intensity at around 279 nm with time, due to the release of more water soluble components in the solution for all the films. However, as the amount of chitosan increases in the films, the observed intensity at 279 nm decreases. The decrease in the intensity at 279 is attributed to the continuous decrease in the amount of red cabbage powder in the biocomposite films, increase in the hydrophobicity and molecular interactions with the increase in the chitosan concentration. The DPPH• standard assay was used to determine the antioxidant activity of the bioplastic films towards lipid oxidation [101]. All bioplastic films showed good antioxidant activity (Figure 72b) that increases with time due to higher release of active component in the solution and reaches 90% after 10 minutes of release for all the developed films except 50% CRC (68% even after 15 minutes of release). The low antioxidant activity of the 50% CRC bioplastic film is due to the lower amount of red cabbage powder components released, that contain the active components responsible for the antioxidant potential (50% less compared to PRC). The results of antioxidant activity are also supported by the release kinetics study where the antioxidant activity increases with time due to the increase in the release of the active components, and decreases with the increase of the chitosan content due to less amount of the active components in the composite responsible for the antioxidant activity. This trend is observed up to 5 minutes of release. After that the antioxidant activity is independent of the release in the active component for all the samples except from the 50% CRC (increase with time or decrease with chitosan content not increasing or decreasing the antioxidant

activity). These results proving that such films are ideal candidates for active food packaging applications.

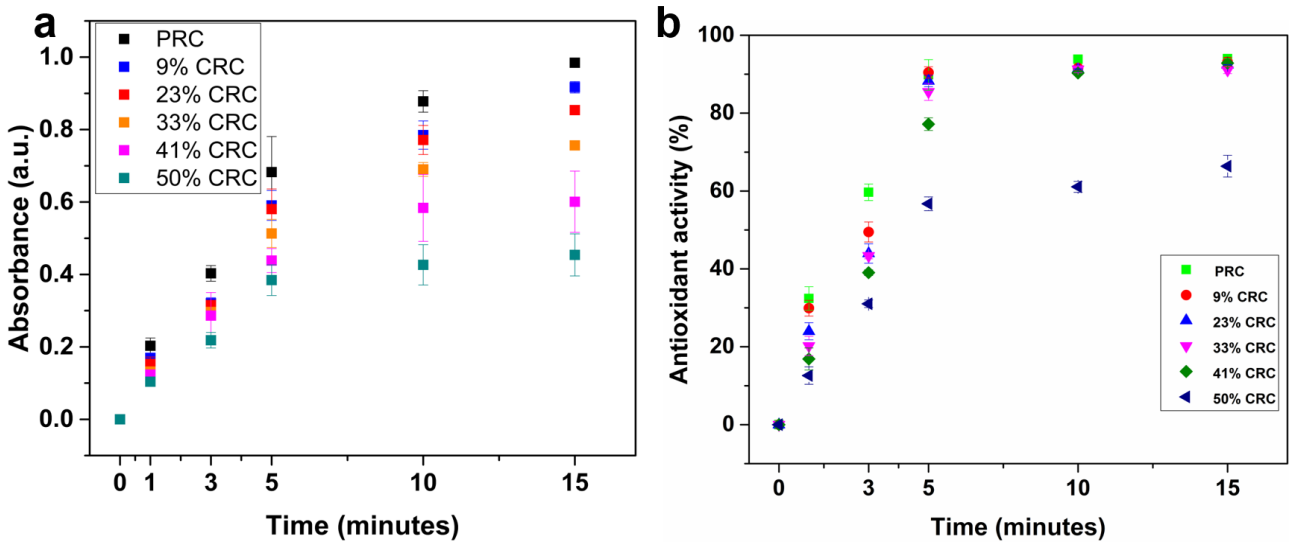

Figure 72. (a) Release kinetics and (b) antioxidant activity for bioplastic films.

4.3.7 Biological oxygen demand (BOD)

The effect of the chitosan on the biodegradability behavior is shown in Figure 73. All the samples show a high level of biodegradability and the general behavior is comparable, although the biodegradability rate slightly decreases with the increase in the concentration of chitosan. The biodegradation kinetics behavior is affected by the chemical composition or the physical properties of the blends [194], [195]. The PRC bioplastic appears to have better biodegradability, while the samples with a higher concentration of chitosan show a slower solubility in water and biodegradation [194], [195]. In addition to this, it becomes more difficult for the microorganisms to break down the polymeric chains into smaller fragments due to strong molecular interactions that increase with the increase in the chitosan concentration as a result biodegradability decreases [194]. In detail, all the samples start to biodegrade after 1-2 days due to the presence of bacteria and microorganisms present in the sea water that uses bioplastic films as a source of nutrients [196]. The amount of oxygen consumed during the digestion/decomposition process is determined and expressed as biological oxygen demand (BOD). After 10 days, the (BOD) is approaching a plateau, achieving values between (38.7 and 49.0 mg O_2/100mg of material for 50% CRC and PRC respectively).

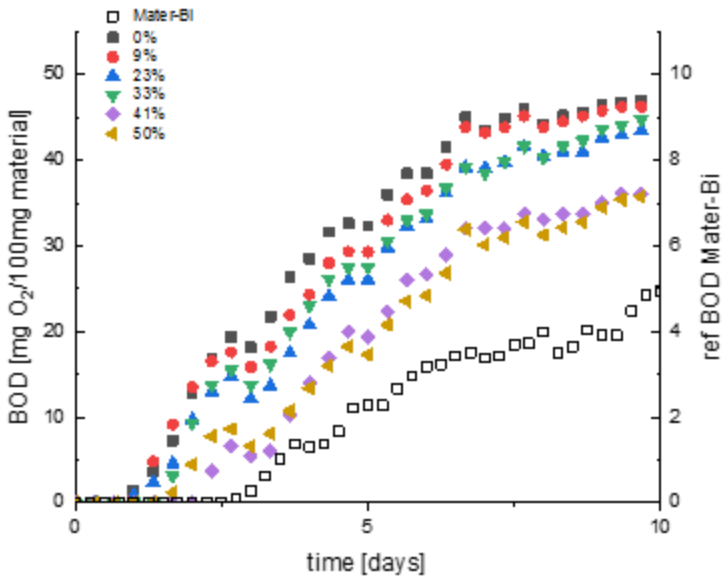

Figure 73. Biological oxygen demand measured for bioplastic films.

All CRC composite films showed stability against water, excellent antioxidant activity and biodegradability but on the basis of mechanical properties 23% CRC bioplastic is selected as the best sample and will be used for further characterization because it gives a fair balance between the tensile modulus and elongation at break that is also a very important parameter for packaging material.

4.3.8 Interaction with the vapors

Red cabbage contains a great variety of anthocyanins, a natural pigment, that can produce color changes upon exposure to environments of different pH (Figure 45 of chapter 3) [64], [178]. Color variations of anthocyanins are produced due to structural changes in the molecules as a result of protonation and deprotonation reactions (Figure 44 of chapter 3) [8], [18], [19]. The response of the 23% CRC bioplastic films upon exposure to HCl and NH_3 vapors is shown in Figure 74-77 and the changes in color were recorded by UV-Vis spectroscopy. As shown in Figure 74 and Figure 75, just after 1 minute of exposure to HCl vapors the film changed color to red and the intensity of the absorbed light (529 nm) keeps increasing with the increase in the reaction time (due to protonation of the red cabbage anthocyanins and the formation of flavylium cations) with the acidic vapors. On the other hand, when the film is exposed to NH_3 vapors, Figure 76 and Figure 77, absorption peaks at around 396 nm and 633 nm appear and their intensity starts increasing with the increase in the exposure time to the NH_3 vapors (due to deprotonation of the red cabbage anthocyanins and the formation of anionic quinoidal base) while the film changes its color just after 1 minute of reaction time, indicating its NH_3 sensing ability. The results of this study suggest that bioplastic films can be used as intelligent packaging materials for monitoring the food freshness.

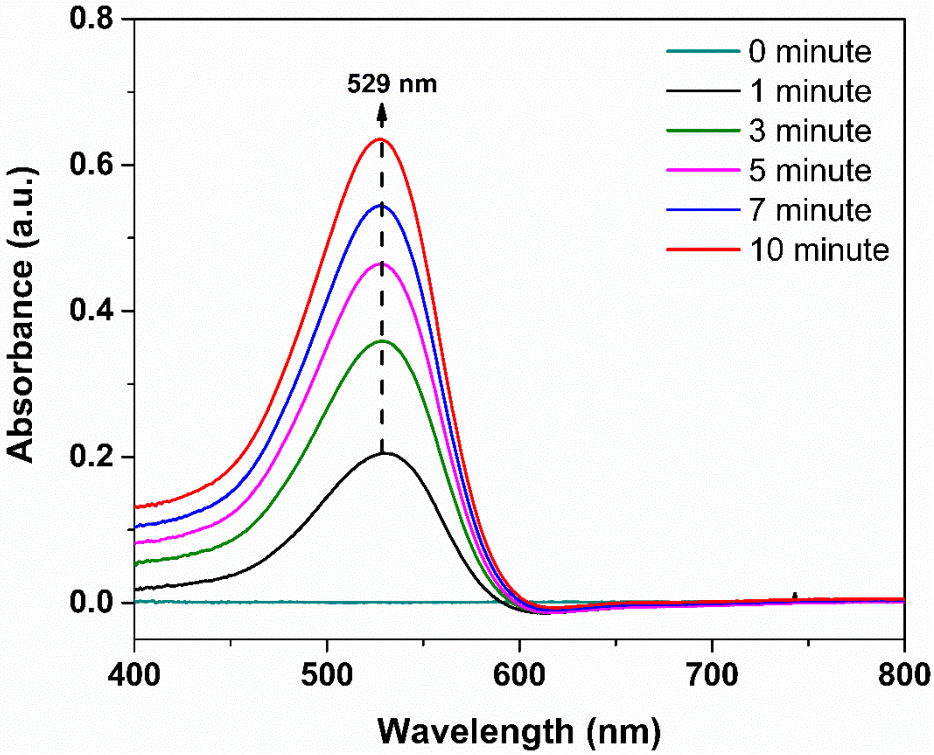

Figure 74. Absorption spectra of the 23% CRC bioplastic film upon exposure to HCl vapors up to 10 minutes.

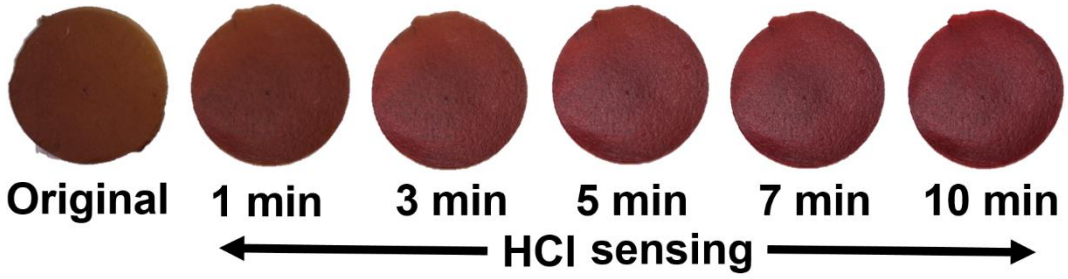

Figure 75. Color modification of the 23% CRC bioplastic film upon exposure to HCl vapors up to 10 minutes.

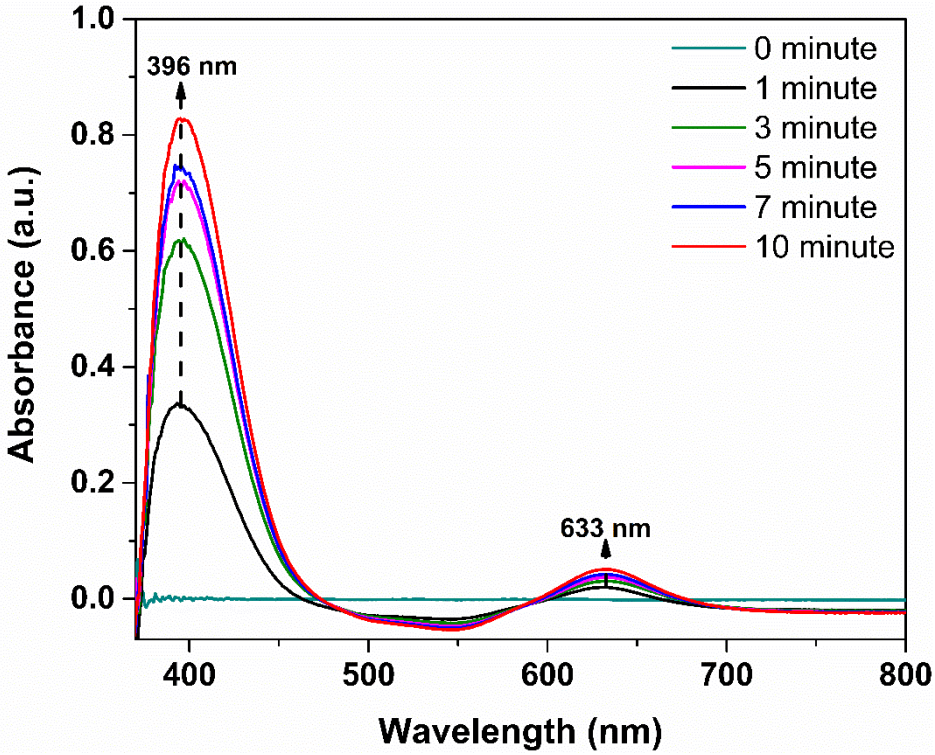

Figure 76. Absorption spectra of the 23% CRC bioplastic film upon exposure to NH_3 vapors up to 10 minutes.

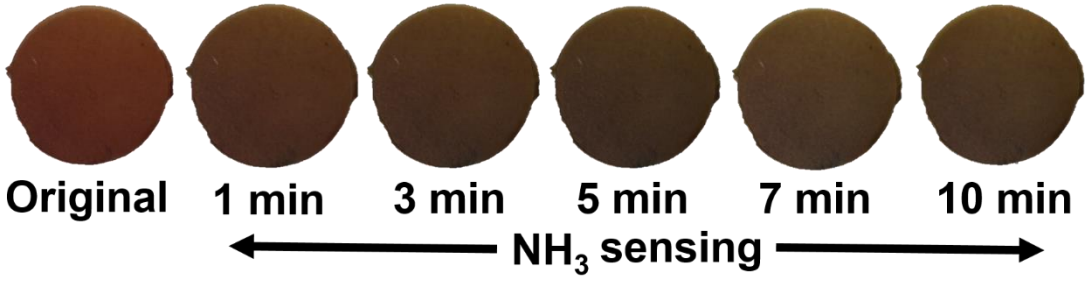

Figure 77. Absorption spectra of the 23% CRC bioplastic film upon exposure to NH_3 vapors up to 10 minutes.

4.4 Conclusion

In the present study, bioplastic films were developed from biomaterials. The chitosan showed good compatibility with the red cabbage powder, improved the stability of the bioplastic films against water and significantly enhanced the water vapor barrier performance and tensile modulus. Compared to pure cellulose and cellulose nanocomposites films, the water vapor barrier performance of the herein presented biocomposites is found to be much better [172], while they present significantly better mechanical performance compared to the one reported for parsley, radicchio and cauliflower bioplastics, and comparable to cocoa and rice bioplastics [132], [171]. In addition, the tensile modulus values of the developed films are higher than the values reported for the commercial oil based packaging films of LDPE and HDPE [132], [171]. The bioplastic films showed excellent antioxidant

activity comparable to other radicchio based bioplastic films [132]. Furthermore, the films showed a fast response to acidic or basic environments, almost 50% faster compared to other anthocyanin based bioplastic films [30]. On top of that, the bioplastic films possess excellent biodegradability, better than the commercial bioplastic Mater-Bi and polylactic acid (PLA) based packaging films [197], and necessary for the minimization of the waste generation caused by the use of the conventional plastic packaging materials. Therefore, the developed multifunctional films may represent an integrated, cost effective and sustainable solution for smart food packaging applications.

Final remarks

This thesis aimed at the development of functional materials for active and intelligent food packaging applications. In the first part of this study, active food packaging films were prepared by the combination of low-density polyethylene (LDPE) and curcumin, a natural antioxidant, through industrially applied methods e.g. extrusion and compression molding. The development of curcumin/LDPE biocomposite packaging films will expand the use of LDPE is active packaging applications and will eliminate the adverse effects that are associated with the use of synthetic antioxidants in active food packaging. In the second part of this study, porous colorimetric indicators were developed by the combination of biopolymers (polyvinyl alcohol and microcrystalline cellulose) and anthocyanin, a natural pigment extracted from red cabbage, for intelligent packaging applications. The development of these biocompatible portable indicators will offer exciting opportunities to enhance the food quality, safety, real time monitoring and shelf life prediction and potentially may overpass conventional techniques e.g. gas chromatography-mass spectrometry and ion exchange chromatography that require the breakage of the package integrity and are not applicable for real time monitoring. In the last part of this study, smart packaging materials were developed by the combination of red cabbage powder and chitosan that integrates the advantages of both the active and intelligent food packaging in a single system. Moreover, the biodegradability of the developed bioplastics will help to reduce the waste generation and harmful effects of the conventional plastics on the ecosystem.

Appendix-I

Table S10. Summary of active packaging materials based on the origin of antioxidants.

Film matrix	**Technique used**	**Antioxidant used / Origin**	**Main activity achieved**	**Reference**
Co-extruded films of high-density polyethylene (HDPE), ethylene vinyl alcohol (EVOH) and low-density polyethylene (LDPE)	Film blowing (Extrusion molding)	Butylated hydroxyanisole (BHA) and butylated hydroxytoluene (BHT) / Synthetic	Active release of antioxidant to whole milk powder	D. Restrepo et al. [17]
Polylactic acid (PLA)	Film blowing (Extrusion molding)	Butylated hydroxyanisole (BHA), butylated hydroxytoluene (BHT), propyl gallate (PG), and tert-butyl hydroquinone (TBHQ) / Synthetic	Active release of antioxidant to food simulant	M. Jamshidian et al. [16]
Polypropylene (PP)	Extrusion molding	Irganox 1076 / Synthetic	Antioxidant for thermal oxidation	V. Ambrogi et al. [18]
Polylactic acid (PLA)	Film blowing (Extrusion molding)	Buthylated hydroxytoluene (BHT) / Synthetic and α-tocopherol / Natural	BHT for thermal oxidation and α-tocopherol for for lipid oxidation	Y. Byun et al. [74]
Polypropylene (PP)	Extrusion and compression molding	Carvacrol and thymol / Natural	Antimicrobial	M. Ramos et al. [14]
Polyethylene (PE)	Extrusion and compression molding	Curcumin / Natural	Antioxidant for thermal oxidation	B. Kirschweng et al. [75]
Polypropylene (PP)	Extrusion and compression molding	Carotenoid solid fraction from tomato waste	Antioxidant for thermal oxidation	P. Cerruti et al. [76]
Chitosan	Solution casting	Green tea extracts / Natural	Antioxidant for lipid oxidation	U. Siripatrawan et al. [12]
Polyethylene (PE)	Extrusion and compression molding	Curcumin / Natural	Antioxidant for thermal oxidation	D. Tatraaljai et a. [77]

Gelatin	Solution casting	Green tea, grape seed, gingko leaf and ginger extracts / Natural	Antioxidant for lipid oxidation	J. Li et al. [13]
Chitosan	Solution casting	Tea polyphenols / Natural	Antioxidant for lipid oxidation	L. Wang et al. [101]
Low-densty polyethylene (LDPE)	Extrusion and compression molding	Carvacrol / Natural	Antimicrobial	M. Perez et al. [22]
Cellulose	Solution casting	Curcumin / Natural	Antimicrobial	N. Luo et al. [100]
Chitosan / Cellulose	Solution casting	Curcumin / Natural	Antimicrobial and antifungal	S. Bajpai et al. [95]
Fish gelatin	Compression molding	Epigallocatechin gallate / Natural	Antioxidant for lipid oxidation	K. Nilsuwan et al. [198]
Low-densty polyethylene (LDPE)	Film blowing (Extrusion molding)	Lotus leaves extracts / Natural	Active release of flavonoids to food	S. Zhang et al. [21]
Chitosan	Solution casting	Black tea and green tea extracts / Natural	Antioxidant for lipid oxidation	Y. Peng et al. [80]
Tara gum / Polyvinyl alcohol	Solution casting	Curcumin / Natural	Antioxidant for lipid oxidation	Q. Ma et al. [102]

Table S11. Summary of intelligent packaging materials based on the origin of pH responsive dyes.

Matrix	**pH senstive dye / Origin**	**Indicator for**	**Reference**
Polyacrylic acid grafted polypropylene films	Methylene blue / Synthetic	Organic acid / Milk	J. Cavallo et al. [59]
Methyl cellulose coatings	Combination of 3 different pH sensitive dyes / Synthetic	CO_2 / Chicken	C. Rukchen et al. [67]
Bacterial cellulose membranes	Bromophenol blue / Synthetic	Acetic acid / Guavas	B. Kuswandi et al. [68]
Cellulose membranes	Methyl red / Synthetic	Amines / Chicken	B. Kuswandi et al. [69]
Silica gel plate	Array of 12 different pH sensitive dyes / Synthetic	Amines / Chicken	U. Khulal et al. [70]
Cellulose acetate membranes	Bromocresol green / Synthetic	Amines / Fish	H. Chun et al. [71]
Silica gel plate	Array of 16 different pH sensitive dyes / Synthetic	Amines / Fish	M. Morsy et al. [72]
TiO_2 nanoporous films	Array of 8 different pH sensitive dyes / Synthetic	Amines	H. Xiao et al. [73]
Filter paper (cellulose) strips	Bromophenol blue / Synthetic	Amines / Buffalo meat	V. Shukla et al. [49]

Polyaniline films	Polyaniline films itself is an indicator	Amines / Fish	B. Kuswandi et al. [50]
Bacterial cellulose membranes	Curcumin / Natural	Amines / Shrimp	B. Kuswandi et al. [51]
Cellophane films	Curcumin / Natural	CO_2 and Amines / Chicken	M. Pávai et al. [52]
PVA / Tara gum films	Curcumin / Natural	Amines / Shrimp	Q. Ma et al. [53]
Pectin films	Curcumin / Natural	Amines / Shrimp	P. Ezati et al. [54]
Chitosan films	Anthocyanin from bauhinia blakeana dunn flower / Natural	CO_2 and Amines / Pork and fish	X. Zhang et al. [31]
Filter paper (cellulose) strip and Agarose gel	Anthocyanin from red cabbage and rose flower / Natural	Amines	V. Shukla et al. [55]
Agar / potato starch films	Anthocyanin from purple sweet potato / Natural	pH indicator and Amines / Pork	I. Choi et al. [56]
Silica gel	Anthocyanin from spinach,red reddish, black rice and jasmin flower / Natural	Amines / Pork	H. Xiao et al. [57]
Hydrophobic nanoporous film	Anthocyanin from 9 different flowers / Natural	Amines / Pork	H. Xiaowei et al. [58]
Chitosan / Polyvinyl alcohol films	Anthocyanin from red cabbage / Natural	pH indicator / Organic acids / Milk	V. Pereira et al. [60]
Bacterial cellulose nanofibers	Anthocyanin from red cabbage / Natural	pH indicator	S. Pourjavaher et al. [61]
Chitosan films	Anthocyanin from grapes / Natural	pH indicator	Yoshida et al. [62]
Chitosan / Pectin films	Anthocyanin from grapes / Natural	pH indicator	V. Maciel et al. [63]
Chitosan / Corn starch films	Anthocyanin from red cabbage / Natural	Amines / Fish	M. Pereira et al. [64]

List of publications

Journals

1. **J. Zia**, U. C. Paul, J. A. Heredia-guerrero, A. Athanassiou, and D. Fragouli, "Low-density polyethylene/curcumin melt extruded composites with enhanced water vapor barrier and antioxidant properties for active food packaging," Polymer., vol. 175, no. May, pp. 137–145, 2019.
2. **J. Zia**, G. Mancini, R. Donno, A. Athanassiou, and D. Fragouli, "Porous pH natural pH indicators for acidic and basic vapor sensing," (Under review).
3. **J. Zia**, G. A. Athanassiou, and D. Fragouli, "Smart food packaging films based on red cabbage and chitosan," (Under preparation).

Book chapter

1. M. E. Genovese, **J. Zia**, and D. Fragouli, "Natural and biocompatible optical indicators for food spoilage detection," (Submitted).

Conferences

1. **J. Zia**, A. Sentahamizhan, A. Athanassiou, and D. Fragouli, "Development and characterization of active food packaging films based on low density polyethylene (LDPE) and natural antioxidant curcumin," 21st International Conference on Food Technology and Processing., October 04-06, London, United Kingdom. 2018.
2. **J. Zia**, A. Athanassiou, and D. Fragouli, "Biocomposite foams as rapid indicators for pH changes," TNT 2019., September 30th - October 4th, San Sebastian, Spain. 2019.

References

[1] M. Ghaani, C. A. Cozzolino, G. Castelli, and S. Farris, “An overview of the intelligent packaging technologies in the food sector,” *Trends Food Sci. Technol.*, vol. 51, pp. 1–11, 2016.

[2] E. Mohebi and L. Marquez, “Intelligent packaging in meat industry: An overview of existing solutions,” *J. Food Sci. Technol.*, vol. 52, no. 7, pp. 3947–3964, 2015.

[3] A. Alhendi and R. Choudhary, “Current Practices in Bread Packaging and Possibility of Improving Bread Shelf Life by Nanotechnology,” vol. 3, no. 4, pp. 55–60, 2013.

[4] De W. Blackburn, *Food spoilage microorganisms*. Cambridge, UK: Woodhead Publishing, 2006.

[5] D. C. Lewis and T. Shibamoto, “Shelf life of fruits,” in *Handbook of Food and Beverage Stability*, G. Charaml., Orlando: Academic Press, 1986.

[6] D. Schaefer and W. M. Cheung, “Smart packaging: opportunities and challenges,” *Procedia CIRP*, vol. 72, pp. 1022–1027, 2018.

[7] J. M. Jay, M. J. Loessner, and D. A. Golden, “Intrinsic and extrinsic parameters of foods that affect microbial growth,” in *Modern Food Microbiology. Food Science Text Series*, Boston: Springer, 2005, pp. 39–59.

[8] J. H. H. In’t Veld, “Microbial and biochemical spoilage of foods,” *Int. J. Food Microbiol.*, vol. 33, no. 1, pp. 1–18, 1996.

[9] J. I. Pitt and A. D. Hocking, *Introduction. Fungi and Food Spoilage*. Boston, 2009.

[10] U. Filtenborg, O., Frisvad, J. C., Thrane, “Moulds in food spoilage,” *Int. J. Food Microbiol.*, vol. 33, no. 1, pp. 85–102, 1996.

[11] M. Ozdemir and J. D. Floros, “Active food packaging technologies,” *Crit. Rev. Food Sci. Nutr.*, vol. 44, no. 3, pp. 185–193, 2004.

[12] U. Siripatrawan and B. R. Harte, “Physical properties and antioxidant activity of an active film from chitosan incorporated with green tea extract,” *Food Hydrocoll.*, vol. 24, no. 8, pp. 770–775, 2010.

[13] J. Li, J. Miao, J. Wu, S. Chen, and Q. Zhang, “Preparation and characterization of active gelatin-based films incorporated with natural antioxidants,” *Food Hydrocoll.*, vol. 37, pp. 166–173, 2014.

[14] M. Ramos, A. Jiménez, M. Peltzer, and M. C. Garrigós, “Characterization and antimicrobial activity studies of polypropylene films with carvacrol and thymol for active packaging,” *J. Food Eng.*, vol. 109, no. 3, pp. 513–519, 2012.

[15] Z. Rehman and A. M. Salariya, “Effect of synthetic antioxidants on storage stability of Khoa – a semi-solid concentrated milk product,” *Food Chem.*, vol. 96, pp. 122–125, 2006.

[16] M. Jamshidian, E. A. Tehrany, and S. Desobry, “Release of synthetic phenolic antioxidants from extruded poly lactic acid (PLA) film,” *Food Control*, vol. 28, no. 2, pp. 445–455, 2012.

[17] D. Granda-Restrepo, E. Peralta, R. Troncoso-Rojas, and H. Soto-Valdez, “Release of antioxidants from co-extruded active packaging developed for whole milk powder,” *Int. Dairy J.*, vol. 19, no. 8, pp. 481–488, 2009.

[18] V. Ambrogi *et al.*, “Natural antioxidants for polypropylene stabilization,” *Polym. Degrad. Stab.*, vol. 96, no. 12, pp. 2152–2158, 2011.

[19] M. Moudache, M. Colon, C. Nerín, and F. Zaidi, “Phenolic content and antioxidant activity of olive by-products and antioxidant film containing olive leaf extract,” *Food Chem.*, vol. 212, pp. 521–527, 2016.

[20] K. A. Iyer, L. Zhang, and J. M. Torkelson, “Direct Use of Natural Antioxidant-rich Agro-wastes as Thermal Stabilizer for Polymer: Processing and Recycling,” *ACS Sustain. Chem. Eng.*, vol. 4, no. 3, pp. 881–889, 2016.

[21] S. Zhang and H. Zhao, “Study on flavonoid migration from active low-density polyethylene film into aqueous food simulants,” *Food Chem.*, vol. 157, pp. 45–50, 2014.

[22] A. B. Properties, “LOW DENSITY POLYETHYLENE (LDPE) NANOCOMPOSITES WITH PASSIVE AND ACTIVE BARRIER PROPERTIES,” *J. Chil. Chem. Soc.*, vol. 2, pp. 3–7, 2014.

[23] D. A. P. De Abreu, J. Maroto, and V. Rodr, “Antioxidants from barley husks impregnated in films of low-density polyethylene and their effect over lipid deterioration of frozen cod (Gadus morhua),” *J. Sci. Food Agric.*, no. August 2011, pp. 427–432, 2012.

[24] D. A. P. De Abreu, P. P. Losada, J. Maroto, and J. M. Cruz, “Natural antioxidant active packaging film and its effect on lipid damage in frozen blue shark (Prionace glauca),” *Innov. Food Sci. Emerg. Technol.*, vol. 12, no. 1, pp. 50–55, 2011.

[25] E. Torrieri *et al.*, “Effect of modified atmosphere and active packaging on the shelf-life of fresh bluefin tuna fillets,” *J. Food Eng.*, vol. 105, no. 3, pp. 429–435, 2011.

[26] R. Ribeiro-Santos, M. Andrade, N. alia R. de Melo, and A. Sanches-Silva, “Use of essential oils in active food packaging : Recent advances and future trends,” *Trends Food Sci. Technol.*, vol. 61, no. January, pp. 132–140, 2017.

[27] H. Yousefi, H.-M. Su, S. M. Imani, K. Alkhaldi, C. D. M. Filipe, and T. F. Didar, “Intelligent Food Packaging: A Review of Smart Sensing Technologies for Monitoring Food Quality,” *ACS Sensors*, vol. 4, pp. 808–821, 2019.

[28] P. Müller and M. Schmid, “Intelligent Packaging in the Food Sector : A Brief Overview,” *Foods*, vol. 8, no. 16, pp. 1–12, 2019.

[29] J. Brockgreitens and A. Abbas, “Responsive Food Packaging : Recent Progress and Technological Prospects,” *Compr. Rev. Food Sci. Food Saf.*, vol. 15, pp. 3–15, 2016.

[30] X. Zhai *et al.*, “Novel colorimetric films based on starch/polyvinyl alcohol incorporated with roselle anthocyanins for fish freshness monitoring,” *Food Hydrocoll.*, vol. 69, pp. 308–317, 2017.

[31] X. Zhang, S. Lu, and X. Chen, “A visual pH sensing film using natural dyes from Bauhinia blakeana Dunn,” *Sensors Actuators, B Chem.*, vol. 198, pp. 268–273, 2014.

[32] M. C. Maria Erminia Genovese, Elena Colusso and cAthanassia A. and D. F. Alessandro Martucci, “Acidochromic fibrous polymer composites for rapidgas detection,” *J. Mater. Chem. A*, vol. 00, no. January 2017, pp. 1–10, 2016.

[33] M. E. Genovese *et al.*, “Photochromic Paper Indicators for Acidic Food Spoilage Detection,” *ACS Omega*, vol. 3, no. October, pp. 13484–13493, 2018.

[34] M. E. Genovese, A. Athanassiou, and D. Fragouli, “Photoactivated acidochromic elastomeric

films for on demand acidic vapor sensing," *J. Mater. Chem. A*, vol. 00, no. October, pp. 1–7, 2015.

[35] J. Geltmeyer *et al.*, "Dye Modification of Nanofibrous Silicon Oxide Membranes for Colorimetric HCl and NH 3 Sensing," *Adv. Funct. Mater*, vol. 26, pp. 5987–5996, 2016.

[36] F. Ebrahimi, M. Moradi, H. Tajik, M. Forough, P. Ezati, and B. Kuswandi, "Cellulose/chitosan pH-responsive indicator incorporated with carrot anthocyanins for intelligent food packaging," *Int. J. Biol. Macromol.*, vol. 136, pp. 920–926, 2019.

[37] B. Tang *et al.*, "Kinetic investigation into pH-dependent color of anthocyanin and its sensing performance," *Dye. Pigment.*, vol. 170, no. June, p. 107643, 2019.

[38] M. Sohail, D. Sun, and Z. Zhu, "Recent Developments in Intelligent Packaging for Enhancing Food Quality and Safety Recent Developments in Intelligent Packaging for Enhancing Food Quality and Safety," *Crit. Rev. Food Sci. Nutr.*, vol. 8398, 2018.

[39] K. B. Biji, C. N. Ravishankar, and C. O. Mohan, "Smart packaging systems for food applications : a review," *J Food Sci Technol*, vol. 52, no. October, pp. 6125–6135, 2015.

[40] M. Smolander, E. Hurme, and R. Ahvenainen, "Leak indicators for modified-atmosphere packages," *Trends food Sci. Technol.*, vol. 108, 1997.

[41] E. Balbinot-alfaro *et al.*, "Intelligent Packaging with pH Indicator Potential," *Food Eng. Rev.*, pp. 235–244, 2019.

[42] J. Liu *et al.*, "Films based on κ-carrageenan incorporated with curcumin for freshness monitoring," *Food Hydrocoll.*, vol. 83, pp. 134–142, 2018.

[43] P. Ezati, H. Tajik, and M. Moradi, "Chemical Fabrication and characterization of alizarin colorimetric indicator based on cellulose-chitosan to monitor the freshness of minced beef," *Sensors Actuators B. Chem.*, vol. 285, no. January, pp. 519–528, 2019.

[44] X. Xie and E. Bakker, "Non-Severinghaus Potentiometric Dissolved CO 2 Sensor with Improved Characteristics," pp. 1332–1336, 2013.

[45] M. Smolander, "Monitoring of the quality of modified atmosphere packaged broiler chicken cuts stored in different temperature conditions . A . Time – temperature indicators as quality-indicating tools," vol. 15, pp. 217–229, 2004.

[46] P. Taylor, C. Ruiz-capillas, F. Jiménez-colmenero, C. Ruiz-capillas, and F. J. I. M. Enez-colmenero, "Biogenic Amines in Meat and Meat," *Crit. Rev. Food Sci. Nutr.*, no. June 2013, pp. 37–41, 2010.

[47] M. Rokka, "Monitoring of the quality of modified atmosphere packaged broiler chicken cuts stored in different temperature conditions B . Biogenic amines as quality-indicating metabolites," *Food Control*, vol. 15, pp. 601–607, 2004.

[48] I. Kaniou, G. Samouris, and T. Mouratidou, "Determination of biogenic amines in fresh unpacked and vacuum-packed beef during storage at 4 C," *Food Chem.*, vol. 74, pp. 515–519, 2001.

[49] V. Shukla, G. Kandeepan, and M. R. Vishnuraj, "Development of On-Package Indicator Sensor for Real-Time Monitoring of Buffalo Meat Quality During Refrigeration Storage," *Food Anal. Methods*, vol. 8, no. 6, pp. 1591–1597, 2015.

[50] B. Kuswandi, Jayus, A. Restyana, A. Abdullah, L. Y. Heng, and M. Ahmad, "A novel colorimetric food package label for fish spoilage based on polyaniline film," *Food Control*,

vol. 25, no. 1, pp. 18–189, 2012.

[51] B. Kuswandi, Jayus, T. S. Larasati, A. Abdullah, and L. Y. Heng, “Real-Time Monitoring of Shrimp Spoilage Using On-Package Sticker Sensor Based on Natural Dye of Curcumin,” *Food Anal. Methods*, vol. 5, no. 4, pp. 881–889, 2012.

[52] M. Pávai, J. Mihály, and A. Paszternák, “pH and CO2 Sensing by Curcumin-Coloured Cellophane Test Strip,” *Food Anal. Methods*, vol. 8, no. 9, pp. 2243–2249, 2015.

[53] Q. Ma, L. Du, and L. Wang, “Tara gum/polyvinyl alcohol-based colorimetric NH3 indicator films incorporating curcumin for intelligent packaging,” *Sensors Actuators B Chem.*, vol. 244, pp. 759–766, 2017.

[54] P. Ezati and J. Rhim, “pH-responsive pectin-based multifunctional films incorporated with curcumin and sulfur nanoparticles,” *Carbohydr. Polym.*, no. October, p. 115638, 2019.

[55] V. Shukla, G. Kandeepan, M. R. Vishnuraj, and A. Soni, “Anthocyanins Based Indicator Sensor for Intelligent Packaging Application,” *Agric. Res.*, vol. 5, no. 2, pp. 205–209, 2016.

[56] I. Choi, J. Y. Lee, M. Lacroix, and J. Han, “Intelligent pH indicator film composed of agar/potato starch and anthocyanin extracts from purple sweet potato,” *Food Chem.*, vol. 218, pp. 122–128, 2017.

[57] X. W. Huang *et al.*, “Determination of pork spoilage by colorimetric gas sensor array based on natural pigments,” *Food Chem.*, vol. 145, pp. 549–554, 2014.

[58] H. Xiaowei, Z. Xiaobo, Z. Jiewen, S. Jiyong, L. Zhihua, and S. Tingting, “Monitoring the biogenic amines in Chinese traditional salted pork in jelly (Yao-meat) by colorimetric sensor array based on nine natural pigments,” *Int. J. Food Sci. Technol.*, vol. 50, no. 1, pp. 203–209, 2015.

[59] J. A. Cavallo, M. C. Strumia, and C. G. Gomez, “Preparation of a milk spoilage indicator adsorbed to a modified polypropylene film as an attempt to build a smart packaging,” *J. Food Eng.*, vol. 136, no. September, pp. 48–55, 2014.

[60] V. A. Pereira, I. N. Q. de Arruda, and R. Stefani, “Active chitosan/PVA films with anthocyanins from Brassica oleraceae (Red Cabbage) as Time-Temperature Indicators for application in intelligent food packaging,” *Food Hydrocoll.*, vol. 43, pp. 180–188, 2015.

[61] S. Pourjavaher, H. Almasi, S. Meshkini, S. Pirsa, and E. Parandi, “Development of a colorimetric pH indicator based on bacterial cellulose nanofibers and red cabbage (Brassica oleraceae) extract,” *Carbohydr. Polym.*, vol. 156, pp. 193–201, 2017.

[62] C. M. P. Yoshida, V. B. V Maciel, M. E. D. Mendon??a, and T. T. Franco, “Chitosan biobased and intelligent films: Monitoring pH variations,” *LWT - Food Sci. Technol.*, vol. 55, no. 1, pp. 83–89, 2014.

[63] V. B. V Maciel, C. M. P. Yoshida, and T. T. Franco, “Chitosan/pectin polyelectrolyte complex as a pH indicator,” *Carbohydr. Polym.*, vol. 132, pp. 537–545, 2015.

[64] A. Teixeira, V. A. Pereira-júnior, M. C. Silva-pereira, and R. Stefani, “Chitosan/corn starch blend films with extract from Brassica oleraceae (red cabbage) as a visual indicator of fi sh deterioration,” vol. 61, pp. 258–262, 2015.

[65] P. Ezati, H. Tajik, and M. Moradi, “Fabrication and characterization of alizarin colorimetric indicator based on cellulose-chitosan to monitor the freshness of minced beef,” *Sensors Actuators B. Chem.*, vol. 285, no. November 2018, pp. 519–528, 2019.

[66] P. Ezati, H. Tajik, M. Moradi, and R. Molaei, “Intelligent pH-sensitive indicator based on starch-cellulose and alizarin dye to track freshness of rainbow trout fi llet,” *Int. J. Biol. Macromol.*, vol. 132, pp. 157–165, 2019.

[67] C. Rukchon, A. Nopwinyuwong, S. Trevanich, T. Jinkarn, and P. Suppakul, “Development of a food spoilage indicator for monitoring freshness of skinless chicken breast,” *Talanta*, vol. 130, pp. 547–554, 2014.

[68] B. Kuswandi, C. Maryska, Jayus, A. Abdullah, and L. Y. Heng, “Real time on-package freshness indicator for guavas packaging,” *J. Food Meas. Charact.*, vol. 7, no. 1, pp. 29–39, 2013.

[69] B. Kuswandi, A. A. Revi Oktaviana, and L. Y. Heng, “A Novel On-Package Sticker Sensor Based on Methyl Red for Real-Time Monitoring of Broiler Chicken Cut Freshness,” *Packag. Technol. Sci.*, vol. 23, no. May, pp. 253–266, 2010.

[70] U. Khulal, J. W. Zhao, W. W. Hu, and Q. S. Chen, “Comparison of different chemometric methods in quantifying total volatile basic-nitrogen (TVB-N) content in chicken meat using a fabricated colorimetric sensor array,” *Rsc Adv.*, vol. 6, no. 6, pp. 4663–4672, 2016.

[71] H. N. Chun, B. Kim, and H. S. Shin, “Evaluation of a freshness indicator for quality of fish products during storage,” *Food Sci. Biotechnol.*, vol. 23, no. 5, pp. 1719–1725, 2014.

[72] M. K. Morsy *et al.*, “Development and validation of a colorimetric sensor array for fish spoilage monitoring,” *Food Control*, vol. 60, pp. 346–352, 2016.

[73] H. Xiao-Wei *et al.*, “Detection of meat-borne trimethylamine based on nanoporous colorimetric sensor arrays,” *Food Chem.*, vol. 197, no. 2, pp. 930–936, 2016.

[74] Y. Byun, Y. T. Kim, and S. Whiteside, “Characterization of an antioxidant polylactic acid (PLA) film prepared with a -tocopherol , BHT and polyethylene glycol using film cast extruder,” *J. Food Eng.*, vol. 100, no. 2, pp. 239–244, 2010.

[75] B. Kirschweng, D. Tátraaljai, E. Földes, and B. Pukánszky, “Efficiency of curcumin, a natural antioxidant, in the processing stabilization of PE: Concentration effects,” *Polym. Degrad. Stab.*, vol. 118, pp. 17–23, 2015.

[76] P. Cerruti, M. Malinconico, J. Rychly, L. Matisova-rychla, and C. Carfagna, “Effect of natural antioxidants on the stability of polypropylene films,” *Polym. Degrad. Stab.*, vol. 94, no. 11, pp. 2095–2100, 2009.

[77] B. Pukánszky, D. Tátraaljai, B. Kirschweng, and J. Kovács, “Processing stabilisation of PE with a natural antioxidant , curcumin,” *Eur. Polym. J.*, vol. 49, pp. 1196–1203, 2013.

[78] R. Geyer, J. R. Jambeck, and K. L. Law, “Production , use , and fate of all plastics ever made,” *Sci. Adv.*, no. July, pp. 25–29, 2017.

[79] P. Sonkaew, A. Sane, and P. Suppakul, “Antioxidant Activities of Curcumin and Ascorbyl Dipalmitate Nanoparticles and Their Activities after Incorporation into Cellulose-Based Packaging Films,” *J. Agric. Food Chem*, vol. 60, pp. 5388–5399, 2012.

[80] Y. Peng, Y. Wu, and Y. Li, “Development of tea extracts and chitosan composite films for active packaging materials,” *Int. J. Biol. Macromol.*, vol. 59, pp. 282–289, 2013.

[81] J. Gómez-Estaca, C. López-de-Dicastillo, P. Hernández-Muñoz, R. Catalá, and R. Gavara, “Advances in antioxidant active food packaging,” *Trends Food Sci. Technol.*, vol. 35, no. 1, pp. 42–51, 2014.

[82] S. Plog, J. Schneider, M. Walker, A. Schulz, and U. Stroth, “Investigations of plasma polymerized SiO x barrier fi lms for polymer food packaging,” *Surf. Coat. Technol.*, vol. 205, pp. 165–170, 2011.

[83] O. Ozcalik and F. Tihminlioglu, “Barrier properties of corn zein nanocomposite coated polypropylene films for food packaging applications,” *J. Food Eng.*, vol. 114, no. 4, pp. 505–513, 2013.

[84] T. V. Duncan, “Applications of nanotechnology in food packaging and food safety: Barrier materials, antimicrobials and sensors,” *J. Colloid Interface Sci.*, vol. 363, no. 1, pp. 1–24, 2011.

[85] P. Oymaci and S. A. Altinkaya, “Improvement of barrier and mechanical properties of whey protein isolate based food packaging films by incorporation of zein nanoparticles as a novel bionanocomposite,” *Food Hydrocoll.*, vol. 54, pp. 1–9, 2016.

[86] A. M. Youssef and S. M. El-Sayed, “Bionanocomposites materials for food packaging applications: Concepts and future outlook,” *Carbohydr. Polym.*, vol. 193, no. March, pp. 19–27, 2018.

[87] F. Xie, E. Pollet, P. J. Halley, and L. Avérous, “Starch-based nano-biocomposites,” *Prog. Polym. Sci.*, vol. 38, no. 10–11, pp. 1590–1628, 2013.

[88] N. El Miri *et al.*, “Bio-nanocomposite films reinforced with cellulose nanocrystals: Rheology of film-forming solutions, transparency, water vapor barrier and tensile properties of films,” *Carbohydr. Polym.*, vol. 129, pp. 156–167, 2015.

[89] Y. Qin, S. Zhang, J. Yu, J. Yang, L. Xiong, and Q. Sun, “Effects of chitin nano-whiskers on the antibacterial and physicochemical properties of maize starch films,” *Carbohydr. Polym.*, vol. 147, pp. 372–378, 2016.

[90] S. R. Kanatt, M. S. Rao, S. P. Chawla, and A. Sharma, “Active chitosan-polyvinyl alcohol films with natural extracts,” *Food Hydrocoll.*, vol. 29, no. 2, pp. 290–297, 2012.

[91] P. R. Salgado, M. E. López-Caballero, M. C. Gómez-Guillén, A. N. Mauri, and M. P. Montero, “Sunflower protein films incorporated with clove essential oil have potential application for the preservation of fish patties,” *Food Hydrocoll.*, vol. 33, no. 1, pp. 74–84, 2013.

[92] C. M. Bitencourt, P. J. A. Sobral, and R. A. Carvalho, “Gelatin-based fi lms additivated with curcuma ethanol extract : Antioxidant activity and physical properties of films,” *Food Hydrocoll.*, vol. 40, pp. 145–152, 2014.

[93] M. H. Le *et al.*, “The dual effect of curcumin nanoparticles encapsulated by 1-3 / 1-6 β - glucan from medicinal mushrooms Hericium erinaceus and Ganoderma lucidum,” *Adv. Nat. Sci. Nanosci. Nanotechnol*, vol. 7, pp. 1–8, 2016.

[94] A. Mey *et al.*, “Enhanced bioavailability and bioefficacy of an amorphous solid dispersion of curcumin,” *FOOD Chem.*, vol. 156, pp. 227–233, 2014.

[95] S. K. Bajpai, N. Chand, and S. Ahuja, “Investigation of curcumin release from chitosan/cellulose micro crystals (CMC) antimicrobial films,” *Int. J. Biol. Macromol.*, vol. 79, pp. 440–448, 2015.

[96] K. Sindhu, A. Rajaram, and K. J. S. and R. Rajaram, “Curcumin conjugated gold nanoparticle synthesis and its biocompatibility,” *RSC Adv.*, vol. 4, pp. 1808–1818, 2014.

[97] T. Esatbeyoglu, K. Ulbrich, C. Rehberg, S. Rohn, and G. Rimbach, “Thermal stability, antioxidant, and antiinflammatory activity of curcumin and its degradation product 4-vinyl guaiacol,” *Food Funct.*, vol. 6, pp. 887–893, 2015.

[98] Y. Cheng, J. Lodge, L. Lu, and J. Lodge, “Evaluation of Natural Plant Powders with Potential Use in Antimicrobial Packaging Applications,” *J. Appl. Packag. Res.*, vol. 6, no. 2, pp. 29–39, 2014.

[99] R. K. Maheshwari, A. K. Singh, J. Gaddipati, and R. C. Srimal, “Multiple biological activities of curcumin : A short review,” *Life Sci.*, vol. 78, no. 18, pp. 2081–2087, 2006.

[100] N. Luo, K. Varaprasad, G. Venkata, S. Reddy, A. Varada, and J. Zhang, “Preparation and characterization of cellulose/curcumin composite films,” *RSC Adv.*, pp. 8483–8488, 2012.

[101] J. Z. Liyan Wang, Yan Dong, Haitao Men, Jin Tong, “Preparation and characterization of active films based on chitosan incorporated tea polyphenols,” *Food Hydrocoll.*, no. February 2017, pp. 35–41, 2013.

[102] Q. Ma, Y. Ren, and L. Wang, “Investigation of antioxidant activity and release kinetics of curcumin from tara gum/polyvinyl alcohol active film,” *Food Hydrocoll.*, vol. 70, pp. 286–292, 2017.

[103] H. Wang, L. Hao, P. Wang, M. Chen, and S. Jiang, “Release kinetics and antibacterial activity of curcumin loaded zein fibers,” *Food Hydrocoll.*, vol. 63, pp. 437–446, 2017.

[104] Y. Liu, Y. Cai, X. Jiang, J. Wu, and X. Le, “Molecular interactions, characterization and antimicrobial activity of curcumin-chitosan blend films,” *Food Hydrocoll.*, vol. 52, pp. 564–572, 2016.

[105] S. J. Risch, “Food Packaging History and Innovations,” *J. Agric. Food Chem.*, vol. 57, no. 18, pp. 8089–8092, 2009.

[106] S. Mrkić, K. Galić, M. Ivanković, S. Hamin, and N. Cikić, “Gas transport and thermal characterization of mono- and Di-polyethylene films used for food packaging,” *J. Appl. Polym. Sci.*, vol. 99, no. 4, pp. 1590–1599, 2006.

[107] L. Axelsson, M. Franzén, M. Ostwald, G. Berndes, G. Lakshmi, and N. H. Ravindranath, “Accounting for the constrained availability of land: a comparison of bio-based ethanol, polyethylene, and PLA with regard to non-renewable energy use and land use,” *Biofuels, Bioprod. Biorefining*, vol. 6, pp. 146–156, 2012.

[108] X. Chen, D. S. Lee, X. Zhu, and K. L. Yam, “Release kinetics of tocopherol and quercetin from binary antioxidant controlled-release packaging films,” *J. Agric. Food Chem.*, vol. 60, no. 13, pp. 3492–3497, 2012.

[109] M. A. Del Nobile, A. Conte, G. G. Buonocore, A. L. Incoronato, A. Massaro, and O. Panza, “Active packaging by extrusion processing of recyclable and biodegradable polymers,” *J. Food Eng.*, vol. 93, no. 1, pp. 1–6, 2009.

[110] N. Laohakunjit and A. Noomhorm, “Effect of plasticizers on mechanical and barrier properties of rice starch film,” *Starch/Staerke*, vol. 56, no. 8, pp. 348–356, 2004.

[111] N. R. Savadekar and S. T. Mhaske, “Synthesis of nano cellulose fibers and effect on thermoplastics starch based films,” *Carbohydr. Polym.*, vol. 89, no. 1, pp. 146–151, 2012.

[112] T. N. Tran *et al.*, “Transparent and flexible amorphous cellulose-acrylic hybrids,” *Chem. Eng. J.*, vol. 287, no. October, pp. 196–204, 2016.

[113] N. Tenn, N. Follain, J. Soulestin, R. Crétois, S. Bourbigot, and S. Marais, “Effect of nanoclay hydration on barrier properties of PLA/montmorillonite based nanocomposites,” *J. Phys. Chem. C*, vol. 117, no. 23, pp. 12117–12135, 2013.

[114] V. Siracusa, “Food packaging permeability behaviour: A report,” *Int. J. Polym. Sci.*, vol. 2012, no. i, pp. 1–11, 2012.

[115] O. P. Sharma and T. K. Bhat, “DPPH antioxidant assay revisited,” *Food Chem.*, vol. 113, no. 4, pp. 1202–1205, 2009.

[116] I. S. B. Thi Nga Tran, Athanassia Athanassiou, Abdul Basit, “Starch-based bio-elastomers functionalized with with red beetroot natural antioxidant,” *Food Chem.*, vol. 216, no. February, pp. 324–333, 2017.

[117] R. A. Silva-buzanello *et al.*, “Preparation of curcumin-loaded nanoparticles and determination of the antioxidant potential of curcumin after encapsulation,” vol. 26, no. 3, pp. 207–214, 2016.

[118] P. J. and K. M. Harshal Pawar, Mugdha Karde, Nilesh Mundle, “Phytochemical Evaluation and Curcumin Content Determination of Turmeric Rhizomes Collected From Bhandara District of Maharashtra,” *Med. Chem. (Los. Angeles).*, vol. 4, no. 8, pp. 588–591, 2014.

[119] A. L. Parize, H. K. Stulzer, M. C. M. Laranjeira, I. M. Da Costa Brighente, and T. C. R. De Souza, “Evaluation of chitosan microparticles containing curcumin and crosslinked with sodium tripolyphosphate produced by spray drying,” *Quim. Nova*, vol. 35, no. 6, pp. 1127–1132, 2012.

[120] P. R. K. Mohan, G. Sreelakshmi, C. V. Muraleedharan, and R. Joseph, “Water soluble complexes of curcumin with cyclodextrins: Characterization by FT-Raman spectroscopy,” *Vib. Spectrosc.*, vol. 62, pp. 77–84, 2012.

[121] “Comparative Study on the Effect of Bentonite or Feldspar Filled Low-Density Polyethylene / Thermoplastic ... Feldspar Filled Low-Density Polyethylene / Thermoplastic Sago Starch / Kenaf Core Fiber,” no. May, 2013.

[122] P. R. Janissek and H. M. Heise, “Polyethylene characterization by FTIR,” vol. 9418, no. January, 2015.

[123] J. M. Chem, S. R. Chowdhury, and S. Sabharwal, “Molecular-scale design of a high performance organic – inorganic hybrid with the help of gamma radiation,” *J. Mater. Chem.*, vol. 21, pp. 6999–7006, 2011.

[124] H. Hagemann, R. G. Snyder, A. J. Peacock, and L. Mandelkern, “Quantitative infrared methods for the measurement of crystallinity and its temperature dependence: polyethylene,” *Macromolecules*, vol. 22, no. 9, pp. 3600–3606, 1989.

[125] S. Krimm, C. Y. Liang, and G. B. B. M. Sutherland, “Infrared spectra of high polymers. II. Polyethylene,” *J. Chem. Phys.*, vol. 25, no. 3, pp. 549–562, 1956.

[126] N. F. Brockmeier, “The effect of temperature on the infrared absorption frequencies of polyethylene and ethylene–propylene copolymer films,” *J. Appl. Polym. Sci.*, vol. 12, no. 9, pp. 2129–2140, 1968.

[127] R. A. A. Fugita *et al.*, “Thermal Behaviour of Curcumin,” *Brazilian J. Therm. Anal.*, vol. 1, pp. 19–23, 2012.

[128] Z. Chen *et al.*, “Thermal degradation kinetics study of curcumin with nonlinear methods,”

Food Chem., vol. 155, pp. 81–86, 2014.

[129] P. K. Roy, P. Surekha, C. Rajagopal, and V. Choudhary, "Thermal degradation studies of LDPE containing cobalt stearate as pro-oxidant," *eXPRESS Polym. Lett.*, vol. 1, no. 4, pp. 208–216, 2007.

[130] M. Kurek, I. Elez, M. Tran, M. Šč, V. Dragovi, and K. Gali, "Development and evaluation of a novel antioxidant and pH indicator film based on chitosan and food waste sources of antioxidants," vol. 84, no. May, pp. 238–246, 2018.

[131] Y. S. Musso, P. R. Salgado, and A. N. Mauri, "Smart edible films based on gelatin and curcumin," *Food Hydrocoll.*, vol. 66, pp. 8–15, 2017.

[132] G. Perotto *et al.*, "Bioplastics from vegetable waste via an eco-friendly water-based process," *Green Chem.*, vol. 20, pp. 894–902, 2018.

[133] S. A. A. Shah *et al.*, "Curcumin incorporated polyurethane urea elastomers with tunable thermo-mechanical properties," *React. Funct. Polym.*, vol. 128, no. March, pp. 97–103, 2018.

[134] S. Gemili, A. Yemenicioğlu, and S. A. Altinkaya, "Development of antioxidant food packaging materials with controlled release properties," *J. Food Eng.*, vol. 96, no. 3, pp. 325–332, 2010.

[135] A. B. Gangurde, H. S. Kundaikar, S. D. Javeer, D. R. Jaiswar, M. S. Degani, and P. D. Amin, "Enhanced solubility and dissolution of curcumin by a hydrophilic polymer solid dispersion and its insilico molecular modeling studies," *J. Drug Deliv. Sci. Technol.*, vol. 29, pp. 226–237, 2015.

[136] L. Golasz, J. Silva, and S. Silva, "Film with anthocyanins as an indicator of chilled pork deterioration," *Ciência e Tecnol. Aliment.*, vol. 2012, pp. 155–162, 2013.

[137] M. Moradi, H. Tajik, H. Almasi, M. Forough, and P. Ezati, "A novel pH-sensing indicator based on bacterial cellulose nano fibers and black carrot anthocyanins for monitoring fish freshness," *Carbohydr. Polym.*, vol. 222, no. June, p. 115030, 2019.

[138] A. PEDROSA-MENABRITO, "SHELF-LIFE EXTENSION OF FRESH FISH - A REVIEW," *J. Food Qual.*, vol. 11, pp. 117–127, 1988.

[139] B. Kuswandi and A. Nurfawaidi, "On-package dual sensors label based on pH indicators for real-time monitoring of beef freshness," *Food Control*, vol. 82, pp. 91–100, 2017.

[140] Y. S. Musso, P. R. Salgado, and A. N. Mauri, "Gelatin based films capable of modifying its color against environmental pH changes," *Food Hydrocoll.*, vol. 61, pp. 523–530, 2016.

[141] Y. Li *et al.*, "A pH-indicating intelligent packaging composed of chitosan-purple potato extractions strength by surface-deacetylated chitin nano fibers," *Int. J. Biol. Macromol.*, vol. 127, pp. 376–384, 2019.

[142] L. Prietto *et al.*, "pH-sensitive films containing anthocyanins extracted from black bean seed coat and red cabbage," *LWT - Food Sci. Technol.*, vol. 80, pp. 492–500, 2017.

[143] M. Koosha and S. Hamedi, "Chitosan/PVA nanocomposite films containing black carrot anthocyanin and bentonite nanoclays with improved mechanical, thermal and antibacterial properties," *Prog. Org. Coatings*, vol. 127, no. October 2018, pp. 338–347, 2019.

[144] M. Vadivel, M. Sankarganesh, and J. Dhaveethu, "Bioactive constituents and bio-waste derived chitosan/xylan based biodegradable hybrid nanocomposite for sensitive detection of fish freshness," *Food Packag. Shelf Life*, vol. 22, no. August, p. 100384, 2019.

[145] K. Devarayan and B. S. Kim, “Reversible and universal pH sensing cellulose nanofibers for health monitor,” *Sensors Actuators, B Chem.*, vol. 209, pp. 281–286, 2015.

[146] K. Halász and L. Csóka, “Black chokeberry (Aronia melanocarpa) pomace extract immobilized in chitosan for colorimetric pH indicator fi lm application,” *Food Packag. Shelf Life*, vol. 16, no. September 2017, pp. 185–193, 2018.

[147] T. Liang, G. Sun, L. Cao, J. Li, and L. Wang, “A pH and NH3 sensing intelligent film based on Artemisia sphaerocephala Krasch . gum and red cabbage anthocyanins anchored by carboxymethyl cellulose sodium added as a host complex,” *Food Hydrocoll.*, vol. 87, no. July 2018, pp. 858–868, 2019.

[148] H. Yu, X. Xu, X. Chen, T. Lu, P. Zhang, and X. Jing, “Preparation and Antibacterial Effects of PVA-PVP Hydrogels Containing Silver Nanoparticles,” 2006.

[149] Y. Nho, Y. Lim, H. Gwon, and E. Choi, “Preparation and characterization of PVA / PVP / glycerin / antibacterial agent hydrogels using γ -irradiation followed by freeze-thawing,” vol. 26, no. 6, pp. 1675–1678, 2009.

[150] M. M. Hawkeye and M. J. Brett, “Optimized Colorimetric Photonic-Crystal Humidity Sensor Fabricated Using Glancing Angle Deposition,” pp. 3652–3658, 2011.

[151] W. S. Mokrzycki and M. Tatol, “Colour difference Delta E-A survey,” in *Machine Graphics and Vision*, no. August, 2011, pp. 383–411.

[152] Z. A. Alothman, “A Review: Fundamental Aspects of Silicate Mesoporous Materials,” no. December 2012, 2016.

[153] L. Campagnolo, D. Morselli, D. Magrì, A. Scarpellini, and C. Demirci, “Silk Fibroin/Orange Peel Foam : An Efficient Biocomposite for Water Remediation,” vol. 1800097, pp. 1–10, 2019.

[154] M. K. Chine, F. Sediri, and N. Gharbi, “Hydrothermal Synthesis of V 3 O 7 · H 2 O Nanobelts and Study of Their Electrochemical Properties,” vol. 2011, no. August, pp. 964–970, 2011.

[155] C. Yang *et al.*, “Compositional controls on pore-size distribution by nitrogen adsorption technique in the Lower Permian Shanxi Shales , Ordos Basin,” *J. Nat. Gas Sci. Eng.*, vol. 34, pp. 1369–1381, 2016.

[156] S. Mallakpour and F. Motirasoul, “Ultrasonics - Sonochemistry Ultrasonication synthesis of PVA / PVP / α -MnO 2 -stearic acid blend nanocomposites for adsorbing Cd II ion,” vol. 40, no. July 2017, pp. 410–418, 2018.

[157] S. Choudhary, “Electrical Properties of Alumina Nanoparticles Filled PVA – PVP Blend Matrix-Based Polymer Nanocomposites,” 2018.

[158] S. Guzman-puyol *et al.*, “Effect of trifluoroacetic acid on the properties of polyvinyl alcohol and polyvinyl alcohol – cellulose composites,” *Chem. Eng. J.*, vol. 277, pp. 242–251, 2015.

[159] M. Contardi *et al.*, “Polyvinylpyrrolidone / hyaluronic acid-based bilayer constructs for sequential delivery of cutaneous antiseptic and antibiotic,” vol. 358, no. October 2018, pp. 912–923, 2019.

[160] J. Coates, “Interpretation of Infrared Spectra , A Practical Approach,” pp. 1–23, 2006.

[161] D. Trache, A. Donnot, K. Khimeche, R. Benelmir, and N. Brosse, “Physico-chemical properties and thermal stability of microcrystalline cellulose isolated from Alfa fibres,”

Carbohydr. Polym., vol. 104, pp. 223–230, 2014.

[162] Y. Liu, L. Li, X. Li, Y. Wang, X. Ren, and J. Liang, "Antibacterial Modification of Microcrystalline Cellulose by Grafting Copolymerization," *BioResources*, vol. 11, no. 1, pp. 519–529, 2016.

[163] J. W. Gilman, D. L. Vanderhart, and T. Kashiwagi, "Thermal Decomposition Chemistry of Poly (vinyl alcohol)," 1995.

[164] W. H. Eisa, T. A. A. Baset, and E. M. A. Mohamed, "Crosslinked PVA / PVP Supported Silver Nanoparticles : A Reusable and Efficient Heterogeneous Catalyst for the 4-Nitrophenol Degradation," *J. Inorg. Organomet. Polym. Mater.*, vol. 27, no. 6, pp. 1703–1711, 2017.

[165] N. A. Betti, "Thermogravimetric Analysis on PVA / PVP Blend Under Air Atmosphere," *Eng. &Tech.Journal*, vol. 34, no. 13, 2016.

[166] Q. Ma, T. Liang, L. Cao, and L. Wang, "Intelligent poly (vinyl alcohol) -chitosan nanoparticles-mulberry extracts films capable of monitoring pH variations," *Int. J. Biol. Macromol.*, vol. 108, pp. 576–584, 2018.

[167] J. Uranga, A. Etxabide, P. Guerrero, and K. De Caba, "Development of active fish gelatin films with anthocyanins by compression molding," *Food Hydrocoll.*, vol. 84, no. May, pp. 313–320, 2018.

[168] I. Dudnyk, E. Janeˇ, J. Vaucher-joset, and F. Stellacci, "Edible sensors for meat and seafood freshness," vol. 259, pp. 1108–1112, 2018.

[169] B. Liu, H. Xu, H. Zhao, W. Liu, L. Zhao, and Y. Li, "Preparation and characterization of intelligent starch/PVA films for simultaneous colorimetric indication and antimicrobial activity for food packaging applications," *Carbohydr. Polym.*, vol. 157, pp. 842–849, 2017.

[170] Q. Ma, Y. Ren, Z. Gu, and L. Wang, "Developing an intelligent film containing Vitis amurensis husk extracts : The effects of pH value of the fi lm-forming solution," *J. Clean. Prod.*, vol. 166, pp. 851–859, 2017.

[171] I. S. Bayer *et al.*, "Direct Transformation of Edible Vegetable Waste into Bioplastics," *Macromolecules*, pp. 5135–5143, 2014.

[172] S. Guzman-puyol, L. Ceseracciu, G. Tedeschi, and S. Marras, "Transparent and Robust All-Cellulose Nanocomposite Packaging Materials Transparent and Robust All -Cellulose Nanocomposite Packaging Materials Prepared in a Mixture of Trifluoroacetic Acid and Trifluoroacetic Anhydride," *Nanomaterials*, vol. 9, no. 368, pp. 1–14, 2019.

[173] M. Nasrollahzadeh, M. Selva, and R. Luque, "Waste-to-wealth: biowaste valorization into valuable bio(nano)materials," *Chem. Soc. Rev.*, vol. 48, no. 18, 2019.

[174] O. Curnow and M. P. Staiger, "A critical review of all-cellulose composites," *J. Mater. Sci.*, vol. 47, pp. 1171–1186, 2012.

[175] M. Ghaderi, M. Mousavi, H. Yousefi, and M. Labbafi, "All-cellulose nanocomposite film made from bagasse cellulose nanofibers for food packaging application All-cellulose nanocomposite film made from bagasse cellulose nanofibers for food packaging application," *Carbohydr. Polym.*, vol. 104, no. April, pp. 59–65, 2014.

[176] T. Tervahartiala, J. P. Valkama, N. C. Hildebrandt, and S. Schabel, "Potential of all - cellulose composites in corrugated board applications : Comparison of chemical pulp raw

materials," *Packag. Technol. Sci.*, no. June 2017, pp. 173–183, 2018.

[177] J. Zia, U. C. Paul, J. A. Heredia-guerrero, A. Athanassiou, and D. Fragouli, "Low-density polyethylene/curcumin melt extruded composites with enhanced water vapor barrier and antioxidant properties for active food packaging," *Polymer (Guildf).*, vol. 175, no. May, pp. 137–145, 2019.

[178] M. Butnariu and A. Butu, "Chemical Composition of Vegetables and Their Products," in *Handbook of Food Chemistry*, 2015, pp. 627–692.

[179] M. F. Borisenkov *et al.*, "Impact of Cabbage Pectin − Protein Complex on Microbial β ‑ Glucuronidase Activity," *J. Agric. Food Chem.*, pp. 1–5, 2013.

[180] T. Hama *et al.*, "Probing the Molecular Structure and Orientation of the Leaf Surface of Brassica oleracea L . by Polarization Modulation- Infrared Reflection-Absorption Spectroscopy," *Plant Cell Physiol*, vol. 60, no. April, pp. 1567–1580, 2019.

[181] A. Sci, "THE EFFECT OF THERMAL PROCESSING OF CRUCIFEROUS VEGETABLES ON THEIR CONTENT OF DIETARY FIBER," *Acta Sci. Pol. Technol. Aliment.*, 2012.

[182] T. W. Kang, G. Chandrasekaran, E. C. Hwang, H. Su, and V. Lakshmanan, "Characterization and antibacterial activity of PVA – PVP – CS carvacrol-loaded polymer composite films for urinary catheter," *Int. J. Polym. Mater. Polym. Biomater.*, vol. 0, no. 0, pp. 1–12, 2018.

[183] M. L. Sanyang, S. M. Sapuan, M. Jawaid, M. R. Ishak, and J. Sahari, "Effect of Plasticizer Type and Concentration on Tensile, Thermal and Barrier Properties of Biodegradable Films Based on Sugar Palm (Arenga pinnata) Starch," *Polymers (Basel).*, no. 7, pp. 1106–1124, 2015.

[184] J. Gustafsson, M. Landberg, B. Veronika, and D. Åkesson, "Development of Bio-Based Films and 3D Objects from Apple Pomace," *Polymers (Basel).*, vol. 11, no. 289, 2019.

[185] Z. W. Abdullah and Y. Dong, "Biodegradable and Water Resistant Poly (vinyl) Alcohol (PVA)/Starch (ST)/Glycerol (GL)/Halloysite Nanotube (HNT) Nanocomposite Films for Sustainable Food Packaging," *Front. Mater.*, vol. 6, no. April, pp. 1–17, 2019.

[186] A. Carolina *et al.*, "Biopolymeric Films of Amphiphilic Derivatives of Chitosan : A Physicochemical Characterization and Antifungal Study," *Int. J. Mol. Sci.*, vol. 20, 2019.

[187] P. González, C. Medina, L. Famá, and S. Goyanes, "Biodegradable and non-retrogradable eco-films based on starch-glycerol with citric acid as crosslinking agent Biodegradable and non-retrogradable eco-films based on starch – glycerol with citric acid as crosslinking agent," *Carbohydr. Polym.*, vol. 138, no. December, pp. 66–74, 2015.

[188] F. M. PELISSARI, M. V. E. GROSSMANN, F. YAMASHITA, and E. A. G. PINEDA, "Antimicrobial, Mechanical, and Barrier Properties of Cassava Starch - Chitosan Films Incorporated with Oregano Essential Oil," *J. Agric. Food Chem.*, pp. 7499–7504, 2009.

[189] L. Ren, X. Yan, J. Zhou, J. Tong, and X. Su, "Influence of chitosan concentration on mechanical and barrier properties of corn starch/chitosan films," *Int. J. Biol. Macromol.*, vol. 105, pp. 1636–1643, 2017.

[190] K. Minh and R. Yoksan, "Morphological characteristics and barrier properties of thermoplastic starch / chitosan blown film," *Carbohydr. Polym.*, vol. 150, pp. 40–47, 2016.

[191] F. M. Pelissari *et al.*, "Constrained mixture design applied to the development of cassava

starch – chitosan blown films," *J. Food Eng.*, vol. 108, no. 2, pp. 262–267, 2012.

[192] U. Putra and M. Processing, "Effect of concentration of chitosan on the mechanical , morphological and optical properties of tapioca starch film," *Int. Food Res. J.*, vol. 23, no. December, pp. 187–193, 2016.

[193] N. Akter, M. Tuhin, and P. Fahmida, "Thermomechanical, barrier, and morphological properties of Chitosan-reinforced starch-based biodegradable composite films," *J. Thermoplast. Compos. Mater.*, no. November, 2014.

[194] S. Rajendran, N. Durai, K. Kannan, and R. A. Arokiaswamy, "The Role of Microbes in Plastic Degradation," in *Environmental Waste Management*, no. August, 2015, pp. 341–370.

[195] Y. Tokiwa, B. P. Calabia, C. U. Ugwu, and S. Aiba, "Biodegradability of Plastics," *Int. J. Mol. Sci.*, pp. 3722–3742, 2009.

[196] M. Ratajska, G. Strobin, M. Wiśniewska-wrona, D. Ciechańska, H. Struszczyk, and S. Boryniec, "Studies on the Biodegradation of Chitosan in an Aqueous Medium," *FIBRES Text. East. Eur.*, vol. 11, no. 3, pp. 75–79, 2003.

[197] G. Scoponi, S. Guzman-puyol, G. Caputo, L. Ceseracciu, A. Athanassiou, and J. A. Heredia-guerrero, "Highly biodegradable, ductile all-polylactide blends," *Polymer (Guildf).*, p. 122371, 2020.

[198] K. Nilsuwan, P. Guerrero, K. De, and S. Benjakul, "Properties of fish gelatin films containing epigallocatechin gallate fabricated by thermo-compression molding," *Food Hydrocoll.*, vol. 97, no. June, p. 105236, 2019.